



HAL
open science

A calibrated optogenetic toolbox of stable zebrafish opsin lines

Paride Antinucci, Adna Dumitrescu, Charlotte Deleuze, Holly Morley, Kristie Leung, Tom Hagley, Fumi Kubo, Herwig Baier, Isaac Bianco, Claire Wyart

► **To cite this version:**

Paride Antinucci, Adna Dumitrescu, Charlotte Deleuze, Holly Morley, Kristie Leung, et al.. A calibrated optogenetic toolbox of stable zebrafish opsin lines. *eLife*, 2020, 9, 10.7554/eLife.54937 . hal-02540191

HAL Id: hal-02540191

<https://hal.sorbonne-universite.fr/hal-02540191>

Submitted on 10 Apr 2020

HAL is a multi-disciplinary open access archive for the deposit and dissemination of scientific research documents, whether they are published or not. The documents may come from teaching and research institutions in France or abroad, or from public or private research centers.

L'archive ouverte pluridisciplinaire **HAL**, est destinée au dépôt et à la diffusion de documents scientifiques de niveau recherche, publiés ou non, émanant des établissements d'enseignement et de recherche français ou étrangers, des laboratoires publics ou privés.

A calibrated optogenetic toolbox of stable zebrafish opsin lines

Antinucci P^{1*}, Dumitrescu AS^{2*}, Deleuze C², Morley HJ¹, Leung K¹, Hagley T¹, Kubo F^{3,4}, Baier H³
Bianco IH^{1*#}, Wyart C^{2*#}

* Equal contribution

Corresponding authors: C.W., claire.wyart@icm-institute.org, I.H.B., i.bianco@ucl.ac.uk

Affiliations

¹Department of Neuroscience, Physiology & Pharmacology, UCL, Gower Street, London, WC1E 6BT, UK.

²Institut du Cerveau et de la Moelle épinière (I.C.M.), Sorbonne Universités, UPMC Univ Paris 06, Inserm, CNRS, Hôpital Pitié-Salpêtrière, Paris, France.

³Department Genes – Circuits – Behavior, Max Planck Institute of Neurobiology, 82152 Martinsried, Germany.

⁴Center for Frontier Research, National Institute of Genetics, 1111 Yata, Mishima, 411-8540, Japan.

Keywords

Optogenetics, opsin, transgene, zebrafish, calibration, photocurrent, behaviour, electrophysiology, channel, pump, CoChR, ChR2(H134R), CheRiff, ChrimsonR, Chronos, eArch3.0, eNpHR3.0, GtACR1, GtACR2

Abstract

Optogenetic actuators with diverse spectral tuning, ion selectivity and kinetics are constantly being engineered providing powerful tools for controlling neural activity with subcellular resolution and millisecond precision. Achieving reliable and interpretable *in vivo* optogenetic manipulations requires reproducible actuator expression and calibration of photocurrents in target neurons. Here, we developed nine transgenic zebrafish lines for stable opsin expression and calibrated their efficacy *in vivo*. We first used high-throughput behavioural assays to compare opsin ability to elicit or silence neural activity. Next, we performed *in vivo* whole-cell electrophysiological recordings to quantify the amplitude and kinetics of photocurrents and test opsin ability to precisely control spiking. We observed substantial variation in efficacy, associated with differences in both opsin expression level and photocurrent characteristics, and identified conditions for optimal use of the most efficient opsins. Overall, our calibrated optogenetic toolkit will facilitate the design of controlled optogenetic circuit manipulations.

31 Introduction

32 Optogenetics has greatly advanced our ability to investigate how neural circuits process
33 information and generate behaviour by allowing manipulation of neural activity with high spatio-
34 temporal resolution in genetically-defined neurons (Miesenbock, 2009; Boyden, 2011; Miesenbock,
35 2011; Adamantidis *et al.*, 2015; Boyden, 2015; Deisseroth, 2015; Deisseroth and Hegemann, 2017).
36 The efficacy with which optogenetic actuators – such as microbial opsins – can control neuronal
37 spiking *in vivo* depends on biophysical properties, expression level and membrane trafficking of the
38 opsin, physiological properties of the target cell and the intensity profile of light delivered within
39 scattering tissue.

40 Accordingly, two primary experimental requirements should be met to enable controlled and
41 reproducible *in vivo* optogenetic circuit manipulations: (i) reproducible opsin expression levels
42 (across cells and animals), with stable expression systems offering higher reliability and
43 homogeneity than transient ones (Kikuta and Kawakami, 2009; Yizhar *et al.*, 2011; Sjulson *et al.*,
44 2016), and (ii) calibrated photocurrents and effects on spiking recorded in target neurons (Huber *et al.*,
45 2008; Mardinly *et al.*, 2018; Li *et al.*, 2019). While previous studies have compared the
46 physiological effects of opsin activation in single cells using standardised conditions [e.g. (Berndt *et al.*,
47 2011; Mattis *et al.*, 2011; Prigge *et al.*, 2012; Klapoetke *et al.*, 2014; Berndt *et al.*, 2016; Mardinly *et al.*,
48 2018)], these comparisons were primarily performed *in vitro* or *ex vivo* using transient expression
49 strategies.

50 In this study, we took advantage of the genetic accessibility and transparency of zebrafish
51 (Arrenberg *et al.*, 2009; Del Bene and Wyart, 2012; Arrenberg and Driever, 2013; Portugues *et al.*,
52 2013; Forster *et al.*, 2017) to generate nine stable transgenic lines for targeted opsin expression using
53 the GAL4/UAS binary expression system (Scheer and Campos-Ortega, 1999; Asakawa and
54 Kawakami, 2008) and quantitatively compare their efficacy for inducing or silencing neuronal
55 spiking. We selected opsins that were reported to induce photocurrents with large amplitude
56 [CoChR (Klapoetke *et al.*, 2014), CheRiff (Hochbaum *et al.*, 2014), ChR2_(H134R) (Gradinaru *et al.*, 2007),
57 eArch3.0 (Mattis *et al.*, 2011), GtACR1,2 (Govorunova *et al.*, 2015)] and/or fast kinetics [Chronos,
58 ChrimsonR (Klapoetke *et al.*, 2014), eNpHR3.0 (Gradinaru *et al.*, 2010)]. We first assessed the efficacy
59 of these stable lines to control activity in intact neural populations via high-throughput behavioural
60 assays at both embryonic and larval stages. Next, we made *in vivo* electrophysiological recordings
61 from single low input-resistance motor neurons to calibrate photocurrents and test the ability of
62 each line to elicit or silence spiking. We observed broad variation in behavioural response rates,
63 photocurrent amplitudes and spike induction, likely due to differences in both opsin properties and
64 expression levels. For the best opsin lines, we identified conditions that allowed control of
65 individual action potentials within high-frequency spike trains. Overall, our toolkit will enable
66 reliable and robust optogenetic interrogation of neural circuit function in zebrafish.

67 Results

68 Generation of stable transgenic lines for targeted opsin expression in zebrafish

69 To maximise the utility of our optogenetic toolkit, we used the GAL4/UAS binary expression
70 system for targeted opsin expression in specific cell populations (Figure 1). We generated nine
71 stable UAS lines for opsins having different ion selectivities and spectral tuning, fused to a
72 fluorescent protein reporter (tdTomato or eYFP; Figure 1A and Supplementary File 1) (Asakawa *et al.*,
73 *et al.*, 2008; Arrenberg *et al.*, 2009; Horstick *et al.*, 2015). GAL4 lines were used to drive expression in
74 defined neuronal populations, such as motor neurons (Figure 1B) (Scott *et al.*, 2007; Wyart *et al.*,
75 2009; Bohm *et al.*, 2016). High levels of expression were achieved in most cases (Figure 1C and
76 Figure 1-figure supplement 1), with only few opsins showing intracellular puncta suggestive of
77 incomplete trafficking to the plasma membrane (CheRiff and GtACR2) or low expression (Chronos).
78 To quantitatively compare opsin lines, we performed standardised behavioural tests at embryonic
79 and larval stages (Figure 1D) and calibrated photocurrents and modulation of spiking in larval
80 primary motor neurons (Figure 1E).

81 Escape behaviour triggered by optogenetic activation of embryonic trigeminal neurons

82 As a first test of our opsin lines, we evaluated their ability to activate embryonic neurons (Figure
83 2A-C), which are characterised by high input resistance (Drapeau *et al.*, 1999; Saint-Amant and
84 Drapeau, 2000). We used the *Tg(isl2b:GAL4)* transgene (Ben Fredj *et al.*, 2010) to drive expression of
85 opsins in the trigeminal ganglion (Figure 2B,C). In this class of somatosensory neuron, optogenetic
86 induction of few spikes has been shown to reliably elicits escape responses (Douglass *et al.*, 2008),
87 characterised by high-amplitude bends of the trunk and tail (Kimmel *et al.*, 1990; Saint-Amant and
88 Drapeau, 1998; Sagasti *et al.*, 2005). Brief pulses of light (5 or 40 ms) induced escape responses in
89 embryos (28–30 hours post fertilisation, hpf) expressing all cation- and anion-conducting
90 channelrhodopsins (Figure 2C-E and Video 1), while no movement was elicited in opsin-negative
91 siblings (Figure 2F,G and Figure 2-figure supplement 1,2; $N = 69 \pm 26$ fish per group, mean \pm SD).
92 The excitatory effect of GtACRs suggests that increasing chloride conductance depolarises neurons
93 at this developmental stage. For all opsins, response probability increased monotonically with light
94 power (Figure 2F,G). Escape behaviour could also be evoked via transient opsin expression, in
95 which animals were tested one day after injection of DNA constructs into single cell-stage
96 *Tg(isl2b:GAL4)* embryos (Figure 2F). Some opsins showed higher response probability in transient
97 transgenic animals (CheRiff, CoChR and GtACRs), likely due to higher expression levels.

98 With blue light, CoChR elicited escapes at the highest response probability (65–100% at 112–
99 $445 \mu\text{W}/\text{mm}^2$; Figure 2F,G) and response latency decreased with increasing irradiance (insets in
100 Figure 2F,G). As expected from its red-shifted absorption spectrum, ChrimsonR was the only cation
101 channelrhodopsin to evoke escapes using amber light ($\sim 70\%$ response probability at $322 \mu\text{W}/\text{mm}^2$;
102 Figure 2F,G) (Klapoetke *et al.*, 2014). Consistent with their respective red- and blue-shifted
103 absorption spectra, GtACR1 triggered escapes upon amber and blue light stimulation whereas
104 GtACR2 elicited responses only with blue light (Figure 2F,G) (Govorunova *et al.*, 2015).

105 Tail movements triggered by optogenetic activation of larval spinal motor neurons

106 Next, we compared the efficacy of cation channelrhodopsin lines to induce behaviour by activation
107 of larval motoneurons, from which we would later record photocurrents. We used the
108 *Tg(mnx1:GAL4)* transgene (Bohm *et al.*, 2016) to target expression to spinal motor neurons
109 (Figure 3A,B) and subjected head-restrained zebrafish (6 days post fertilisation, dpf; N = 28 ± 8 fish
110 per group, mean ± SD) to either single light pulses (2 or 10 ms) or pulse trains at 20 or 40 Hz (Figure
111 3C,D and Video 2,3) while monitoring tail movements.

112 Optogenetically-evoked tail movements were triggered with short latency following light onset
113 (8.3 ± 6.9 ms, mean ± SD) in opsin-expressing larvae only, whereas visually-evoked swim bouts
114 occurred at much longer latency (316 ± 141 ms, mean ± SD) in both opsin-expressing larvae and
115 control siblings (Figure 3E). We restricted our analyses to optogenetically-evoked movements,
116 initiated within 50 ms of stimulus onset (corresponding to a minimum of the probability density
117 distribution of latency; dotted line in Figure 3E). Optogenetically-evoked tail movements comprised
118 a sequence of left-right alternating half beats, thereby resembling natural swim bouts (Figure 3C,D
119 and Video 2,3). Response probability increased with irradiance (Figure 3F and Figure 3-figure
120 supplement 1) and CoChR again elicited tail movements with the highest probability and shortest
121 latency in response to blue light (96 - 100% at 0.63–2.55 mW/mm²; Figure 3F,G). Only the
122 ChrimsonR line responded to red light (~ 78% response probability at 1 mW/mm²; Figure 3F). Tail
123 movements evoked by single light pulses typically had shorter duration and fewer cycles than
124 visually-evoked swims (Figure 3H–K). However, longer movements (> 100 ms, 4–5 cycles) were
125 often observed in response to single light pulses (see response to 2 ms pulse in Figure 3D and
126 Video 2) indicating engagement of spinal central pattern generators. This may occur through
127 recruitment of glutamatergic V2a interneurons connected to motor neurons via gap junctions (Song
128 *et al.*, 2016) and/or by proprioceptive feedback via cerebrospinal fluid-contacting neurons (Wyart *et al.*,
129 2009; Fidelin *et al.*, 2015; Bohm *et al.*, 2016). Pulse train stimuli evoked swim bouts of longer
130 duration, with swims in CoChR and ChrimsonR lines showing modest frequency-dependent
131 modulation of cycle number (Figure 3L–Q).

132 *In vivo* whole-cell recording of photocurrents in larval primary motor neurons

133 To calibrate photocurrents *in vivo*, we performed whole-cell voltage clamp recordings from single
134 primary motor neurons (pMNs) in 5–6 dpf larvae (Figure 4A). Each opsin was stimulated with a
135 wavelength close to its absorption peak (1–30 mW/mm²; Figure 4-figure supplement 1A). We
136 recorded over 138 neurons, including control cells from opsin-negative animals, from which 90 cells
137 were selected following strict criteria for recording quality (see Material and methods; N = 3–19
138 included cells per group; Figure 4-figure supplement 1B). Opsin-expressing pMNs displayed
139 physiological properties, such as membrane resistance, resting membrane potential and cell
140 capacitance, comparable to control opsin-negative cells (Figure 4B,C and Figure 4-figure
141 supplement 1C,D). All cation channelrhodopsins induced inward currents upon light stimulation,
142 which were not observed in opsin-negative pMNs (Figure 4D). Notably, CoChR and ChrimsonR
143 generated the largest photocurrents (CoChR 475 ± 186 pA, mean ± SD, N = 8 cells, ChrimsonR

144 251 ± 73 pA, N = 7; Figure 4E), consistent with their higher expression level (Figure 1-figure
145 supplement 1D) and efficacy in behavioural assays (Figure 2,3). We did not observe significant
146 irradiance-dependent modulation of photocurrent amplitude in any opsin line, likely due to the
147 high range of irradiance we tested (Figure 4-figure supplement 1F). Photocurrent kinetics influence
148 the temporal precision with which single action potentials can be evoked (Mattis *et al.*, 2011).
149 Therefore, we measured the photocurrent activation time (i.e. time to peak response from light
150 onset), which results from the balance between activation and inactivation of the opsin, and
151 deactivation time constant, which is determined by the rate of channel closure at light offset (Mattis
152 *et al.*, 2011; Schneider *et al.*, 2015). Comparable activation times were observed across opsin lines (4-
153 5 ms; Figure 4F). Deactivation time constants were more variable between opsins, with Chronos
154 showing the fastest deactivation kinetics (4.3 ± 0.4 ms, N = 3 cells, mean ± SD) and the other opsins
155 displaying longer time constants (12-20 ms; Figure 4G).

156 **Optogenetic induction of spiking in larval pMNs**

157 To investigate whether our cation channelrhodopsin lines can induce action potentials in pMNs, we
158 performed *in vivo* current clamp recordings while providing single light pulses (0.1-5 ms duration).
159 In all opsin lines, light stimulation induced voltage depolarisations, which were never observed in
160 opsin-negative pMNs, and voltage responses above -30 mV were classified as spikes (Figure 5A).

161 CoChR and ChrimsonR were the only opsin lines capable of triggering spiking in this cell type
162 (Figure 5A and Figure 5-figure supplement 1A-C), as expected from their peak photocurrents
163 exceeding pMN rheobase (dotted lines in Figure 4E). Notably, 5 ms light pulses induced spikes in
164 all CoChR-expressing neurons (N = 11 out of 11 cells at 3-30 mW/mm²), 92% of cells spiked with 1-
165 2 ms pulses and only 50% spiked in response to 0.5 ms pulses (Figure 5-figure supplement 1A).
166 ChrimsonR was less effective than CoChR in inducing action potentials, with 36-38% of neurons
167 spiking when using 2-5 ms pulses (2 ms, N = 4 out of 11; 5 ms, N = 3 out of 8 cells) and only 1 cell
168 out of 8 spiking in response to 1 ms pulses. In both lines, the number of evoked spikes increased
169 with longer pulse duration (Figure 5B and Figure 5-figure supplement 1D).

170 For experiments aiming to replay physiological firing patterns, optogenetic actuators should be
171 capable of inducing spike trains with millisecond precision and at biological firing frequencies. We
172 thus tested the ability of CoChR and ChrimsonR to evoke pMN firing patterns across a range of
173 frequencies (1-100 Hz; Figure 5C). pMNs can spike at high frequency (up to 300-500 Hz, (Menelaou
174 and McLean, 2012), hence optogenetic induction of high-frequency firing should not be limited by
175 cell intrinsic physiological properties, but rather by opsin properties and light stimulation
176 parameters. To assess the fidelity of firing patterns at each stimulation frequency, we measured
177 spike number per light pulse as well as spike latency and jitter (i.e. standard deviation of spike
178 latency). ChrimsonR could induce firing up to the highest frequency tested (100 Hz), with each light
179 pulse typically evoking a single spike (Figure 5C,D). CoChR generated bursts of spikes in response
180 to light pulses, even at the shortest stimulation duration and spiking consistently attenuated in the
181 second half of the stimulation train (Figure 5E,F). Overall, spikes were induced with short latency

182 (3–4 ms mean latency) and low jitter (0.25 – 1.25 ms jitter) with both opsin lines (Figure 5G,H and
183 Figure 5–figure supplement 1E).

184 **Optogenetic suppression of coiling behaviour in embryos**

185 Next, we tested the ability of our opsin lines to suppress spontaneous behaviour of zebrafish
186 embryos (Saint-Amant and Drapeau, 1998; Warp *et al.*, 2012; Mohamed *et al.*, 2017; Bernal Sierra *et al.*
187 *et al.*, 2018). We targeted expression of the anion-conducting channels GtACR1 and GtACR2
188 (Govorunova *et al.*, 2015), the outward proton pump eArch3.0 (Mattis *et al.*, 2011) and the inward
189 chloride pump eNpHR3.0 (Gradinaru *et al.*, 2010) to spinal cord neurons using the *Tg(s1020t:GAL4)*
190 transgene (Scott *et al.*, 2007) and examined changes in spontaneous coiling behaviour in response to
191 light (Figure 6A–D and Video 4). Embryos were tested between 24 and 27 hpf, a stage at which
192 embryos coil spontaneously (Saint-Amant and Drapeau, 1998) but show only minimal light-induced
193 photomotor responses, which mostly occur later in development (30–40 hpf) (Kokel *et al.*, 2013). In
194 opsin-expressing embryos, light exposure led to a suppression of coiling behaviour that was
195 followed by a synchronised restart at light offset (Figure 6D,E and Figure 6–figure supplement 1;
196 $N = 91 \pm 16$ fish per group, mean \pm SD), as previously reported (Warp *et al.*, 2012; Mohamed *et al.*,
197 2017). As expected from behaviour with *Tg(isl2b:GAL4)* embryos (Figure 2F,G), GtACR activation in
198 spinal neurons occasionally induced movements in the initial 1–2 s following light onset (black
199 arrows in Figure 6D,E), a phenomenon that was not observed with Cl^-/H^+ pumps. Given these two
200 effects, changes in coil rate were separately quantified for the initial 2 s (Figure 6–figure supplement
201 2) and subsequent 8 s period of light exposure ('late LED ON'; grey horizontal bars in Figure 6E).

202 All opsin lines suppressed coiling behaviour during the 'late LED ON' period (Figure 6F,G). As
203 previously observed (Friedmann *et al.*, 2015), light also decreased coiling in control opsin-negative
204 embryos, yet to a significantly lesser degree than in opsin-expressing animals (Figure 6F,G).
205 Optogenetically evoked suppression was likely a result of distinct mechanisms in the different
206 transgenic lines. While Cl^-/H^+ pumps systematically induce hyperpolarisation, anion
207 channelrhodopsins can silence cells via shunting as well as depolarisation block depending upon
208 the reversal potential of chloride *in vivo* (see below and Discussion). GtACRs achieved the strongest
209 suppression of coil rate using blue light (90–95% decrease at 8.4–225 $\mu\text{W}/\text{mm}^2$; Figure 6F). With
210 amber light, GtACR1, eArch3.0 and eNpHR3.0 showed comparable suppression (80–90% decrease
211 at 50.5–227 $\mu\text{W}/\text{mm}^2$), with GtACR1 achieving \sim 83% decrease in coil rate even at low irradiance
212 (15.9 $\mu\text{W}/\text{mm}^2$; Figure 6G).

213 **Optogenetic suppression of swimming in larvae**

214 To compare the efficacy of our opsin lines to suppress behaviour in larvae, we targeted opsin
215 expression to spinal motor neurons and interneurons using *Tg(s1020t:GAL4)*, as above, and
216 examined changes in spontaneous swimming behaviour of 6 dpf animals in response to 10 s light
217 pulses (Figure 7A–C and Video 5; $N = 25 \pm 9$ fish per group, mean \pm SD).

218 Expression of GtACR1, GtACR2 and eArch3.0 in motor neurons and interneurons reduced swim
219 bout rate relative to control larvae in response to blue light, with GtACRs achieving the greatest

220 suppression (20–45% decrease; Figure 7D,E) (Sternberg *et al.*, 2016). Consistent with a previous
221 report (Andalman *et al.*, 2019), opsin-negative larvae showed a 20–30% increase in bout rate during
222 illumination with blue light (Figure 7E and Figure 7–supplement 1), while no increase was observed
223 with red light (Figure 7F). Using red light, only eNpHR3.0 could reduce bout rate and suppression
224 increased with higher irradiance (45% decrease at 1 mW/mm²; Figure 7F). No increase in bout rate
225 was found in larvae expressing anion channelrhodopsins even when analysis was restricted to the
226 initial 2 s of the light period (Figure 7–figure supplement 2A), suggesting GtACRs do not induce
227 excitatory effects at larval stages. Opsin activation did not affect bout speed (Figure 7–figure
228 supplement 2B). By contrast, using the *Tg(mnx1:GAL4)* transgene to selectively drive expression
229 only in motor neurons resulted in a decrease in bout speed (~20% reduction), but not bout rate
230 (Figure 7–figure supplement 3,4).

231 Photocurrents induced by anion channelrhodopsins and chloride/proton pumps

232 To analyse the physiological effects induced by anion channelrhodopsins and Cl⁻/H⁺ pumps, we
233 measured their photocurrents through *in vivo* voltage clamp recordings from larval pMNs (5–6 dpf).
234 Since anion channelrhodopsin function depends on chloride homeostasis (Figure 8A) (Govorunova
235 *et al.*, 2015) and chloride reversal potential (ECl) is known to change over development (Ben-Ari,
236 2002; Reynolds *et al.*, 2008; Zhang *et al.*, 2010), we recorded GtACR1 photocurrents using two
237 intracellular solutions: one mimicking ECl in embryonic neurons (-50 mV) (Saint-Amant and
238 Drapeau, 2003) and the second approximating intracellular chloride concentration in more mature,
239 larval neurons (ECl = -70 mV, see Materials and methods). Inspection of I-V curves for GtACR1
240 photocurrents showed that, in both solutions, currents reversed with a positive 5–10 mV shift
241 relative to ECl (Figure 8–supplement 1A,B), as previously observed (Govorunova *et al.*, 2015) and
242 within the expected error margin given our access resistance (Figure 4–figure supplement 1C;
243 estimated voltage error for ECl_{-50 mV} solution, 4.6 ± 6.4 mV, mean ± SD, N = 5 cells; ECl_{-70 mV} solution,
244 1.2 ± 1.3 mV, N = 3). This suggests that GtACR1 photocurrents were primarily driven by chloride
245 ions, as expected (Govorunova *et al.*, 2015). The other opsin lines were tested using the ECl_{-50 mV}
246 solution only. Neurons were stimulated with light (1 s pulse) at a holding potential matching their
247 measured resting membrane potential (Figure 4C).

248 Anion channelrhodopsins induced inward, `depolarising` photocurrents (as expected from the
249 combination of ECl and holding potential), while Cl⁻/H⁺ pumps generated outward,
250 `hyperpolarising` currents (Figure 8B). All opsins except eNpHR3.0 showed bi-phasic photocurrent
251 responses comprising a fast activation followed by a slow inactivation (Figure 8B), likely due to a
252 fraction of the opsin population transitioning to an inactive state (Chow *et al.*, 2010; Mattis *et al.*,
253 2011; Schneider *et al.*, 2015). We measured both the peak photocurrent (Figure 8C) as well as the
254 steady-state current during the last 5 ms of the light period (Figure 8D). GtACRs induced
255 photocurrents with peak amplitude 3–10 times larger than those generated by Cl⁻/H⁺ pumps
256 (Figure 8C), while steady-state currents were similar across opsins (Figure 8D). Some degree of
257 irradiance-dependent modulation of photocurrents was observed, primarily in peak amplitude
258 (Figure 8–supplement 1C–E). To characterise photocurrent kinetics, we computed activation,

259 inactivation and deactivation time constants (Mattis *et al.*, 2011). GtACR photocurrents had the
260 fastest activation kinetics (~ 1 ms at 30 mW/mm²; Figure 8E and Figure 8-figure supplement 1F).
261 However, deactivation kinetics of Cl⁻/H⁺ pumps were 2–10 times faster than those induced by
262 GtACRs (14–22 ms eNpHR3.0, 27–37 ms eArch3.0; Figure 8G and Figure 8-figure supplement 1H)
263 and showed little inactivation (600–1000 ms eArch3.0; Figure 8F and Figure 8-figure supplement
264 1G).

265 **Optogenetic inhibition of pMN spiking**

266 To investigate the ability of anion channelrhodopsins and Cl⁻/H⁺ pumps to suppress neural
267 activity, we recorded pMNs in current clamp mode. In control opsin-negative neurons, light
268 delivery (1 s) induced negligible voltage deflections (Figure 9A). By contrast, anion
269 channelrhodopsins generated membrane depolarisation towards ECl while the Cl⁻/H⁺ pumps
270 hyperpolarised the cell (Figure 9A), in accordance with recorded photocurrents. The absolute peak
271 amplitude of voltage deflections was comparable between opsin lines (10–25 mV), with 10–40%
272 decrease between peak and steady-state responses in all cases except eNpHR3.0, which generated
273 stable hyperpolarisation (Figure 9B,C and Figure 9-figure supplement 1A,B). In a subset of
274 GtACR1- (N = 4 out of 7) and GtACR2-expressing neurons (N = 2 out of 6), spiking was induced at
275 light onset when using the ECL_{50 mV} solution (Figure 9A; GtACR1 6.7 ± 7.1 spikes; GtACR2 1.5 ± 0.7 ,
276 mean \pm SD). This is consistent with the movements evoked at light onset in young, 1 dpf embryos
277 expressing GtACRs (Figure 2 and 6). The kinetics of voltage decay to baseline following light offset
278 matched those of recorded photocurrents (Figure 9D and Figure 9-figure supplement 1C).

279 Next, we compared the utility of our opsin lines to inhibit pMN firing. First, we induced larval
280 pMNs to fire at 5 Hz by injecting pulses of depolarising current (5 ms, 1.2–1.5 \times rheobase) and
281 simultaneously delivered 5 ms light pulses to inhibit selected spikes (Figure 9E). We found that
282 GtACRs and eNpHR3.0 could effectively inhibit spikes (80–95% suppression), while light pulses did
283 not alter firing in opsin-negative neurons (Figure 9F). In agreement with our current clamp
284 recordings, a subset of GtACR1-expressing neurons (N = 4 out of 7) tested in the embryonic ECL
285 _{50 mV} solution failed to suppress spikes and instead induced extra action potentials in response to
286 light pulses, resulting in a negative spike inhibition efficacy (Figure 9F). Data from eArch3.0-
287 expressing neurons could not be collected due to degradation in the quality of recordings or cells
288 becoming highly depolarised (i.e. resting membrane potential > -50 mV) by the later stages of the
289 protocol, suggesting that repeated eArch3.0 activation may alter electrical properties of neurons
290 (Williams *et al.*, 2019).

291 Lastly, we asked whether we could inhibit firing over periods of tens to hundreds of milliseconds.
292 We injected long pulses of depolarising current (200–800 ms) to elicit tonic pMN firing, and
293 simultaneously provided shorter light pulses (50–200 ms; 3–10 mW/mm²) in the middle of the spike
294 train (Figure 9G). Both GtACR1 and eNpHR3.0 successfully inhibited spiking during the light
295 pulse, with complete suppression in 60–100% of cells at 10 mW/mm² irradiance (Figure 9G,H).
296 Notably, GtACR1 could inhibit tonic spiking even when using the embryonic ECL_{50 mV} solution

297 (Figure 9G,H), consistent with the suppression of coiling behaviour upon prolonged illumination of
298 GtACR-expressing embryos (Figure 6).

299 Discussion

300 In this study, we generated a set of stable transgenic lines for GAL4/UAS-mediated opsin
301 expression in zebrafish and evaluated their efficacy in controlling neural activity *in vivo*. High-
302 throughput behavioural assays and whole-cell electrophysiological recordings provided
303 complementary insights to guide tool selection (Figure 10). Behavioural assays enabled efficient
304 evaluation of opsin lines in various sensory and motor cell types and revealed developmental stage-
305 specific effects in intact neural populations. Electrophysiological recordings from single motor
306 neurons afforded quantification of photocurrents and systematic evaluation of the ability of these
307 optogenetic tools to elicit or silence activity at single action potential resolution.

308 An *in vivo* platform for opsin tool selection

309 The selection of optogenetic actuators should be based on their ability to reliably control neural
310 activity *in vivo*. While previous efforts compared opsin efficacy using transient expression strategies
311 [e.g. through viral or plasmid-mediated opsin gene delivery, see Mattis *et al.* (2011) and
312 Introduction], here we calibrated opsin effects in stable transgenic lines, which offer more
313 reproducible expression across experiments and laboratories (Kikuta and Kawakami, 2009; Yizhar *et al.*,
314 2011). Overall, there was good qualitative agreement between behavioural and
315 electrophysiological results, with efficacy in behavioural assays (even with transient expression)
316 largely predicting rank order in photocurrent amplitudes. This illustrates the utility of high-
317 throughput behavioural assays for rapid evaluation and selection of expression constructs prior to
318 more time-consuming generation and characterisation of stable lines and electrophysiological
319 calibration. We observed broad variation in efficacy across lines, likely attributable to differences in
320 both the intrinsic properties of the opsin as well as variation in expression and membrane targeting.
321 Membrane trafficking can also be influenced by the fluorescent protein fused to the actuator
322 (Arrenberg *et al.*, 2009). In our hands, we observed better expression with the tdTomato fusion
323 reported here than with previous attempts using a tagRFP fusion protein. In the future, expression
324 might be further improved through codon optimisation (Horstick *et al.*, 2015), trafficking-enhancing
325 sequences (Gradinaru *et al.*, 2010; Mattis *et al.*, 2011), alternative expression targeting systems (Luo *et al.*,
326 2008; Sjulson *et al.*, 2016) and optimisation of the fluorescent reporter protein.

327 Behavioural and electrophysiological readouts complemented one another and enriched the
328 interpretation of our results. Electrophysiological recordings in a defined cell type allowed direct
329 and comparative calibration of photocurrents. Although several opsin lines did not evoke action
330 potentials in low-input-resistance pMNs, behavioural assays showed that all lines induced tail
331 movements in larvae. This is likely due to recruitment of secondary motor neurons labelled by the
332 *Tg(mnx1:GAL4)* transgene, which have higher input resistance (Menelaou and McLean, 2012).
333 Behavioural assays at multiple ages revealed that anion channelrhodopsins can excite neurons in
334 1 dpf embryos which was corroborated by making whole-cell recordings using a patch solution

335 reproducing the high intracellular chloride concentration observed in embryonic neurons (Reynolds
336 *et al.*, 2008; Zhang *et al.*, 2010).

337 Overall, our platform enables efficient selection and calibration of optogenetic tools for *in vivo*
338 neuroscience. It also enables opsin-specific optimisation of light delivery (i.e. wavelength, pulse
339 duration, frequency and intensity). For example, we found that equivalent stimulation regimes
340 produced different rates of spiking adaptation that impacted the ability to control high-frequency
341 firing, depending on the specific opsin line in question.

342 **Robust and precise optogenetic induction of spiking**

343 Which opsin lines are best suited for reliable neural activation? Photocurrent amplitude, measured
344 in pMNs, was proportional to estimated opsin expression level (Figure 1-figure supplement 1D)
345 and was predictive of the ability of opsin lines to induce behaviour via activation of distinct cell
346 types at both larval and embryonic stages (CoChR > ChrimsonR > ChR2_(HI134R) > Chronos ≥ CheRiff).
347 The CoChR and ChrimsonR lines showed the highest expression levels among cation
348 channelrhodopsins and were the only lines capable of inducing action potentials in pMNs,
349 consistent with their photocurrent amplitudes exceeding pMN rheobase. Notably, CoChR evoked
350 spikes in all pMNs tested and triggered behaviour with maximal response probability in larvae at
351 irradiance levels as low as 0.63 mW/mm².

352 Where precise control of a cell's firing pattern is desired, electrophysiological calibration is essential
353 to tune stimulation parameters for a specific opsin/cell-type combination. Our data indicate that in
354 primary motor neurons, light pulses can lead to bursts of spikes and substantial firing rate
355 adaptation during high-frequency stimulation, likely a result of plateau potentials and inactivation
356 of voltage-gated sodium channels. Thus, although the CoChR line produced large-amplitude
357 photocurrents and was highly efficient and precise in evoking the first spike, in this particular cell
358 type it was also prone to burst firing even for short (0.5 ms) light pulses, which compromised
359 spiking entrainment with high-frequency stimulations. However, CoChR has been used to elicit
360 single spikes in mouse pyramidal cells with 1 ms light pulses at frequencies up to 50 Hz (Ronzi *et al.*
361 *et al.*, 2017). A thorough calibration in the cell type of interest *in vivo* is therefore necessary for precise
362 control of spike number and timing. Compared to CoChR, we observed that ChrimsonR, although
363 less efficient at firing primary motor neurons overall, led to less spike adaptation during
364 stimulation and fewer bursts of spikes.

365 **Excitatory effects of anion channelrhodopsins**

366 Anion channelrhodopsins induced movements at light onset in 1 dpf embryos as well as transient
367 spiking in pMNs when using an intracellular solution that mimicked the high ECl⁻ (-50 mV) of
368 immature neurons. This is consistent with GtACRs functioning as a light-gated chloride
369 conductance (Govorunova *et al.*, 2015). The transient nature of spiking and motor activity might be
370 due to the initial large inward photocurrent depolarising neurons above spiking threshold.
371 Transient induction of action potentials with GtACRs has also been observed in rat cortical
372 pyramidal neurons in brain slices (Malyshev *et al.*, 2017) as well as cultured hippocampal neurons

373 (Mahn *et al.*, 2018) and has been attributed to antidromic spiking resulting from a positively shifted
374 ECl in the axon (Mahn *et al.*, 2016; Mahn *et al.*, 2018). In light of this, the use of GtACRs in immature
375 neurons or subcellular structures should be carefully calibrated and use of Cl⁻/H⁺ pumps may be
376 preferable. The likely mechanism of silencing induced by activation of GtACRs is shunting as the
377 large photocurrents are associated with a reduction in the input resistance of the cell. In addition,
378 GtACRs bring the membrane potential close to ECl, which may – depending on the physiological
379 values of ECl *in vivo* – also lead to depolarisation block.

380 **Precise optogenetic inhibition of neural activity**

381 To accurately suppress action potentials, opsin tools must be carefully selected with consideration
382 for developmental stage and ECl-dependent effects as well as photocurrent kinetics. GtACRs
383 generated large photocurrents with fast activation kinetics, which can explain why GtACR1 was
384 effective in inhibiting single action potentials with short light pulses in larval pMNs. Cl⁻/H⁺ pump
385 photocurrents instead showed fast deactivation kinetics, which allowed eNpHR3.0-expressing
386 neurons to rapidly resume spiking at light offset. Differences in photocurrent kinetics between
387 opsin classes – i.e. channels vs. pumps – may thus differentially affect the temporal resolution of
388 activity inhibition and recovery, respectively. The combined behavioural and electrophysiological
389 approach can be extended in the future to optogenetic silencers based on K⁺ channel activation,
390 such as the recently introduced PAC-K (Bernal Sierra *et al.*, 2018).

391 In conclusion, our calibrated optogenetic toolkit and associated methodology provide an *in vivo*
392 platform for designing controlled optogenetic experiments and benchmarking novel opsins.

393 **Acknowledgements**

394 The authors thank members of the Bianco lab and Wyart lab for helpful discussions. We thank staff
395 from the UCL and ICM PHENO fish facilities for fish care and husbandry (UCL: Carole Wilson and
396 team; ICM: Sophie Nunes-Figueiredo, Bogdan Buzurin, Monica Dicu and Antoine Arneau). Irene
397 Arnold-Ammer and Enrico Kühn (MPI of Neurobiology) assisted with generation of transgenic
398 lines. We also acknowledge support from the ICM electrophysiology core facility (CELIS-ePhys)
399 and Mingyue Wu for electrophysiology experimental assistance. P.A. was supported by a Sir Henry
400 Wellcome Postdoctoral Fellowship (204708/Z/16/Z). A.D. was supported by a Marie Curie
401 Incoming International Fellowship (H2020-MSCA-IF-2016 Project #752199). F.K. was supported by
402 a HFSP long-term fellowship (LT393/2010). Generation of opsins in H. B.'s laboratory was
403 supported by the Max Planck Society (H. B. and F. K.) and the DFG (SPP1926 Next-Generation
404 Optogenetics). A Sir Henry Dale Fellowship from the Royal Society & Wellcome Trust
405 (101195/Z/13/Z) and a UCL Excellence Fellowship were awarded to I.H.B. C.W. was funded by
406 Human Frontier Science Program (HFSP) Research Grant (RGP063-2018) and the New York Stem
407 Cell Foundation (NYSCF-R-NI39). The work on electrophysiological calibration of opsins
408 performed in ICM has also received funding from the ICM foundation, the program
409 `Investissements d'avenir` ANR-10-IAIHU-06 (Big Brain Theory ICM Program), ANR-11-INBS-0011
410 (NeurATRIS: Translational Research Infrastructure for Biotherapies in Neurosciences).

411 **Competing Interests**

412 The authors declare no competing interests.

Key Resources Table				
Reagent type (species) or resource	Designation	Source or reference	Identifiers	Additional information
Genetic reagent (<i>Danio rerio</i>)	<i>Tg(UAS:ChrimsonR-tdTomato)u328Tg</i>	This study	ZFIN ID: ZDB-ALT-190226-2	Available from EZRC
Genetic reagent (<i>Danio rerio</i>)	<i>Tg(UAS:Chronos-tdTomato)u330Tg</i>	This study	ZFIN ID: ZDB-ALT-190226-3	Available from EZRC
Genetic reagent (<i>Danio rerio</i>)	<i>Tg(UAS:CoChR-tdTomato)u332Tg</i>	This study	ZFIN ID: ZDB-ALT-190226-4	Available from EZRC
Genetic reagent (<i>Danio rerio</i>)	<i>Tg(UAS:CheRiff-tdTomato)u334Tg</i>	This study	ZFIN ID: ZDB-ALT-190226-5	Available from EZRC
Genetic reagent (<i>Danio rerio</i>)	<i>Tg(UAS:GtACR1-tdTomato)u336Tg</i>	This study	ZFIN ID: ZDB-ALT-190226-6	Available from EZRC
Genetic reagent (<i>Danio rerio</i>)	<i>Tg(UAS:GtACR2-tdTomato)u338Tg</i>	This study	ZFIN ID: ZDB-ALT-190226-7	Available from EZRC
Genetic reagent (<i>Danio rerio</i>)	<i>Tg(UAS:eArch3.0-eYFP)mpn120</i>	This study	transgene	Available from Baier lab
Genetic reagent (<i>Danio rerio</i>)	<i>Tg(UAS:eNpHR3.0-eYFP)mpn121</i>	This study	transgene	Available from Baier Lab

Genetic reagent (<i>Danio rerio</i>)	<i>Tg(UAS:Cr.ChR2-YFP)icm11Tg</i>	PMID: 26752076	ZFIN ID: ZDB-ALT- 150324-2	Available from EZRC (Fidelin <i>et al.</i> , 2015)
Genetic reagent (<i>Danio rerio</i>)	<i>Tg(UAS:GFP)zf82</i>	PMID: 19835787	ZFIN ID: ZDB-ALT- 080528-1	Asakawa <i>et al.</i> , 2008
Genetic reagent (<i>Danio rerio</i>)	<i>Tg(isl2b.2:GAL4-VP16, myl7:EGFP)zc60Tg</i>	PMID: 20702722	ZFIN ID: ZDB-ALT- 101130-1	Ben Fredj <i>et al.</i> , 2010
Genetic reagent (<i>Danio rerio</i>)	<i>Tg(isl2b:GAL4-VP16, myl7:TagRFP)zc65</i>	PMID: 21905164	ZFIN ID: ZDB-FISH- 150901- 13523	Fujimoto <i>et al.</i> , 2011
Genetic reagent (<i>Danio rerio</i>)	<i>Et(-0.6hsp70l:GAL4-VP16)s1020tEt</i>	PMID: 17369834	ZFIN ID: ZDB-ALT- 070420-21	Scott <i>et al.</i> , 2007
Genetic reagent (<i>Danio rerio</i>)	<i>Tg(mnx1:GAL4)icm23Tg</i>	PMID: 26946992	ZFIN ID: ZDB-ALT- 160120-1	Böhm <i>et al.</i> , 2016
Genetic reagent (<i>Danio rerio</i>)	<i>Et(-109Xla.Eef1a1:GFP)mn2Et</i>	PMID: 15347431	ZFIN ID: ZDB-ALT- 080625-1	Balciunas <i>et al.</i> , 2004
Recombinant DNA reagent	<i>pTol1-UAS:ChrimsonR-tdTomato</i>	This study	Addgene ID: 124231	Available from Addgene
Recombinant DNA reagent	<i>pTol1-UAS:Chronos-tdTomato</i>	This study	Addgene ID: 124232	Available from Addgene
Recombinant DNA reagent	<i>pTol1-UAS:CoChR-tdTomato</i>	This study	Addgene ID: 124233	Available from Addgene
Recombinant DNA reagent	<i>pTol1-UAS:CheRiff-tdTomato</i>	This study	Addgene ID: 124234	Available from Addgene

Recombinant DNA reagent	<i>pTol1-UAS:GtACR1-tdTomato</i>	This study	Addgene ID: 124235	Available from Addgene
Recombinant DNA reagent	<i>pTol1-UAS:GtACR2-tdTomato</i>	This study	Addgene ID: 124236	Available from Addgene
Recombinant DNA reagent	<i>pTol1-UAS:ChR2(H134R)-tdTomato</i>	This study	Addgene ID: 124237	Available from Addgene
Recombinant DNA reagent	<i>pTol2-UAS:eArch3.0-eYFP</i>	This study	plasmid	Available from Baier lab
Recombinant DNA reagent	<i>pTol2-UAS:eNpHR3.0-eYFP</i>	This study	plasmid	Available from Baier lab
Software, algorithm	MATLAB	MathWorks	RRID: SCR_001622	https://uk.mathworks.com/products/matlab.html
Software, algorithm	Python	Anaconda	RRID: SCR_008394	https://www.anaconda.com
Software, algorithm	LabView	National Instruments	RRID: SCR_014325	http://www.ni.com/en-gb/shop/labview.html
Software, algorithm	Prism	GraphPad	RRID: SCR_002798	https://www.graphpad.com/scientific-software/prism/

414 **Experimental model**

415 Animals were reared on a 14/10 h light/dark cycle at 28.5°C. For all experiments, we used zebrafish
416 (*Danio rerio*) embryos and larvae homozygous for the *mitfa*^{w2} skin-pigmentation mutation (Lister *et*
417 *al.*, 1999). All larvae used for behavioural assays were fed *Paramecia* from 4 dpf onward. Animal
418 handling and experimental procedures were approved by the UCL Animal Welfare Ethical Review
419 Body and the UK Home Office under the Animal (Scientific Procedures) Act 1986.

420 *In vivo* electrophysiological recordings were performed in 5–6 dpf zebrafish larvae from AB and
421 Tüpfel long fin (TL) strains in accordance with the European Communities Council Directive
422 (2010/63/EU) and French law (87/848) and approved by the Institut du Cerveau et de la Moelle
423 épinière, the French ministry of Research and the Darwin Ethics Committee (APAFIS protocol
424 #16469-2018071217081175v5).

425 Cloning and transgenesis

426 To generate the *UAS:opsin-tdTomato* DNA constructs used for transient opsin expression and for
427 creating the stable *Tg(UAS:opsin-tdTomato)* transgenic lines, the coding sequences of the opsins
428 listed below and the red fluorescent protein tdTomato (from *pAAV-Syn-Chronos-tdTomato*) were
429 cloned in frame into a UAS Tol1 backbone (*pT1UciMP*).

430 The source plasmids used for cloning *UAS:opsin-tdTomato* DNA constructs were:

- 431 • ChrimsonR from *pCAG-ChrimsonR-tdT* (Addgene plasmid # 59169)
- 432 • Chronos from *pAAV-Syn-Chronos-tdTomato* (Addgene plasmid # 62726)
- 433 • CoChR from *pAAV-Syn-CoChR-GFP* (Addgene plasmid # 59070)
- 434 • CheRiff from *FCK-CheRiff-eGFP* (Addgene plasmid # 51693)
- 435 • GtACR1 from *pFUGW-hGtACR1-EYFP* (Addgene plasmid # 67795)
- 436 • GtACR2 from *pFUGW-hGtACR2-EYFP* (Addgene plasmid # 67877)
- 437 • ChR2_(H134R) from *pAAV-Syn-ChR2(H134R)-GFP* (Addgene plasmid # 58880)

438 The *pCAG-ChrimsonR-tdT*, *pAAV-Syn-Chronos-tdTomato*, *pAAV-Syn-CoChR-GFP* and *pAAV-Syn-*
439 *ChR2(H134R)-GFP* plasmids were gifts from Edward Boyden (Boyden *et al.*, 2005; Klapoetke *et al.*,
440 2014). The *FCK-CheRiff-eGFP* plasmid was a gift from Adam Cohen (Hochbaum *et al.*, 2014). The
441 *pFUGW-hGtACR1-EYFP* and *pFUGW-hGtACR2-EYFP* plasmids were gifts from John Spudich
442 (Govorunova *et al.*, 2015). The *pT1UciMP* plasmid was a gift from Harold Burgess (Addgene
443 plasmid # 62215) (Horstick *et al.*, 2015).

444 The cloning was achieved using the In-Fusion HD Cloning Plus CE kit (Clontech) with the
445 following primers:

- 446 • ChrimsonR_fw, CTCAGCGTAAAGCCACCATGGGCGGAGCT
- 447 • Chronos_fw, CGTAAAGCCACCATGGAAACAGCC
- 448 • CoChR_fw, CTCAGCGTAAAGCCACCATGCTGGGAAACG
- 449 • CoChR_rev, TACTACCGGTGCCGCCACTGT
- 450 • CoChR_tdT_fw, ACAGTGGCGGCACCGGTAGTA
- 451 • CheRiff_fw, CTCAGCGTAAAGCCACCATGGGCGGAGCT
- 452 • CheRiff_rev, CTACCGGTGCCGCCACTTTATCTTCTCCTCTGTCACG
- 453 • CheRiff_tdT_fw, TAAAGTGGCGGCACCGGTAGTAGCAGTGAG
- 454 • GtACR1_fw, CTCAGCGTAAAGCCACCATGAGCAGCATCACCTGTGATC
- 455 • GtACR1_rev, CTACCGGTGCCCGCGGTCTCGCCGGCTCTGG
- 456 • GtACR1_tdT_fw, CGAGACCGCGGCACCGGTAGTAGCAGTGAG
- 457 • GtACR2_fw, CTCAGCGTAAAGCCACCATGGCCTCCCAGGTTCGT
- 458 • GtACR2_rev, CTACCGGTGCCGCCCTGCCGAACATTCTG
- 459 • GtACR2_tdT_fw, CGGCAGGGCGGCACCGGTAGTAGCAGTGAG
- 460 • ChR2(H134R)_fw, CTCAGCGTAAAGCCACCATGGACTATGGCGGCG
- 461 • ChR2(H134R)_rev, TACTCACTGCTACTACCGGTGCCGCCAC
- 462 • ChR2(H134R)_tdT_fw, ACCGGTAGTAGCAGTGAGTAAGG
- 463 • tdT_rev_40bp, CTCGAGATCTCCATGTTTACTTATAACAGCTCATCCATGCC
- 464 • tdT_rev_45bp, CTAGTCTCGAGATCTCCATGTTTACTTATAACAGCTCATCCATGCC

465 To generate the stable *Tg(UAS:opsin-tdTomato)* lines, purified *UAS:opsin-tdTomato* DNA constructs
466 were first sequenced to confirm gene insertion and integrity and, subsequently, co-injected
467 (35 ng/μl) with *Tol1* transposase mRNA (80 ng/μl) into *Tg(KalTA4u508)* zebrafish embryos
468 (Antinucci *et al.*, 2019) at the early one-cell stage. Transient expression, visible as tdTomato
469 fluorescence, was used to select injected embryos that were then raised to adulthood. Zebrafish
470 codon-optimised *Tol1* transposase mRNA was prepared by *in vitro* transcription from NotI-
471 linearised *pCS2-Tol1.zf1* plasmid using the SP6 transcription mMessage mMachine kit (Life
472 Technologies). The *pCS2-Tol1.zf1* was a gift from Harold Burgess (Addgene plasmid # 61388)
473 (Horstick *et al.*, 2015). RNA was purified using the RNeasy MinElute Cleanup kit (Qiagen). Germ
474 line transmission was identified by mating sexually mature adult fish to *mitfa^{w2/w2}* fish and
475 subsequently examining their progeny for tdTomato fluorescence. Positive embryos from a single
476 fish were then raised to adulthood. Once this second generation of fish reached adulthood, positive
477 embryos from a single `founder` fish were again selected and raised to adulthood to establish stable
478 *Tg(KalTA4u508;UAS:opsin-tdTomato)* double-transgenic lines.

479 To generate the *UAS:opsin-eYFP* DNA constructs used for creating the stable *Tg(UAS:opsin-eYFP)*
480 transgenic lines, the coding sequences of the opsins fused with eYFP listed below were cloned into a
481 *UAS Tol2* backbone (*pTol2 14xUAS:MCS*).

- 482 • *eArch3.0-eYFP* from *pAAV-CaMKIIa-eArch_3.0-EYFP* (Addgene plasmid # 35516)
- 483 • *eNpHR3.0-eYFP* from *pAAV-Ef1a-DIO-eNpHR 3.0-EYFP* (Addgene plasmid # 26966)

484 The *pAAV-CaMKIIa-eArch_3.0-EYFP* and *pAAV-Ef1a-DIO-eNpHR 3.0-EYFP* plasmids were gifts from
485 Karl Deisseroth (Gradinaru *et al.*, 2010; Mattis *et al.*, 2011).

486 The coding sequences were amplified by PCR using the following primers and cloned into either
487 EcoRI/NcoI (for eArch3.0) or EcoRI/SphI (for eNpHR3.0) sites of the *pTol2 14xUAS:MCS* plasmid:

- 488 • eArch3.0_fw, ATGAATTCGCCACCATGGACCCCATCGCTCT
- 489 • eArch3.0_rev, ATGCATGCTCATTACACCTCGTTCTCGTAG
- 490 • eNpHR3.0_fw, ATGAATTCGCCACCATGACAGAGACCCTGC
- 491 • eNpHR3.0_rev, TACCATGGTTACACCTCGTTCTCGTAGC

492 To generate the stable *Tg(UAS:opsin-eYFP)* lines, purified *UAS:opsin-eYFP* DNA constructs were first
493 sequenced to confirm gene insertion and integrity and, subsequently, co-injected (25 ng/μl) with
494 *Tol2* transposase mRNA (25 ng/μl) into *Tg(isl2b:GAL4-VP16, myl7:TagRFP)zc65* (Fujimoto *et al.*,
495 2011) (for eArch3.0-eYFP) or *Tg(s1020t:GAL4)* (Scott *et al.*, 2007) (for eNpHR3.0-eYFP) zebrafish
496 embryos at the early one-cell stage. Transient expression, visible as eYFP fluorescence, was used to
497 select injected embryos that were then raised to adulthood. Zebrafish codon-optimised *Tol2*
498 transposase mRNA was prepared by *in vitro* transcription from NotI-linearised *pCS2-zT2TP*
499 plasmid using the SP6 transcription mMessage mMachine kit (Life Technologies). The *pCS2-zT2TP*
500 was a gift from Koichi Kawakami (Suster *et al.*, 2011). RNA was purified using the NucleoSpin Gel
501 and PCR Clean-up kit (Macherey-Nagel). Germ line transmission was identified by mating sexually
502 mature adult fish to *mitfa^{w2/w2}* fish and, subsequently, examining their progeny for eYFP

503 fluorescence. Positive embryos from each injected fish were then raised to adulthood. Once this
504 second generation of fish reached adulthood, positive embryos from a single `founder` fish were
505 again selected and raised to adulthood to establish stable *Tg(Isl2b:GAL4;UAS:eArch3.0-eYFP)* or
506 *Tg(s1020t:GAL4;UAS:eNpHR3.0-eYFP)* double-transgenic lines.

507 **Fluorescence image acquisition**

508 Zebrafish embryos or larvae were mounted in 1% low-melting point agarose (Sigma-Aldrich) and
509 anesthetised using tricaine (MS-222, Sigma-Aldrich). Imaging was performed using a custom-built
510 2-photon microscope [XLUMPLFLN 20× 1.0 NA objective (Olympus), 580 nm PMT dichroic, band-
511 pass filters: 510/84 (green), 641/75 (red) (Semrock), R10699 PMT (Hamamatsu Photonics),
512 Chameleon II ultrafast laser (Coherent Inc)]. Imaging was performed at 1040 nm for opsin-
513 tdTomato lines, while 920 nm excitation was used for opsin-eYFP lines. In both cases, the same laser
514 power at sample (10.7 mW) and PMT gain were used. For the images displayed in Figure 1C, 3B
515 and 7B and Figure 7-figure supplement 3B, equivalent imaging field of view and pixel size were
516 used (1200 × 800 px, 0.385 μm/px). The imaging field of view and pixel size for images displayed in
517 Figure 2C and 6B were 960 × 680 px, 0.385 μm/px. For all these images, the same acquisition
518 averaging (mean image from 12 frames) and z-spacing of imaging planes (2 μm) were used.

519 The image displayed in Figure 4A was acquired from a single plane on a fluorescence microscope
520 [AxioExaminer D1 (Zeiss), 63× 1.0 NA objective (Zeiss), Xcite (Xcelitas, XT600) 480 nm LED
521 illumination, 38HE filtercube (Zeiss), Imagem camera (Hamamatsu)], with an imaging field of
522 view of 512 × 512 px and 0.135 μm/px pixel size.

523 **Opsin expression analysis**

524 Image stacks were acquired from the spinal cord of 5 dpf *Tg(mnx1:GAL4;UAS:opsin)* larvae using a
525 2-photon microscope and acquisition parameters described above. Maximum intensity z-projections
526 spanning 5–10 μm in depth were used to estimate opsin expression at the plasma membrane of
527 motor neurons. First, automated cell body segmentation was performed using Cellpose to obtain
528 `cell body masks` (Stringer *et al.*, 2020) (<https://github.com/MouseLand/cellpose>). Then, `membrane
529 masks` corresponding to outlines of the `cell body masks` (see Figure 1-figure supplement 1A) were
530 generated by running a boundary tracing routine for binary objects in MATLAB (MathWorks). For
531 each cell, we computed the mean fluorescence intensity across all pixels in the corresponding
532 membrane mask. Cells were grouped into primary or secondary motor neurons according to both
533 area of cell body mask and location along the dorsal-ventral axis of the spinal cord (Menelaou and
534 McLean, 2012). Cells with soma area larger than 60 μm² located in the dorsal half of the spinal cord
535 were classified as primary motor neurons, cells with area smaller than 50 μm² were classified as
536 secondary motor neurons (see Figure 1-figure supplement 1B).

537 **Behavioural assays**

538 The same monitoring system was used for all behavioural assays (see schematic in Figure 2A) with
539 some differences. Images were acquired under infrared illumination (850 nm) using a high-speed

540 camera (Mikrotron MC1362, 500 μ s shutter-time) equipped with a machine vision lens (Fujinon
541 HF35SA-1) and an 850 nm bandpass filter to block visible light. The 850 nm bandpass filter was
542 removed during embryonic activation assays (in which images were acquired at 1,000 fps) to
543 determine time of light stimulus onset. In all other assays, lower acquisition rates were used (i.e. 50
544 or 500 fps) and, within each assay, the frames corresponding to stimulus onset/offset were
545 consistent across trials.

546 Light was delivered across the whole arena from above using the following LEDs (spectral
547 bandwidth at half maximum for each LED is reported in parenthesis):

548 *For embryonic assays*

- 549 • 470 nm OSRAM Golden Dragon Plus LED (LB W5AM; 25 nm).
- 550 • 590 nm ProLight LED (PM2B-3LAE-SD; 18 nm).

551 *For larval assays*

- 552 • 459 nm OSRAM OSTAR Projection Power LED (LE B P2W; 27 nm).
- 553 • 617 nm OSRAM OSTAR Projection Power LED (LE A P2W; 18 nm).

554 The 459 and 617 nm LEDs were projected onto the arena with an aspheric condenser with diffuser
555 surface. Irradiance was varied using constant current drive electronics with pulse-width
556 modulation at 5 kHz. Irradiance was calibrated using a photodiode power sensor (Thorlabs S121C).
557 LED and camera control were implemented using LabVIEW (National Instruments).

558 Before experiments, animals were screened for opsin expression in the target neural population at
559 either 22 hpf (embryonic assays) or 3 dpf (larval assays) using a fluorescence stereomicroscope
560 (Olympus MVX10). For each opsin, animals with similar expression level were selected for
561 experiments together with control opsin-negative siblings. To reduce variability in opsin expression
562 level, all animals used for behavioural experiments were heterozygous for both the GAL4 and UAS
563 transgenes. Animals were placed in the arena in the dark for around 2 min before starting
564 experiments. For all assays, each light stimulus was repeated at least 3 times. Each trial lasted 1 s in
565 behavioural activation assays and 30 s in behavioural inhibition assays.

566 ***Embryonic activation assay***

567 Opsin expression was targeted to trigeminal ganglion neurons using the *Tg(isl2b:GAL4)* transgene
568 (Ben Fredj *et al.*, 2010). Behaviour was monitored at 1,000 fps across embryos (28–30 hpf)
569 individually positioned in agarose wells (~2 mm diameter) in fish facility water and free to move
570 within their chorion. Embryos were subjected to 5 or 40 ms pulses of blue (470 nm) or amber
571 (590 nm) light at different irradiance levels (4.5–445 μ W/mm²) and with a 15 s inter-stimulus
572 interval in the dark.

573 ***Embryonic inhibition assay***

574 Opsin expression was targeted to spinal primary and secondary motor neurons and interneurons
575 (Kolmer-Agduhr cells and ventral longitudinal descending interneurons) using the *Tg(s1020t:GAL4)*
576 transgene (Scott *et al.*, 2007). Behaviour was monitored at 50 fps across embryos (24–27 hpf)
577 individually positioned in agarose wells (~2 mm diameter) with fish facility water and free to move

578 within their chorion. Embryos were subjected to 10 s pulses of blue (470 nm) or amber (590 nm)
579 light at different irradiance levels (0–227 $\mu\text{W}/\text{mm}^2$) with a 50 s inter-stimulus interval in the dark.

580 *Larval activation assay*

581 Opsin expression was targeted to primary and secondary spinal motor neurons using the
582 *Tg(mnx1:GAL4)* transgene (Bohm *et al.*, 2016). Behaviour was monitored at 500 fps in 6 dpf larvae
583 with their head restrained in 2% low-melting point agarose (Sigma-Aldrich) and their tail free to
584 move. Larvae were subjected to 2 or 10 ms pulses of blue (459 nm) or red (617 nm) light at different
585 irradiance levels (0.04–2.55 mW/mm^2) with a 20 s inter-stimulus interval in the dark. We also
586 provided 250 ms trains of light pulses (1 ms pulse duration for blue light at 2.55 mW/mm^2 or 10 ms
587 for red light at 1 mW/mm^2) at two pulse frequencies (20 or 40 Hz).

588 *Larval inhibition assays*

589 Opsin expression was targeted to spinal cord neurons using either the *Tg(s1020t:GAL4)* or
590 *Tg(mnx1:GAL4)* transgene, as above. Behaviour was monitored at 50 fps across larvae individually
591 positioned in agarose wells (~1.4 cm diameter) with fish facility water in which they were free to
592 swim. Larvae were subjected to 10 s pulses of blue (459 nm) or red (617 nm) light at different
593 irradiance levels (0.24–2.55 mW/mm^2) with a 50 s inter-stimulus interval in the dark. Control trials
594 during which no light pulse was provided were interleaved between light stimulation trials.

595 **Behavioural data analysis**

596 Movie data was analysed using MATLAB (MathWorks). Region of interests (ROIs) containing
597 individual fish were manually specified. For each ROI, the frame-by-frame change in pixel intensity
598 – ΔPixel – was computed in the following way. For each trial, pixel intensity values were low-pass
599 filtered across time frames and the absolute frame-by-frame difference in intensity (dI) was obtained
600 for each pixel. Pixels showing the highest variance in dI (top 5th percentile) were selected to compute
601 their mean dI , corresponding to the ROI ΔPixel trace for the trial.

602 With the exception of the larval inhibition assay (see below), onset and offset of animal movements
603 were detected from ΔPixel traces in the following way. For each ROI, ΔPixel traces were
604 concatenated across all trials to estimate the probability density function (pdf) of ΔPixel values. The
605 portion of the distribution with values below the pdf peak was mirror-reflected about the x -axis and
606 a Gaussian was fitted to the obtained symmetric distribution. The mean (μ) and standard deviation
607 (σ) of the fitted Gaussian were then used to compute ROI-specific ΔPixel thresholds for detecting
608 onset ($\mu + 6\sigma$) and offset ($\mu + 3\sigma$) of animal movements.

609 For embryonic and larval activation assays, behavioural response latency corresponds to the time
610 from light stimulus onset to the start of the first detected movement. Movements were classified as
611 optogenetically-evoked if their response latency was shorter than 200 ms for the embryonic assay or
612 50 ms for the larval assay, which corresponds to the minimum in the pdf of response latency from all
613 opsin-expressing larvae (Figure 3E). For each animal, response probability to each light stimulus
614 type corresponds to the fraction of trials in which at least one optogenetically-evoked movement
615 was detected.

616 In the larval activation assay, the tail was tracked by performing consecutive annular line-scans,
617 starting from a manually-selected body centroid and progressing towards the tip of the tail so as to
618 define nine equidistant x-y coordinates along the tail. Inter-segment angles were computed between
619 the eight resulting segments. Reported tail curvature was computed as the sum of these inter-
620 segment angles. Rightward bending of the tail is represented by positive angles and leftward
621 bending by negative angles. Number of tail beats corresponds to the number of full tail oscillation
622 cycles. Tail theta-1 angle is the amplitude of the first half beat. Tail beat frequency was computed as
623 the reciprocal of the mean full-cycle period during the first four tail oscillation cycles of a swim
624 bout. Bout duration was determined from Δ Pixel traces using the movement onset/offset
625 thresholds described above.

626 For larval inhibition assays, images were background-subtracted using a background model
627 generated over each trial (30 s duration). Images were then thresholded and the fish body centroid
628 was found by running a particle detection routine for binary objects within suitable area limits.
629 Tracking of body centroid position was used to compute fish speed, and periods in which speed
630 was higher than 1 mm/s were classified as swim bouts. Bout speed was computed as the mean
631 speed over the duration of each bout.

632 To account for group differences in baseline coil/bout rate and bout speed in inhibition assays, data
633 was normalised at a given irradiance level by divided by the mean rate/speed across fish in control
634 (no light) trials.

635 **Electrophysiological recordings**

636 *Transgenic lines*

637 Opsin expression was targeted to primary motor neurons using the *Tg(mnx1:GAL4)* transgene
638 (Bohm *et al.*, 2016) with one exception: 11 out of 19 eNpHR3.0-expressing cells were recorded in
639 *Tg(s1020t:GAL4)* larvae (Scott *et al.*, 2007). As in behavioural assays, all animals used for
640 electrophysiological experiments were heterozygous for both the GAL4 and UAS transgenes. For
641 control recordings, we targeted opsin-negative GFP-expressing primary motor neurons in
642 *Tg(mnx1:GAL4;UAS:EGFP)* (Asakawa *et al.*, 2008) or *Tg(parga-GFP)* (Balciunas *et al.*, 2004) larvae. In
643 all transgenic lines used, primary motor neurons could be unambiguously identified as the 3–4
644 largest cell somas, located in the dorsal-most portion of the motor column (Beattie *et al.*, 1997; Bello-
645 Rojas *et al.*, 2019). We verified primary motor neuron identity in a small subset of recordings from
646 eYFP-expressing cells in *Tg(mnx1:GAL4;UAS:Chr2(H134R)-eYFP)* larvae by adding 0.025%
647 sulforhodamine-B acid chloride dye in the intracellular solution (Sigma-Aldrich) and filling the
648 neuron to reveal its morphology. To maximise data acquisition in our *in vivo* preparation, when the
649 first attempts of primary motor neuron recordings were not successful, we recorded neighbouring,
650 dorsally-located presumed secondary motor neurons (11 out of 86 included cells).

651 *Data acquisition*

652 Zebrafish larvae (5–6 dpf) were first paralysed in 1 mM α -Bungarotoxin solution (Tocris) for 3–
653 6 min after which they were pinned in a lateral position to a Sylgard-coated recording dish

654 (Sylgard 184, Dow Corning) with tungsten pins inserted through the notochord. The skin was
655 removed between the trunk and midbody regions using sharp forceps, after which the dorsal
656 muscle from 2–3 somites was suctioned with glass pipettes (~50 μm opening made from capillaries
657 of 1.5 mm outer diameter, 1.1 mm inner diameter; Sutter). Patch pipettes were made from capillary
658 glass (1 mm outer diameter, 0.58 mm inner diameter; WPI) with a horizontal puller (Sutter
659 Instrument P1000) and had resistances between 8–16 M Ω . To first pass the dura, we applied a
660 higher positive pressure (30–40 mm Hg) to the recording electrode via a pneumatic transducer
661 (Fluke Biomedical, DPM1B), which was then lowered (20–25 mm Hg) once the electrode was near
662 the cells. We generally recorded data from a single cell per larva. In a few instances, two cells from
663 separate adjacent somites were recorded in the same fish.

664 External bath recording solution contained the following: 134 mM NaCl, 2.9 mM KCl, 2.1 mM
665 $\text{CaCl}_2\text{-H}_2\text{O}$, 1.2 mM MgCl_2 , 10 mM glucose, and 10 mM HEPES, with pH adjusted to 7.8 with 9 mM
666 NaOH and an osmolarity of 295 mOsm. We blocked glutamatergic and GABAergic synaptic
667 transmission with a cocktail of: 20 μM CNQX or DNQX, 50 μM D-AP5, 10 μM Gabazine (Tocris)
668 added to the external recording solution. The -50 mV ECl solution contained: 115 mM K-gluconate,
669 15 mM KCl, 2 mM MgCl_2 , 4 mM Mg-ATP, 0.5 mM EGTA, 10 mM HEPES, with pH adjusted to 7.2
670 with 11mM KOH solution, and a 285 mOsm. In these conditions, we calculated the liquid junction
671 potential (LJP; Clampfit calculator) to be 12.4 mV. The -70 mV ECl solution contained: 126 mM K-
672 gluconate, 4 mM KCl, 2 mM MgCl_2 , 4 mM Mg-ATP, 0.5 mM EGTA, 10 mM HEPES, pH adjusted to
673 7.2 with 11mM KOH solution, 285 mOsm and a 13.3 mV LJP. All reagents were obtained from
674 Sigma-Aldrich unless otherwise stated.

675 Recordings were made with an Axopatch 700B amplifier and digitised with Digidata 1440A or
676 1550B (Molecular Devices). pClamp software was used to acquire electrophysiological data at a
677 sampling rate of 20 kHz and low-pass filtered at 2 kHz (voltage clamp) or 10 kHz (current clamp).
678 Voltage clamp recordings were acquired with full whole-cell compensation and ~60% series
679 resistance compensation, while corrections for bridge balance and electrode capacitance were
680 applied in current clamp mode. Cells were visualised with a 63 \times /1.0 NA or a 60 \times /1.0 NA water-
681 immersion objective (Zeiss or Nikon, respectively) on a fluorescence microscope equipped with
682 differential interference contrast optics (AxioExaminer D1, Zeiss or Eclipse FN1, Nikon).

683 *Optogenetic stimulation*

684 Light stimulation was performed with either a X-Cite (Xcelitas, XT600) or a broadband white LED
685 (Prizmatix, UHP-T-HCRI_DI) light source equipped with a combination of different bandpass and
686 neutral density filters to modulate irradiance at specific wavelengths (see Figure 4-figure
687 supplement 1A and Supplemental File 4 for centre wavelengths/bandwidth and irradiance levels
688 used to activate opsins). The onset, duration and irradiance level of light pulses were triggered and
689 controlled via the Digidata device used for electrophysiological recordings.

690 For all cells, data was acquired in the following order: (1) series resistance was checked at the
691 beginning, middle and end of recording; (2) action potential rheobase was determined by injecting
692 5 ms pulses of current (160–340 pA) in current-clamp gap-free mode; (3) voltage clamp recording of

693 opsin photocurrents; (4) current clamp recording of voltage responses induced by opsin activation.
694 Light stimuli were provided from low to high irradiance levels across all protocols. For each
695 protocol, inter-stimulus intervals were between 10 and 15 s.

696 For cation channelrhodopsins, we used a range of short light pulses. Voltage clamp recordings were
697 paired with a 5 ms light pulse, while current clamp recordings were performed with 0.1, 0.5, 1, 2 or
698 5 ms pulses. In addition, we tested whether we could optogenetically entrain neurons to spike at
699 frequencies ranging from 1 to 100 Hz using stimulus trains composed of 0.5, 1, 2 or 5 ms light
700 pulses.

701 For anion channelrhodopsins and Cl^-/H^+ pumps, voltage and current clamp recordings were paired
702 with a 1 s light pulse. In addition, we used two different tests of optogenetic inhibition during
703 active spiking. To assess single spike inhibition efficacy and precision, we evoked spiking by
704 injecting 5 ms pulses of current at 1.2–1.5 \times rheobase for 10 trains at 5 Hz (1 s inter-train interval,
705 total of 100 spikes triggered in 30 s), during which we provided 5 ms light pulses paired to the first
706 current stimulus of the train and a subsequent one with progressively longer latency (Zhang *et al.*,
707 2007). To test opsin ability to inhibit tonic firing over longer time periods, we evoked spiking with
708 longer pulses of current (200–800 ms) at 1.2–1.5 \times rheobase paired with a light pulse (50–200 ms) in
709 the middle of the current stimulation. We first recorded a control current injection-only trial,
710 followed by current and light pulse trials with a 20 s inter-stimulus interval.

711 *Data analysis*

712 Data were analysed using the pyABF module in Spyder (3.3.6 MIT, running Python 3.6, scripts
713 available here: https://github.com/wyartlab/Antinucci_Dumitrescu_et_al_2020), MATLAB
714 (MathWorks) and Clampfit (Molecular Devices). Series resistance (R_s) was calculated as a cell
715 response to a 5 or 10 mV hyperpolarisation step in voltage clamp from a holding potential of -60
716 mV, with whole-cell compensation disabled. Membrane resistance (R_m) was obtained from the
717 steady holding current at the new step, and membrane capacitance (C_m) corresponds to the area
718 under the exponentially decaying current from peak to holding. We used the following cell
719 inclusion criteria: (1) cell spiking upon injection of a 5 ms pulse of current; (2) membrane resting
720 potential < -50 mV at all times; (3) > 150 pA current injection necessary to maintain the cell at a
721 holding potential equal to resting potential in current clamp; (4) series resistance < 6 \times pipette
722 resistance at all times during the recording. We chose this conservative series resistance range as per
723 previous electrophysiological procedures in other animal models: i.e. mammalian *in vivo* recordings
724 with pipette resistance between 4–7 M Ω and max series resistance between 10–100 M Ω (Margrie *et*
725 *al.*, 2002). All reported membrane voltages were liquid junction potential corrected.

726 For voltage clamp recordings, we measured the maximum photocurrent amplitude in a time
727 window of 100 ms (for cation channelrhodopsins) or 1 s (for anion channelrhodopsins and Cl^-/H^+
728 pumps) duration starting from light onset. To characterise photocurrent kinetics of cation
729 channelrhodopsins, we measured the time to peak photocurrent from light onset (i.e. activation
730 time) and computed the response decay time constant by fitting a monoexponential decay function
731 to the photocurrent from peak to baseline (i.e. deactivation time constant). To compute

732 photocurrent kinetics of anion channelrhodopsins and Cl⁻/H⁺ pumps, we fitted monoexponential
733 functions to the following components of the response: activation time constant was computed from
734 light onset to peak response, inactivation time constant from peak response to steady state (last 5 ms
735 of light stimulation), deactivation time constant from steady state to baseline (1 s following light
736 offset)

737 To characterise voltage responses induced by opsins under current clamp, we first classified events
738 as spikes (when max voltage depolarisation was > - 30 mV) or sub-threshold (peak voltage
739 deflection < - 30 mV). For each response type, we measured the absolute peak of the response, the
740 time to reach maximum response from light onset and the time-decay to baseline from peak by
741 fitting a monoexponential decay function, as above. To assess firing pattern fidelity, we calculated
742 the number of spikes per light pulse in a train, the latency from light onset to the first spike
743 occurring within a 10 ms time window, and the spike jitter as the standard deviation of spike
744 latency values across a pulse train with given frequency.

745 Opsin efficacy in inhibiting single spikes was quantified using the following equation:

$$I = \frac{S_C - S_{C+L}}{S_C} \times 100$$

746 where S_C is the mean number of spikes elicited by current pulses when no light was provided, S_{C+L}
747 is the mean number of spikes elicited during time periods in which a light pulse was paired with a
748 current pulse, and I is the inhibition index (100% being perfect inhibition and negative values
749 indicating additional spikes were generated during light pulses). Tonic firing inhibition efficacy was
750 quantified by counting the number of spikes occurring during the light delivery period and
751 normalising this count to provide spikes generated per 50 ms.

752 **Statistical analysis**

753 All statistical analyses were performed using Prism (GraphPad). Sample distributions were first
754 assessed for normality and homoscedasticity. Details regarding the statistical tests used are
755 reported in Supplementary File 2 for behavioural data and Supplementary File 3 for
756 electrophysiological data. Significance threshold was set to 0.05 and all reported p-values were
757 corrected for multiple comparisons. Tests were two-tailed for all experiments. Statistical analysis
758 performed during the peer-review process has been reported as exploratory analyses (see
759 Supplementary File 3). Number of animals/cells are provided for each graph. No outliers were
760 excluded from the analyses.

761 **Figure legends**

762 **Figure 1. Toolkit for targeted opsin expression**

763 **A** List of selected opsins, with spectral absorption and opsin class.

764 **B** Schematics of expression patterns in the GAL4 transgenic driver lines used in this study.

765 **C** Opsin expression in spinal neurons in *Tg(mnx1:GAL4;UAS:opsin-FP)* larvae at 5 dpf (for
766 eNpHR3.0, the *s1020t:GAL4* transgene was used). Insets show magnified cell bodies to illustrate
767 opsin membrane expression (for insets, brightness and contrast were adjusted independently for
768 each opsin to aid visualisation). A, anterior; D, dorsal; P, posterior; V, ventral. Scale bar 20 μm in
769 large images, 5 μm in insets.

770 **D** Behavioural assays and corresponding figure numbers.

771 **E** *In vivo* electrophysiological recordings and figure numbers.

772 See also Figure 1–figure supplement 1.

773 **Figure 1–figure supplement 1. Analysis of opsin expression in larval motor neurons**

774 **A** Opsin expression in spinal motor neurons in a *Tg(mnx1:GAL4;UAS:ChrimsonR-tdTomato)* larva at
775 5 dpf. Middle panel shows masks used to compute cell body area. Bottom panel shows masks used
776 to estimate membrane expression. A, anterior; D, dorsal; P, posterior; V, ventral. Scale bar 30 μm .

777 **B** Cell body area and dorsoventral location in the spinal cord were used to classify cells as primary
778 or secondary motor neurons (MNs) (Menelaou and McLean, 2012). Black line corresponds to sum of
779 two Gaussians fit. Grey bars indicate unclassified neurons.

780 **C** Opsin expression estimated as mean fluorescence intensity per membrane pixel in primary MNs
781 (pMNs, dark) and secondary MNs (sMN, light). Opsins are grouped according to the fluorescent
782 protein they are linked to. Box plots range from 10th to 90th percentiles. a. u., arbitrary units.

783 **D** Opsin expression in pMNs vs. photocurrents in pMNs for cation channelrhodopsins linked to
784 tdTomato. Error bars indicate standard deviation. Dotted line and grey areas correspond to linear fit
785 with 95% confidence intervals.

786 **E** Opsin expression across all neurons in individual fish (N = 5 larvae per opsin; Chronos, n = 302
787 cells; CheRiff, n = 998; ChrimsonR, n = 771; CoChR, n = 514; GtACR2, n = 1002; GtACR1, n = 735;
788 eNpHR3.0, n = 386; ChR2_(H134R), n = 910; eArch3.0, n = 487).

789 **Figure 2. Optogenetic activation of embryonic trigeminal neurons triggers escape responses**

790 **A** Experimental setup for optogenetic stimulation and behavioural monitoring. IR, infrared.

791 **B** Schematic of behavioural assay.

792 **C** Opsin expression in trigeminal neurons in a *Tg(isl2b:GAL4;UAS:CoChR-tdTomato)* embryo at 1 dpf.
793 Imaging field of view corresponds to black box in (B). A, anterior; D, dorsal; P, posterior; V, ventral.
794 Scale bar 50 μm .

795 **D** *Tg(isl2b:GAL4;UAS:CoChR-tdTomato)* embryos positioned in individual agarose wells. Behaviour
796 was monitored at 1,000 frames per second across multiple embryos (28–30 hpf; N = 69 \pm 26 fish per
797 opsin group, mean \pm SD) subjected to 5 or 40 ms pulses of full-field illumination (470 or 590 nm,
798 4.5–445 $\mu\text{W}/\text{mm}^2$) with a 15 s inter-stimulus interval.

799 **E** Optogenetically-triggered escape responses detected from ΔPixel traces in the 3 embryos
800 indicated in (D). Dotted line indicates maximum latency (200 ms) for a response to be considered
801 optogenetically-triggered.

802 **F,G** Response probability for transient (**E**) or stable (**F**) transgenic embryos expressing different
803 opsins (mean \pm SEM, across fish). Insets show response latency for 5 ms blue light pulses in CoChR-
804 expressing embryos (median \pm 95% CI, across fish).
805 See also Figure 2–figure supplements 1 and 2 and Video 1.

806 **Figure 2–figure supplement 1. Response probability vs. time in transient transgenic embryos**
807 **expressing opsins in trigeminal neurons**

808 **A–D** Distribution of response probability vs. time for *Tg(isl2b:GAL4)* embryos (28–30 hpf)
809 expressing different opsins through transient transgenesis (mean + SD, across fish). Embryos were
810 stimulated with 5 ms (**A,B**) or 40 ms (**C,D**) pulses of blue (470 nm; **A,C**) or amber (590 nm; **B,D**)
811 light. Each time bin corresponds to 8 ms.

812 **Figure 2–figure supplement 2. Response probability vs. time in stable transgenic embryos**
813 **expressing opsins in trigeminal neurons**

814 **A–D** Distribution of response probability vs. time for *Tg(isl2b:GAL4)* embryos (28–30 hpf)
815 expressing different opsins through stable transgenesis (mean + SD, across fish). Embryos were
816 stimulated with 5 ms (**A,B**) or 40 ms (**C,D**) pulses of blue (470 nm; **A,C**) or amber (590 nm; **B,D**)
817 light. Each time bin corresponds to 8 ms.

818 **Video 1. Escape responses elicited by optogenetic stimulation of embryonic trigeminal neurons**

819 Escape responses in *Tg(isl2b:GAL4;UAS:CoChR-tdTomato)* embryos (28–30 hpf) triggered by a 5 ms
820 pulse of blue light (470 nm, 445 μ W/mm²). Images were acquired at 1,000 frames per second and
821 the video plays at 0.1 \times speed. Related to Figure 2.

822 **Figure 2–Source Data 1. Data related to Figure 2.**

823 Data provided as a XLSX file.

824 **Figure 3. Optogenetic activation of larval spinal motor neurons triggers tail movements**

825 **A** Schematics of behavioural assay. Head-restrained, tail-free larvae (6 dpf; N = 28 \pm 8 fish per opsin
826 group, mean \pm SD) were exposed to 2 or 10 ms pulses of light (459 or 617 nm, 0.04–2.55 mW/mm²)
827 with a 20 s inter-stimulus interval while their behaviour was monitored at 500 fps. We also
828 provided 250 ms trains of light pulses at 20 or 40 Hz.

829 **B** Opsin expression in spinal motor neurons in a *Tg(mnx1:GAL4;UAS:CoChR-tdTomato)* larva at
830 5 dpf. Imaging field of view corresponds to black box in (**A**). A, anterior; D, dorsal; P, posterior; V,
831 ventral. Scale bar 50 μ m.

832 **C** Swim bouts elicited by a pulse train in *Tg(mnx1:GAL4;UAS:CoChR-tdTomato)* larvae (left). The
833 control, opsin-negative larva (right), does not respond within 148 ms after stimulus onset.

834 **D** Tail tracking, showing optogenetically-evoked swim bouts in a CoChR-expressing larva (bottom
835 three rows) and a visually-evoked swim in a control opsin-negative larva (top). tbf, tail beat
836 frequency.

837 **E** Distribution of response latencies for all tail movements in opsin-expressing (red) and control
838 opsin-negative larvae (grey). Dotted line indicates maximum latency (50 ms) for a response to be
839 considered optogenetically-triggered. Control larvae exclusively show long latency responses. Each
840 time bin corresponds to 25 ms.

841 **F,L** Response probability of larvae expressing different opsins for single-pulse (**F**) or pulse-train (**L**)
842 stimulation (mean \pm SEM, across fish).

843 **G-Q** Latency (**G,M**), bout duration (**H,N**), tail angle of the first half beat (θ_1 ; **I,O**), number of cycles
844 (**J,P**) and tail beat frequency (**K,Q**) for single-pulse (**G-K**) or pulse-train (**M-Q**) stimulation
845 (mean \pm SEM, across fish).

846 See also Figure 3–figure supplement 1 and Video 2 and 3.

847 **Figure 3–figure supplement 1. Response probability vs. time in larvae expressing opsins in**
848 **spinal motor neurons**

849 **A–D** Distribution of response probability vs. time for *Tg(mnx1:GAL4)* larvae (6 dpf) expressing
850 different opsins (mean + SD, across fish). Larvae were stimulated with single 2 ms (**A,B**) or 10 ms
851 (**C,D**) pulses of blue (459 nm; **A,C**) or red (617 nm; **B,D**) light. Each time bin corresponds to 2 ms.

852 **Video 2. Swim bouts elicited by single-pulse optogenetic stimulation of larval spinal motor**
853 **neurons**

854 Swim responses in 3 head-restrained tail-free *Tg(mnx1:GAL4;UAS:CoChR-tdTomato)* larvae (6 dpf,
855 left) triggered by a single 2 ms pulse of blue light (459 nm, 0.63 mW/mm²). A control opsin-
856 negative larva is positioned on the right. Images were acquired at 500 frames per second and the
857 video plays at 0.04 \times speed. Related to Figure 3.

858 **Video 3. Swim bouts elicited by 20 Hz pulse train optogenetic stimulation of larval spinal motor**
859 **neurons**

860 Swim responses in 3 head-restrained tail-free *Tg(mnx1:GAL4;UAS:CoChR-tdTomato)* larvae (6 dpf,
861 left) triggered by a train of 1 ms pulses of blue light (459 nm, 20 Hz, 2.55 mW/mm², 250 ms train
862 duration). A control opsin-negative larva is positioned on the right. Images were acquired at
863 500 frames per second and the video plays at 0.04 \times speed. Related to Figure 3.

864 **Figure 3–Source Data 1. Data related to Figure 3.**

865 Data provided as a XLSX file.

866 **Figure 4. Electrophysiological recording of photocurrents in primary motor neurons**

867 **A** Schematics of experimental setup for optogenetic stimulation with *in vivo* whole-cell patch clamp
868 recordings. Image shows a patched primary motor neuron (pMN) expressing CoChR in a 6 dpf
869 *Tg(mnx1:GAL4;UAS:CoChR-tdTomato)* larva. Scale bar 5 μ m.

870 **B** Membrane resistance was not affected by opsin expression (mean \pm SD, across cells).

871 **C** Resting membrane potential was similar between opsin-expressing and control neurons
872 (mean \pm SD).

873 **D** Examples of inward photocurrents in response to 5 ms light pulses (20 mW/mm²).

874 **E** Peak photocurrent amplitude. CoChR and ChrimsonR induced the largest photocurrents
875 (mean \pm SEM, across cells). Dotted lines show range of pMN rheobase. Data is pooled across
876 stimulus intensity (1–30 mW/mm²) but see Figure 4–figure supplement 1 for currents at varying
877 irradiance.

878 **F** Photocurrent activation time was similar across opsins (mean \pm SEM).

879 **G** Chronos photocurrents had the fastest deactivation time constant, while CoChR and ChrimsonR
880 showed similar deactivation kinetics (mean \pm SEM).

881 See also Figure 4-figure supplement 1.

882 **Figure 4-figure supplement 1. Wavelengths used in electrophysiological recordings and**
883 **photocurrent properties vs. irradiance**

884 **A** LED emission wavelength (centre/bandwidth, nm) and irradiance levels used for each opsin line
885 and control cells.

886 **B** Number of cells patched in each group. Numbers and coloured bars indicate included cells while
887 grey bars indicate excluded cells (see Materials and methods for inclusion criteria).

888 **C,D** Access resistance (**C**) and cell capacitance (**D**) were comparable between groups (mean \pm SD,
889 across cells).

890 **E** Example photocurrents from a CoChR-expressing cell at different irradiance levels (3–
891 20 mW/mm²).

892 **F–H** Peak photocurrent amplitude (**F**), activation time (**G**) and deactivation time constant (**H**) vs.
893 irradiance (mean \pm SEM, across cells). Dotted lines in (**F**) show range of pMN rheobase. Asterisks
894 indicate a significant non-zero slope.

895 **Figure 4-Source Data 1. Data related to Figure 4.**

896 Data provided as a XLSX file.

897 **Figure 5. CoChR and ChrimsonR can elicit spiking in primary motor neurons**

898 **A** Example membrane depolarisations induced by 5 ms light pulses (20 mW/mm²).

899 **B** Number of optogenetically-evoked spikes vs. pulse duration (across irradiance levels 1–30
900 mW/mm²). Longer pulse duration induced more spikes in both CoChR- and ChrimsonR-
901 expressing cells. Left plots show single neurons and right plot shows mean \pm SEM across cells.

902 **C** Example voltage responses from CoChR- and ChrimsonR-expressing cells upon pulse train
903 stimulation (1–100 Hz, 2–5 ms pulse duration).

904 **D** Number of spikes vs. pulse number within a train (mean \pm SEM, across cells; shaded area depicts
905 average number of spikes is below 1). In CoChR-expressing cells, the initial 3–4 pulses within the
906 train induced bursts of 2–4 spikes.

907 **E** Heatmap of mean spike number elicited via CoChR stimulation, separated according to
908 stimulation frequency and pulse duration. Primary motor neurons often responded with bursts of
909 action potentials, even for short light pulses.

910 **F** Example responses to the 1st (top) and last (bottom) 0.5 ms light pulse in a train, recorded from a
911 CoChR-positive neuron.

912 **G** Spike latency vs. pulse frequency (mean \pm SEM).

913 **H** Spike jitter (mean \pm SEM) vs. pulse frequency shows that ChrimsonR-expressing cells exhibited
914 lower spike jitter than CoChR-expressing cells.

915 See also Figure 5-figure supplement 1.

916
917 **Figure 5-figure supplement 1. Optogenetically-evoked voltage responses**

918 **A** Fraction of cells that generated spikes in response to single light pulses (0.1–5 ms).

919 **B** Peak depolarisation across irradiance levels (1–30 mW/mm²; mean \pm SEM, across cells). Orange
920 line indicates threshold for spike detection (-30 mV).

921 **C** Time to peak depolarisation (mean \pm SEM).

922 **D** Number of evoked spikes vs. irradiance (1–5 ms pulse duration). In CoChR-expressing cells, 2–
923 5 ms light pulses induced spike bursts (mean ± SEM).

924 **E** Spike latency vs. pulse number (mean ± SEM). With increasing pulse frequency, CoChR-
925 expressing cells showed progressively longer spike latency throughout the pulse train.

926 **Figure 5–Source Data 1. Data related to Figure 5.**

927 Data provided as a XLSX file.

928 **Figure 6. Optogenetic suppression of coiling behaviour in embryos**

929 **A** Schematic of the behavioural assay.

930 **B** Opsin expression in spinal motor neurons and interneurons in a *Tg(s1020t:GAL4;UAS:GtACR1-*
931 *tdTomato)* embryo at 1 dpf. Imaging field of view corresponds to black box in (A). A, anterior; D,
932 dorsal; P, posterior; V, ventral. Scale bar 50 μm.

933 **C** Camera field of view showing *Tg(s1020t:GAL4;UAS:GtACR1-tdTomato)* embryos positioned in
934 individual agarose wells. Behaviour was monitored at 50 frames per second across multiple
935 embryos (24–27 hpf; N = 91 ± 16 fish per group, mean ± SD) subjected to 10 s light periods
936 (470 or 590 nm, 0–227 μW/mm²) with a 50 s inter-stimulus interval.

937 **D** Tracking of coiling behaviour (mean ΔPixel from 3 trials) for the 3 embryos shown in (C). Black
938 arrow indicates movements at light onset, whereas grey arrowhead indicates synchronised restart
939 of coiling behaviour following light offset.

940 **E** Optogenetically-induced changes in coil rate (mean + SD, across fish) in embryos expressing the
941 anion channelrhodopsin GtACR1 (N = 77 embryos, top) or the Cl⁻ pump eNpHR3.0
942 (N = 111 embryos, bottom). Horizontal dark grey bars indicate the 'late LED On' period. Each time
943 bin corresponds to 2 s.

944 **F,G** Normalised coil rate during the 'late LED On' period in embryos expressing different opsins
945 (mean ± SEM, across fish). Control opsin-negative siblings were subjected to the same light stimuli.
946 See also Figure 6–figure supplements 1 and 2 and Video 4.

947 **Figure 6–figure supplement 1. Coil rate vs. time in embryos expressing different opsins in spinal**
948 **neurons**

949 **A,B** Distribution of coil rate vs. time for *Tg(s1020t:GAL4)* embryos (24–27 hpf) expressing different
950 opsins (mean + SD, across fish). Embryos were subjected to 10 s pulses of blue (470 nm; **A**) or amber
951 (590 nm; **B**) light. Each time bin corresponds to 2 s.

952 **Figure 6–figure supplement 2. Coil rate vs. irradiance for the initial 2 seconds of light exposure**

953 **A,B** Normalised coil rate during the initial 2 s of the LED On period in embryos (24–27 hpf)
954 expressing different opsins (mean ± SEM, across fish). Control opsin-negative siblings were
955 subjected to the same light stimuli.

956 **Video 4. Monitoring of coiling behaviour upon opsin activation in embryonic spinal neurons**

957 Coiling behaviour in *Tg(s1020t:GAL4;UAS:GtACR2-tdTomato)* embryos (24–27 hpf) subjected to a
958 10 s period of blue light (470 nm, 225 μW/mm²). Images were acquired at 50 frames per second and
959 the video plays at 3× speed. Related to Figure 6.

960 **Figure 6–Source Data 1. Data related to Figure 6.**

961 Data provided as a XLSX file.

962 **Figure 7. Optogenetic suppression of swimming in larvae**

963 **A** Schematic of behavioural assay.

964 **B** Opsin expression in spinal motor neurons and interneurons in a *Tg(s1020t:GAL4;UAS:GtACR1-*
965 *tdTomato)* larva at 5 dpf. Imaging field of view corresponds to black box in (A). A, anterior; D,
966 dorsal; P, posterior; V, ventral. Scale bar 50 μm .

967 **C** *Tg(s1020t:GAL4;UAS:GtACR1-tdTomato)* larvae were positioned in individual agarose wells (left)
968 and instantaneous swim speed was monitored by centroid tracking (right) at 50 fps (6 dpf;
969 $N = 25 \pm 9$ fish per group, mean \pm SD). 10 s light periods were delivered (459 or 617 nm, 0-
970 $2.55 \text{ mW}/\text{mm}^2$) with a 50 s inter-stimulus interval.

971 **D** Optogenetically-induced changes in bout rate (mean + SEM, across fish) in *Tg(s1020t:GAL4)*
972 larvae expressing GtACR1 ($N = 24$ larvae, left) or eNpHR3.0 ($N = 40$ larvae, right). Horizontal grey
973 bars indicate the time windows used to quantify behavioural changes. Each time bin corresponds to
974 2 s.

975 **E,F** Normalised bout rate during the `LED On` period in larvae expressing different opsins
976 (mean \pm SEM, across fish) and in control, opsin-negative, siblings.

977 See also Figure 7-figure supplements 1-4 and Video 5.

978 **Figure 7-figure supplement 1. Bout rate vs. time in larvae expressing different opsins in spinal**
979 **neurons**

980 **A,B** Distribution of bout rate vs. time for *Tg(s1020t:GAL4)* larvae (6 dpf) expressing different opsins
981 (mean + SD, across fish). Larvae were subjected to 10 s pulses of blue (459 nm; A) or red (617 nm; B)
982 light. Each time bin corresponds to 2 s.

983 **Figure 7-figure supplement 2. Bout rate and speed vs. irradiance during different time periods in**
984 ***Tg(s1020t:GAL4)* larvae**

985 **A,B** Normalised bout rate (A) or bout speed (B) during the whole LED On period, the initial 2 s of
986 light exposure and the `post LED` 8 s period in *Tg(s1020t:GAL4)* larvae (6 dpf) expressing different
987 opsins (mean \pm SEM, across fish). Control opsin-negative siblings were subjected to the same light
988 stimuli.

989 **Figure 7-figure supplement 3. Optogenetic suppression of swimming in *Tg(mnx1:GAL4)* larvae**

990 **A** Schematics of opsin expression pattern and behavioural assay.

991 **B** Opsin expression in spinal motor neurons in a *Tg(mnx1:GAL4;UAS:GtACR1-tdTomato)* larva at 5
992 dpf. Imaging field of view corresponds to black box in (A). A, anterior; D, dorsal; P, posterior; V,
993 ventral. Scale bar 50 μm .

994 **C** Background-subtracted camera field of view showing *Tg(mnx1:GAL4;UAS:GtACR1-tdTomato)*
995 larvae positioned in individual agarose wells (left) and tracking of swimming speed for selected
996 larvae (right). Behaviour was monitored at 50 fps across multiple freely-swimming larvae (6 dpf;
997 $N = 24 \pm 6$ fish per group, mean \pm SD) while they were subjected to 10 s light periods
998 (459 or 617 nm, 0- $2.55 \text{ mW}/\text{mm}^2$) with a 50 s inter-stimulus interval.

999 **D** Optogenetically-induced changes in bout rate (mean + SEM, across fish) in *Tg(mnx1:GAL4)* larvae
1000 expressing GtACR1 ($N = 29$ larvae, left) or eArch3.0 ($N = 23$ larvae, right). Horizontal grey bars
1001 indicate the time windows used for comparative quantification of behavioural changes. Each time
1002 bin corresponds to 2 s.

1003 E,F Normalised bout speed during the `LED On` period in larvae expressing different opsins
1004 (mean \pm SEM, across fish). Control opsin-negative siblings were subjected to the same light stimuli.

1005 **Figure 7-figure supplement 4. Bout rate and speed vs. irradiance during different time periods in**
1006 ***Tg(mnx1:GAL4)* larvae**

1007 A-D Normalised bout rate (A-C) or bout speed (D) during the whole `LED On` period (A), the
1008 initial 2 s of the light period (B), or the `post LED` 8 s period (C,D) in *Tg(mnx1:GAL4)* larvae (6 dpf)
1009 expressing different opsins (mean \pm SEM, across fish). Control opsin-negative siblings were
1010 subjected to the same light stimuli.

1011 **Video 5. Suppression of swimming upon opsin activation in larval spinal neurons**

1012 Suppression of swimming in *Tg(s1020t:GAL4;UAS:GtACR1-tdTomato)* larvae (6 dpf) during 10 s of
1013 blue light (459 nm, 0.24 mW/mm²). Images were acquired at 50 frames per second and the video
1014 plays at 3 \times speed. Related to Figure 7.

1015 **Figure 7-Source Data 1. Data related to Figure 7.**

1016 Data provided as a XLSX file.

1017 **Figure 8. Photocurrents induced by anion channelrhodopsins and chloride/proton pumps**

1018 A Action of anion channelrhodopsins (top) and Cl⁻/H⁺ pumps (bottom). For anion
1019 channelrhodopsins, photocurrent magnitude and direction depend on chloride reversal potential
1020 (ECl) and holding potential (V_{hold}), while Cl⁻/H⁺ pumps always induce outward currents.

1021 B Example photocurrents in response to a 1 s light exposure (20 mW/mm²).

1022 C,D Photocurrent peak (C) and steady-state (D) amplitude (mean \pm SEM, across cells). GtACRs
1023 induced larger photocurrents than Cl⁻/H⁺ pumps.

1024 E-G Photocurrent activation (E), inactivation (F) and deactivation (G) time constants (mean \pm SEM).
1025 Photocurrents induced by Cl⁻/H⁺ pumps showed minimal inactivation and faster deactivation
1026 kinetics than GtACRs. eNpHR3.0 photocurrents did not inactivate hence no inactivation time
1027 constant was computed.

1028 See also Figure 8-figure supplement 1.

1029 **Figure 8-figure supplement 1. Photocurrent properties vs. irradiance**

1030 A Example GtACR1 photocurrents obtained by providing a 1 s light periods at different holding
1031 potentials (V_{hold}) using intracellular solutions approximating either embryonic or larval ECl. Orange
1032 traces denote holding potentials closest to ECl.

1033 B GtACR1 photocurrent I-V curves (mean \pm SD). Photocurrents reverse with a positive 5-10 mV
1034 shift relative to ECl (dotted lines) in both solutions.

1035 C Example photocurrents from an eNpHR3.0-expressing cell at different irradiance levels (3-
1036 20 mW/mm²).

1037 D,E Photocurrent peak (D) and steady-state (E) amplitude vs. irradiance (mean \pm SEM, across cells).
1038 Asterisks indicate a significant non-zero slope.

1039 F-H Photocurrent activation (F), inactivation (G) and deactivation (H) time constants vs. irradiance
1040 (mean \pm SEM). eNpHR3.0 photocurrents did not inactivate hence no inactivation time constant was
1041 computed.

1042 **Figure 8–Source Data 1. Data related to Figure 8.**

1043 Data provided as a XLSX file.

1044 **Figure 9. GtACRs and eNpHR3.0 effectively inhibited spiking**

1045 **A** Example voltage deflections induced by anion channelrhodopsins and Cl^-/H^+ pumps in response
1046 to a 1 s light pulse (20 mW/mm²).

1047 **B–D** Peak (**B**) and steady-state (**C**) responses and deactivation time constant (**D**) of voltage
1048 deflections. All opsins induced similar absolute voltage changes. Anion channelrhodopsins
1049 generated depolarisation with both intracellular solutions while Cl^-/H^+ pumps generated
1050 hyperpolarisation.

1051 **E** Example recordings demonstrating inhibition of single spikes in GtACR1- and eNpHR3.0-
1052 expressing cells with 5 ms light pulses (3 mW/mm²).

1053 **F** Fraction of spikes that were optogenetically inhibited (mean \pm SEM, across cells). All opsins
1054 achieved high suppression efficacy, but GtACR1 induced additional spikes upon light delivery with
1055 the embryonic intracellular solution.

1056 **G** Example recordings demonstrating inhibition of sustained spiking in GtACR1- and eNpHR3.0-
1057 expressing cells.

1058 **H** Quantification of suppression using protocol illustrated in G. Number of spikes per 50 ms during
1059 light delivery (0–10 mW/mm²) is plotted against irradiance. GtACR1 and eNpHR3.0 inhibited tonic
1060 spiking with similar efficacy (mean \pm SEM).

1061 See also Figure 9–figure supplement 1.

1062 **Figure 9-figure supplement 1. Optogenetically-evoked voltage responses vs. irradiance**

1063 **A–C** Peak (**A**) and steady-state (**B**) responses and deactivation time constant (**C**) of voltage
1064 deflections vs. irradiance (mean \pm SEM, across cells). eArch3.0 was the only opsin showing
1065 irradiance-dependent modulation of peak voltage response.

1066 **Figure 9–Source Data 1. Data related to Figure 9.**

1067 Data provided as a XLSX file.

1068 **Figure 10. Summary of opsin line efficacy**

1069 **A** Efficacy of cation channelrhodopsin lines in inducing neural activity across behavioural assays,
1070 electrophysiological recordings, developmental stages and wavelengths. The radius of each circle is
1071 proportional to efficacy.

1072 **B** Efficacy of anion channelrhodopsins and Cl^-/H^+ pumps in suppressing neural activity.

1073 **References**

- 1074 Adamantidis, A., Arber, S., Bains, J.S., Bamberg, E., Bonci, A., Buzsaki, G., Cardin, J.A., Costa, R.M., Dan,
1075 Y., Goda, Y., *et al.* (2015). Optogenetics: 10 years after ChR2 in neurons--views from the community. *Nat*
1076 *Neurosci* *18*, 1202-1212.
- 1077 Andalman, A.S., Burns, V.M., Lovett-Barron, M., Broxton, M., Poole, B., Yang, S.J., Grosenick, L., Lerner,
1078 T.N., Chen, R., Benster, T., *et al.* (2019). Neuronal Dynamics Regulating Brain and Behavioral State
1079 Transitions. *Cell* *177*, 970-985.e920.
- 1080 Antinucci, P., Folgueira, M., and Bianco, I.H. (2019). Pretectal neurons control hunting behaviour. *Elife* *8*.
- 1081 Arrenberg, A.B., Del Bene, F., and Baier, H. (2009). Optical control of zebrafish behavior with
1082 halorhodopsin. *Proc Natl Acad Sci U S A* *106*, 17968-17973.
- 1083 Arrenberg, A.B., and Driever, W. (2013). Integrating anatomy and function for zebrafish circuit analysis.
1084 *Front Neural Circuits* *7*, 74.
- 1085 Asakawa, K., and Kawakami, K. (2008). Targeted gene expression by the Gal4-UAS system in zebrafish. *Dev*
1086 *Growth Differ* *50*, 391-399.
- 1087 Asakawa, K., Suster, M.L., Mizusawa, K., Nagayoshi, S., Kotani, T., Urasaki, A., Kishimoto, Y., Hibi, M.,
1088 and Kawakami, K. (2008). Genetic dissection of neural circuits by Tol2 transposon-mediated Gal4 gene and
1089 enhancer trapping in zebrafish. *Proc Natl Acad Sci U S A* *105*, 1255-1260.
- 1090 Balciunas, D., Davidson, A.E., Sivasubbu, S., Hermanson, S.B., Welle, Z., and Ekker, S.C. (2004). Enhancer
1091 trapping in zebrafish using the Sleeping Beauty transposon. *BMC Genomics* *5*, 62.
- 1092 Beattie, C.E., Hatta, K., Halpern, M.E., Liu, H., Eisen, J.S., and Kimmel, C.B. (1997). Temporal separation
1093 in the specification of primary and secondary motoneurons in zebrafish. *Dev Biol* *187*, 171-182.
- 1094 Bello-Rojas, S., Istrate, A.E., Kishore, S., and McLean, D.L. (2019). Central and peripheral innervation
1095 patterns of defined axial motor units in larval zebrafish. *J Comp Neurol* *527*, 2557-2572.
- 1096 Ben Fredj, N., Hammond, S., Otsuna, H., Chien, C.B., Burrone, J., and Meyer, M.P. (2010). Synaptic
1097 activity and activity-dependent competition regulates axon arbor maturation, growth arrest, and territory in
1098 the retinotectal projection. *J Neurosci* *30*, 10939-10951.
- 1099 Ben-Ari, Y. (2002). Excitatory actions of gaba during development: the nature of the nurture. *Nat Rev*
1100 *Neurosci* *3*, 728-739.

1101 Bernal Sierra, Y.A., Rost, B.R., Pofahl, M., Fernandes, A.M., Kopton, R.A., Moser, S., Holtkamp, D.,
1102 Masala, N., Beed, P., Tukker, J.J., *et al.* (2018). Potassium channel-based optogenetic silencing. *Nat*
1103 *Commun* 9, 4611.

1104 Berndt, A., Schoenenberger, P., Mattis, J., Tye, K.M., Deisseroth, K., Hegemann, P., and Oertner, T.G.
1105 (2011). High-efficiency channelrhodopsins for fast neuronal stimulation at low light levels. *Proc Natl Acad*
1106 *Sci U S A* 108, 7595-7600.

1107 Berndt, A., Lee, S.Y., Wietek, J., Ramakrishnan, C., Steinberg, E.E., Rashid, A.J., Kim, H., Park, S.,
1108 Santoro, A., Frankland, P.W., *et al.* (2016). Structural foundations of optogenetics: Determinants of
1109 channelrhodopsin ion selectivity. *Proc Natl Acad Sci U S A* 113, 822-829.

1110 Bohm, U.L., Prendergast, A., Djenoune, L., Nunes Figueiredo, S., Gomez, J., Stokes, C., Kaiser, S., Suster,
1111 M., Kawakami, K., Charpentier, M., *et al.* (2016). CSF-contacting neurons regulate locomotion by relaying
1112 mechanical stimuli to spinal circuits. *Nat Commun* 7, 10866.

1113 Boyden, E.S., Zhang, F., Bamberg, E., Nagel, G., and Deisseroth, K. (2005). Millisecond-timescale,
1114 genetically targeted optical control of neural activity. *Nat Neurosci* 8, 1263-1268.

1115 Boyden, E.S. (2011). A history of optogenetics: the development of tools for controlling brain circuits with
1116 light. *F1000 Biol Rep* 3, 11.

1117 Boyden, E.S. (2015). Optogenetics and the future of neuroscience. *Nat Neurosci* 18, 1200-1201.

1118 Chow, B.Y., Han, X., Dobry, A.S., Qian, X., Chuong, A.S., Li, M., Henninger, M.A., Belfort, G.M., Lin,
1119 Y., Monahan, P.E., *et al.* (2010). High-performance genetically targetable optical neural silencing by light-
1120 driven proton pumps. *Nature* 463, 98-102.

1121 Deisseroth, K. (2015). Optogenetics: 10 years of microbial opsins in neuroscience. *Nat Neurosci* 18, 1213-
1122 1225.

1123 Deisseroth, K., and Hegemann, P. (2017). The form and function of channelrhodopsin. *Science* 357.

1124 Del Bene, F., and Wyart, C. (2012). Optogenetics: a new enlightenment age for zebrafish neurobiology. *Dev*
1125 *Neurobiol* 72, 404-414.

1126 Douglass, A.D., Kraves, S., Deisseroth, K., Schier, A.F., and Engert, F. (2008). Escape behavior elicited by
1127 single, channelrhodopsin-2-evoked spikes in zebrafish somatosensory neurons. *Curr Biol* 18, 1133-1137.

1128 Drapeau, P., Ali, D.W., Buss, R.R., and Saint-Amant, L. (1999). In vivo recording from identifiable neurons
1129 of the locomotor network in the developing zebrafish. *J Neurosci Methods* 88, 1-13.

1130 Fidelin, K., Djenoune, L., Stokes, C., Prendergast, A., Gomez, J., Baradel, A., Del Bene, F., and Wyart, C.
1131 (2015). State-Dependent Modulation of Locomotion by GABAergic Spinal Sensory Neurons. *Curr Biol* 25,
1132 3035-3047.

1133 Forster, D., Dal Maschio, M., Laurell, E., and Baier, H. (2017). An optogenetic toolbox for unbiased
1134 discovery of functionally connected cells in neural circuits. *Nat Commun* 8, 116.

1135 Friedmann, D., Hoagland, A., Berlin, S., and Isacoff, E.Y. (2015). A spinal opsin controls early neural
1136 activity and drives a behavioral light response. *Curr Biol* 25, 69-74.

1137 Fujimoto, E., Gaynes, B., Brimley, C.J., Chien, C.B., and Bonkowsky, J.L. (2011). Gal80 intersectional
1138 regulation of cell-type specific expression in vertebrates. *Dev Dyn* 240, 2324-2334.

1139 Govorunova, E.G., Sineshchekov, O.A., Janz, R., Liu, X., and Spudich, J.L. (2015). Natural light-gated
1140 anion channels: A family of microbial rhodopsins for advanced optogenetics. *Science* 349, 647-650.

1141 Gradinaru, V., Thompson, K.R., Zhang, F., Mogri, M., Kay, K., Schneider, M.B., and Deisseroth, K.
1142 (2007). Targeting and readout strategies for fast optical neural control in vitro and in vivo. *J Neurosci* 27,
1143 14231-14238.

1144 Gradinaru, V., Zhang, F., Ramakrishnan, C., Mattis, J., Prakash, R., Diester, I., Goshen, I., Thompson,
1145 K.R., and Deisseroth, K. (2010). Molecular and cellular approaches for diversifying and extending
1146 optogenetics. *Cell* 141, 154-165.

1147 Hochbaum, D.R., Zhao, Y., Farhi, S.L., Klapoetke, N., Werley, C.A., Kapoor, V., Zou, P., Kralj, J.M.,
1148 Maclaurin, D., Smedemark-Margulies, N., *et al.* (2014). All-optical electrophysiology in mammalian neurons
1149 using engineered microbial rhodopsins. *Nat Methods* 11, 825-833.

1150 Horstick, E.J., Jordan, D.C., Bergeron, S.A., Tabor, K.M., Serpe, M., Feldman, B., and Burgess, H.A.
1151 (2015). Increased functional protein expression using nucleotide sequence features enriched in highly
1152 expressed genes in zebrafish. *Nucleic Acids Res* 43, e48.

1153 Huber, D., Petreanu, L., Ghitani, N., Ranade, S., Hromadka, T., Mainen, Z., and Svoboda, K. (2008).
1154 Sparse optical microstimulation in barrel cortex drives learned behaviour in freely moving mice. *Nature* 451,
1155 61-64.

1156 Kikuta, H., and Kawakami, K. (2009). Transient and stable transgenesis using tol2 transposon vectors.
1157 *Methods Mol Biol* 546, 69-84.

1158 Kimmel, C.B., Hatta, K., and Metcalfe, W.K. (1990). Early axonal contacts during development of an
1159 identified dendrite in the brain of the zebrafish. *Neuron* 4, 535-545.

1160 Klapoetke, N.C., Murata, Y., Kim, S.S., Pulver, S.R., Birdsey-Benson, A., Cho, Y.K., Morimoto, T.K.,
1161 Chuong, A.S., Carpenter, E.J., Tian, Z., *et al.* (2014). Independent optical excitation of distinct neural
1162 populations. *Nat Methods* *11*, 338-346.

1163 Kokel, D., Dunn, T.W., Ahrens, M.B., Alshut, R., Cheung, C.Y., Saint-Amant, L., Bruni, G., Mateus, R.,
1164 van Ham, T.J., Shiraki, T., *et al.* (2013). Identification of nonvisual photomotor response cells in the
1165 vertebrate hindbrain. *J Neurosci* *33*, 3834-3843.

1166 Li, N., Chen, S., Guo, Z.V., Chen, H., Huo, Y., Inagaki, H.K., Chen, G., Davis, C., Hansel, D., Guo, C., *et*
1167 *al.* (2019). Spatiotemporal constraints on optogenetic inactivation in cortical circuits. *Elife* *8*.

1168 Lister, J.A., Robertson, C.P., Lepage, T., Johnson, S.L., and Raible, D.W. (1999). nacre encodes a zebrafish
1169 microphthalmia-related protein that regulates neural-crest-derived pigment cell fate. *Development* *126*, 3757-
1170 3767.

1171 Luo, L., Callaway, E.M., and Svoboda, K. (2008). Genetic dissection of neural circuits. *Neuron* *57*, 634-660.

1172 Mahn, M., Prigge, M., Ron, S., Levy, R., and Yizhar, O. (2016). Biophysical constraints of optogenetic
1173 inhibition at presynaptic terminals. *Nat Neurosci* *19*, 554-556.

1174 Mahn, M., Gibor, L., Patil, P., Cohen-Kashi Malina, K., Oring, S., Printz, Y., Levy, R., Lampl, I., and
1175 Yizhar, O. (2018). High-efficiency optogenetic silencing with soma-targeted anion-conducting
1176 channelrhodopsins. *Nat Commun* *9*, 4125.

1177 Malyshev, A.Y., Roshchin, M.V., Smirnova, G.R., Dolgikh, D.A., Balaban, P.M., and Ostrovsky, M.A.
1178 (2017). Chloride conducting light activated channel GtACR2 can produce both cessation of firing and
1179 generation of action potentials in cortical neurons in response to light. *Neurosci Lett* *640*, 76-80.

1180 Mardinly, A.R., Oldenburg, I.A., Pegard, N.C., Sridharan, S., Lyall, E.H., Chesnov, K., Brohawn, S.G.,
1181 Waller, L., and Adesnik, H. (2018). Precise multimodal optical control of neural ensemble activity. *Nat*
1182 *Neurosci* *21*, 881-893.

1183 Margrie, T.W., Brecht, M., and Sakmann, B. (2002). In vivo, low-resistance, whole-cell recordings from
1184 neurons in the anaesthetized and awake mammalian brain. *Pflugers Arch* *444*, 491-498.

1185 Mattis, J., Tye, K.M., Ferenczi, E.A., Ramakrishnan, C., O'Shea, D.J., Prakash, R., Gunaydin, L.A., Hyun,
1186 M., Fenno, L.E., Gradinaru, V., *et al.* (2011). Principles for applying optogenetic tools derived from direct
1187 comparative analysis of microbial opsins. *Nat Methods* *9*, 159-172.

1188 Menelaou, E., and McLean, D.L. (2012). A gradient in endogenous rhythmicity and oscillatory drive matches
1189 recruitment order in an axial motor pool. *J Neurosci* *32*, 10925-10939.

- 1190 Miesenbock, G. (2009). The optogenetic catechism. *Science* 326, 395-399.
- 1191 Miesenbock, G. (2011). Optogenetic control of cells and circuits. *Annu Rev Cell Dev Biol* 27, 731-758.
- 1192 Mohamed, G.A., Cheng, R.K., Ho, J., Krishnan, S., Mohammad, F., Claridge-Chang, A., and Jesuthasan, S.
1193 (2017). Optical inhibition of larval zebrafish behaviour with anion channelrhodopsins. *BMC Biol* 15, 103.
- 1194 Portugues, R., Severi, K.E., Wyart, C., and Ahrens, M.B. (2013). Optogenetics in a transparent animal:
1195 circuit function in the larval zebrafish. *Curr Opin Neurobiol* 23, 119-126.
- 1196 Prigge, M., Schneider, F., Tsunoda, S.P., Shilyansky, C., Wietek, J., Deisseroth, K., and Hegemann, P.
1197 (2012). Color-tuned channelrhodopsins for multiwavelength optogenetics. *J Biol Chem* 287, 31804-31812.
- 1198 Reynolds, A., Brustein, E., Liao, M., Mercado, A., Babilonia, E., Mount, D.B., and Drapeau, P. (2008).
1199 Neurogenic role of the depolarizing chloride gradient revealed by global overexpression of KCC2 from the
1200 onset of development. *J Neurosci* 28, 1588-1597.
- 1201 Ronzitti, E., Conti, R., Zampini, V., Tanese, D., Foust, A.J., Klapoetke, N., Boyden, E.S., Papagiakoumou,
1202 E., and Emiliani, V. (2017). Submillisecond Optogenetic Control of Neuronal Firing with Two-Photon
1203 Holographic Photoactivation of Chronos. *J Neurosci* 37, 10679-10689.
- 1204 Sagasti, A., Guido, M.R., Raible, D.W., and Schier, A.F. (2005). Repulsive interactions shape the
1205 morphologies and functional arrangement of zebrafish peripheral sensory arbors. *Curr Biol* 15, 804-814.
- 1206 Saint-Amant, L., and Drapeau, P. (1998). Time course of the development of motor behaviors in the
1207 zebrafish embryo. *J Neurobiol* 37, 622-632.
- 1208 Saint-Amant, L., and Drapeau, P. (2000). Motoneuron activity patterns related to the earliest behavior of the
1209 zebrafish embryo. *J Neurosci* 20, 3964-3972.
- 1210 Saint-Amant, L., and Drapeau, P. (2003). Whole-cell patch-clamp recordings from identified spinal neurons
1211 in the zebrafish embryo. *Methods Cell Sci* 25, 59-64.
- 1212 Scheer, N., and Campos-Ortega, J.A. (1999). Use of the Gal4-UAS technique for targeted gene expression in
1213 the zebrafish. *Mech Dev* 80, 153-158.
- 1214 Schneider, F., Grimm, C., and Hegemann, P. (2015). Biophysics of Channelrhodopsin. *Annu Rev Biophys*
1215 44, 167-186.

1216 Scott, E.K., Mason, L., Arrenberg, A.B., Ziv, L., Gosse, N.J., Xiao, T., Chi, N.C., Asakawa, K., Kawakami,
1217 K., and Baier, H. (2007). Targeting neural circuitry in zebrafish using GAL4 enhancer trapping. *Nat*
1218 *Methods* 4, 323-326.

1219 Sjulson, L., Cassataro, D., DasGupta, S., and Miesenbock, G. (2016). Cell-Specific Targeting of Genetically
1220 Encoded Tools for Neuroscience. *Annu Rev Genet* 50, 571-594.

1221 Song, J., Ampatzis, K., Bjornfors, E.R., and El Manira, A. (2016). Motor neurons control locomotor circuit
1222 function retrogradely via gap junctions. *Nature* 529, 399-402.

1223 Sternberg, J.R., Severi, K.E., Fidelin, K., Gomez, J., Ihara, H., Alcheikh, Y., Hubbard, J.M., Kawakami, K.,
1224 Suster, M., and Wyart, C. (2016). Optimization of a Neurotoxin to Investigate the Contribution of
1225 Excitatory Interneurons to Speed Modulation In Vivo. *Curr Biol* 26, 2319-2328.

1226 Stringer, C., Michaelos, M., and Pachitariu, M. (2020). Cellpose: a generalist algorithm for cellular
1227 segmentation. *bioRxiv*, 2020.2002.2002.931238.

1228 Suster, M.L., Abe, G., Schouw, A., and Kawakami, K. (2011). Transposon-mediated BAC transgenesis in
1229 zebrafish. *Nat Protoc* 6, 1998-2021.

1230 Warp, E., Agarwal, G., Wyart, C., Friedmann, D., Oldfield, C.S., Conner, A., Del Bene, F., Arrenberg,
1231 A.B., Baier, H., and Isacoff, E.Y. (2012). Emergence of patterned activity in the developing zebrafish spinal
1232 cord. *Curr Biol* 22, 93-102.

1233 Williams, R.H., Tsunematsu, T., Thomas, A.M., Bogyo, K., Yamanaka, A., and Kilduff, T.S. (2019).
1234 Transgenic Archaelrhodopsin-3 Expression in Hypocretin/Orexin Neurons Engenders Cellular Dysfunction
1235 and Features of Type 2 Narcolepsy. *J Neurosci*.

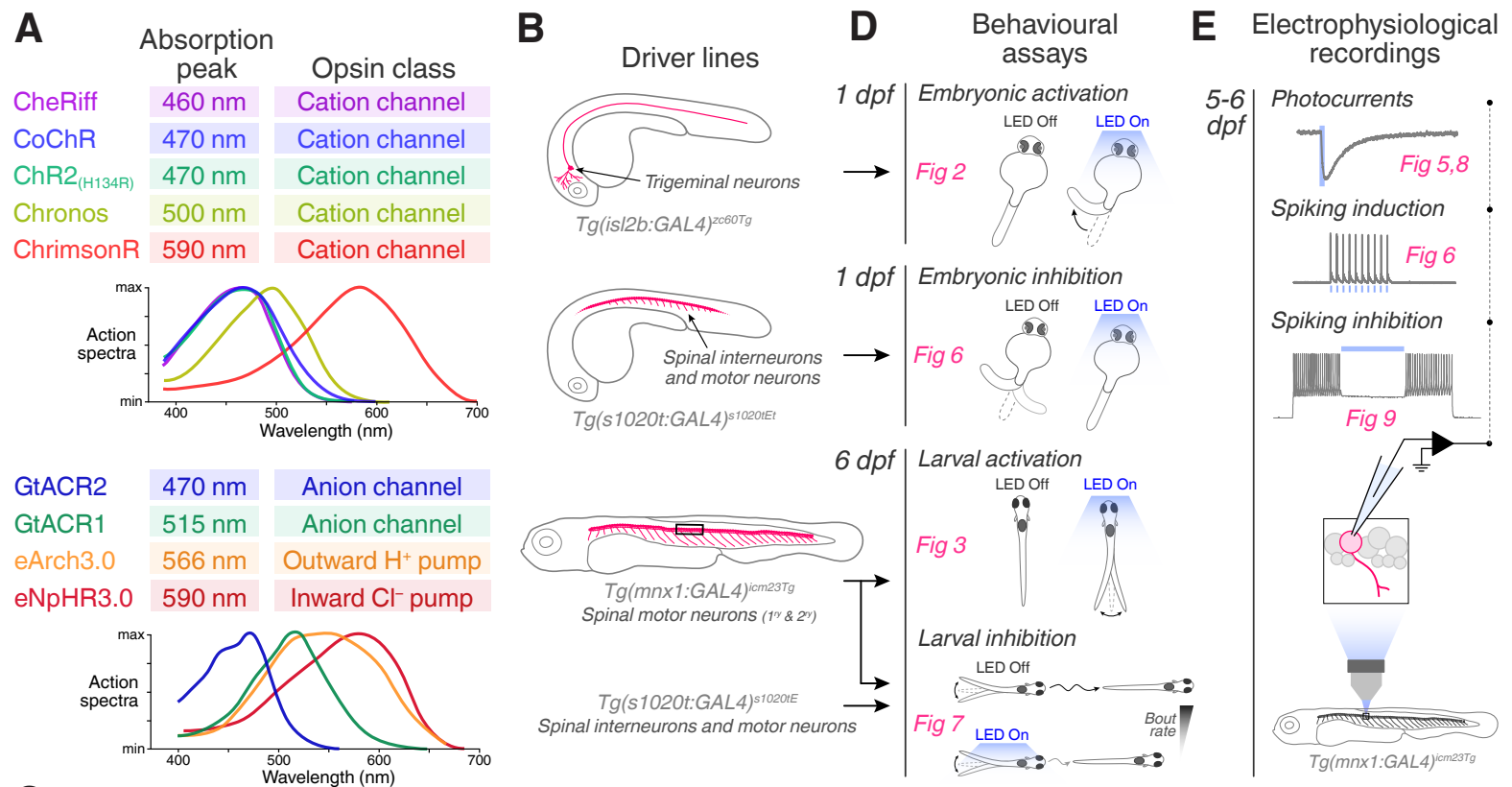
1236 Wyart, C., Del Bene, F., Warp, E., Scott, E.K., Trauner, D., Baier, H., and Isacoff, E.Y. (2009).
1237 Optogenetic dissection of a behavioural module in the vertebrate spinal cord. *Nature* 461, 407-410.

1238 Yizhar, O., Fenno, L.E., Davidson, T.J., Mogri, M., and Deisseroth, K. (2011). Optogenetics in neural
1239 systems. *Neuron* 71, 9-34.

1240 Zhang, F., Wang, L.P., Brauner, M., Liewald, J.F., Kay, K., Watzke, N., Wood, P.G., Bamberg, E., Nagel,
1241 G., Gottschalk, A., *et al.* (2007). Multimodal fast optical interrogation of neural circuitry. *Nature* 446, 633-
1242 639.

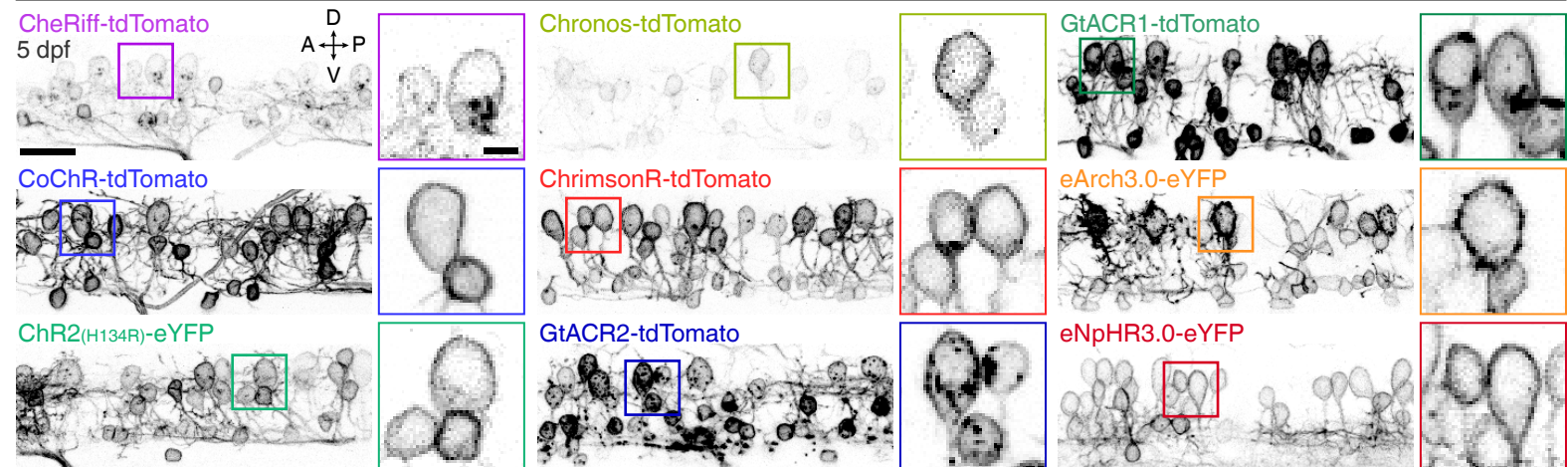
1243 Zhang, R.W., Wei, H.P., Xia, Y.M., and Du, J.L. (2010). Development of light response and GABAergic
1244 excitation-to-inhibition switch in zebrafish retinal ganglion cells. *J Physiol* 588, 2557-2569.

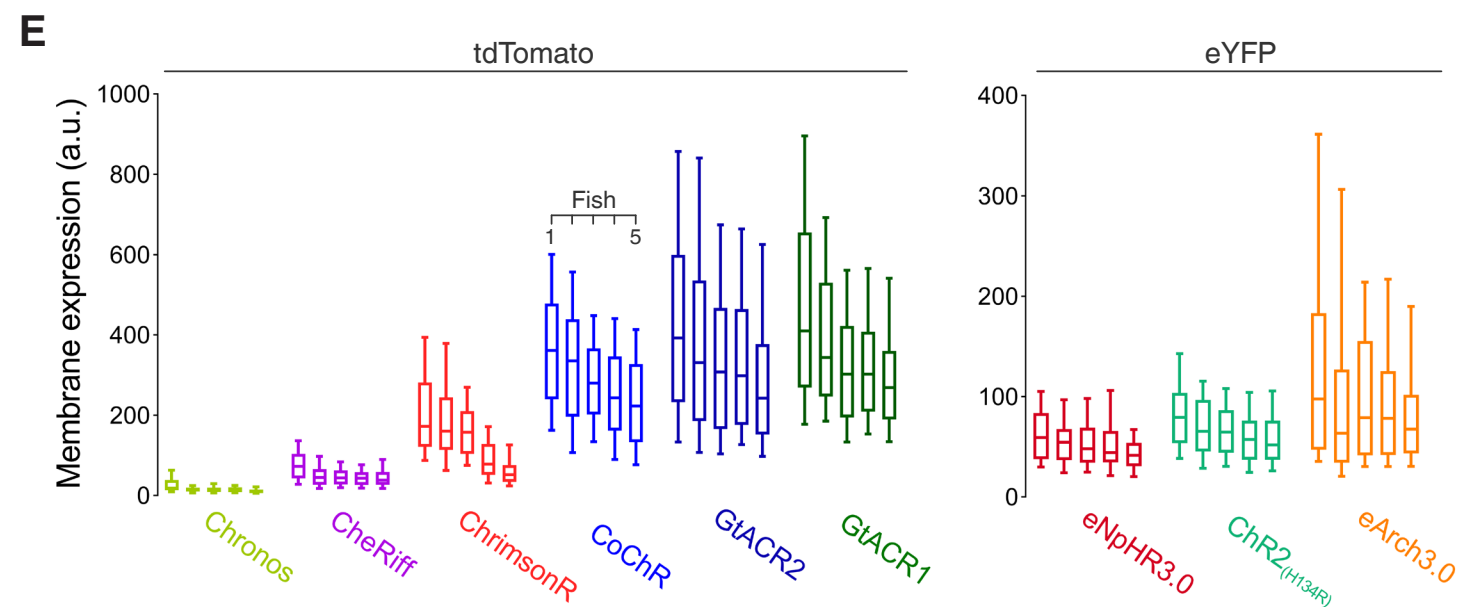
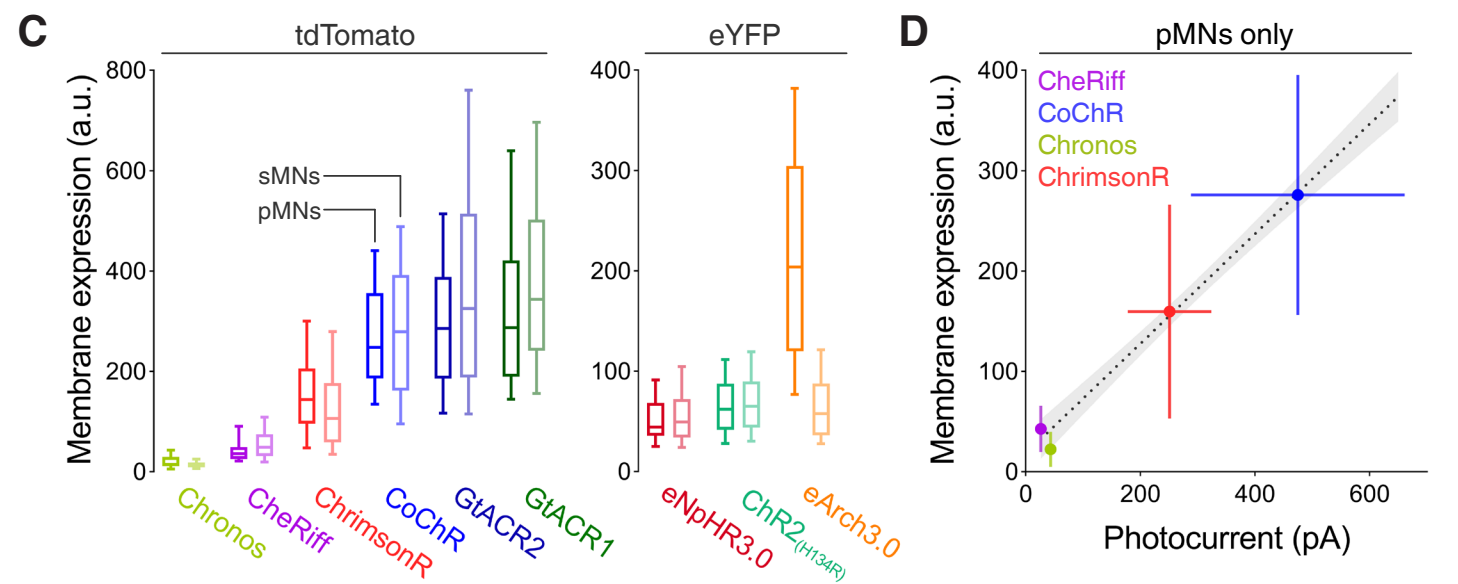
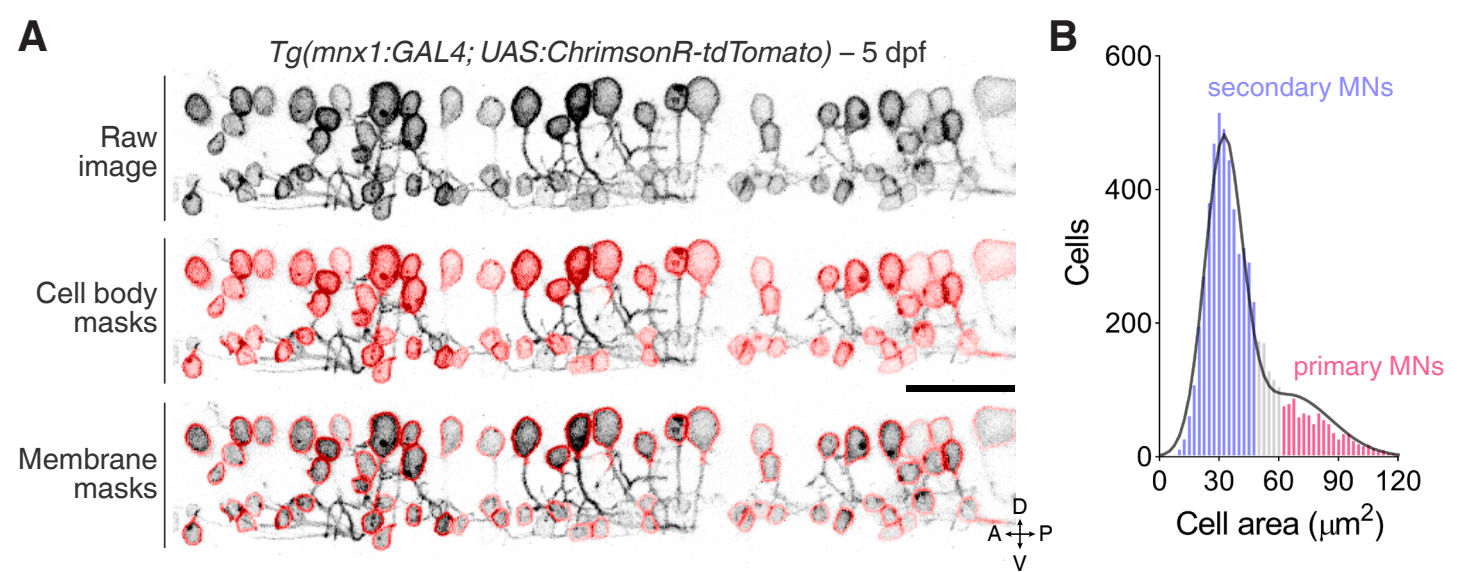
1245

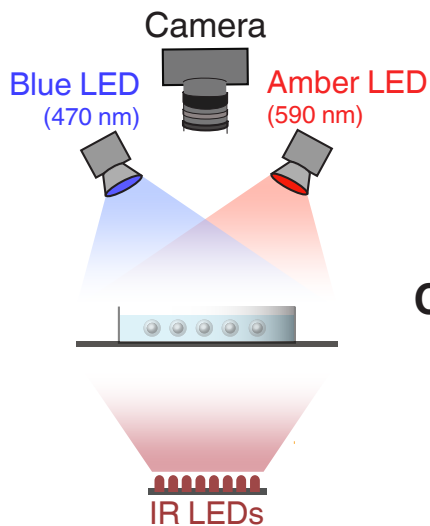
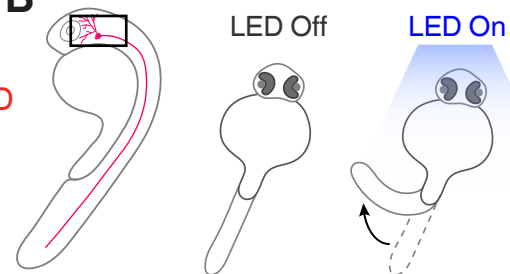
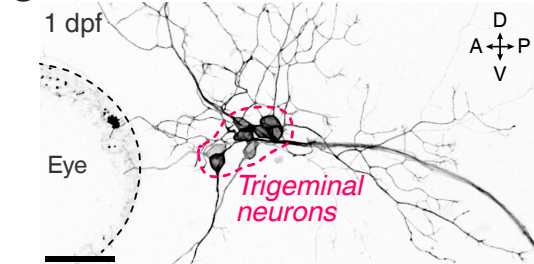
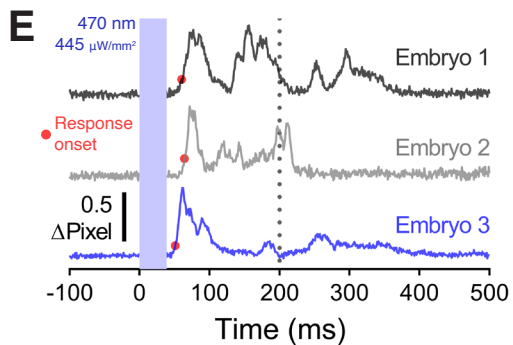
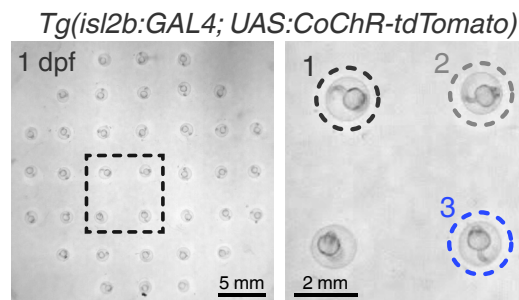


C

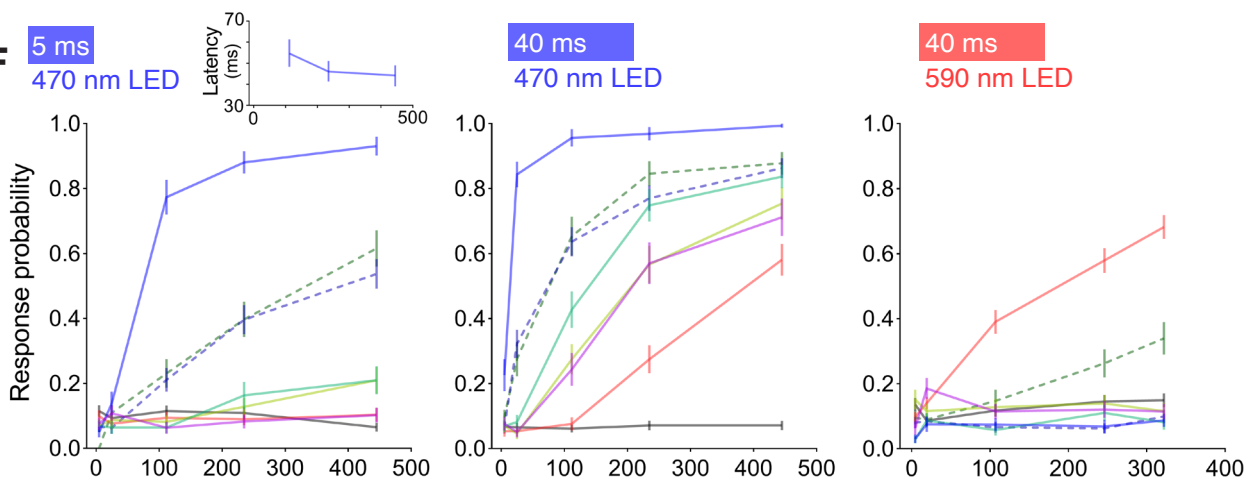
Opsin expression



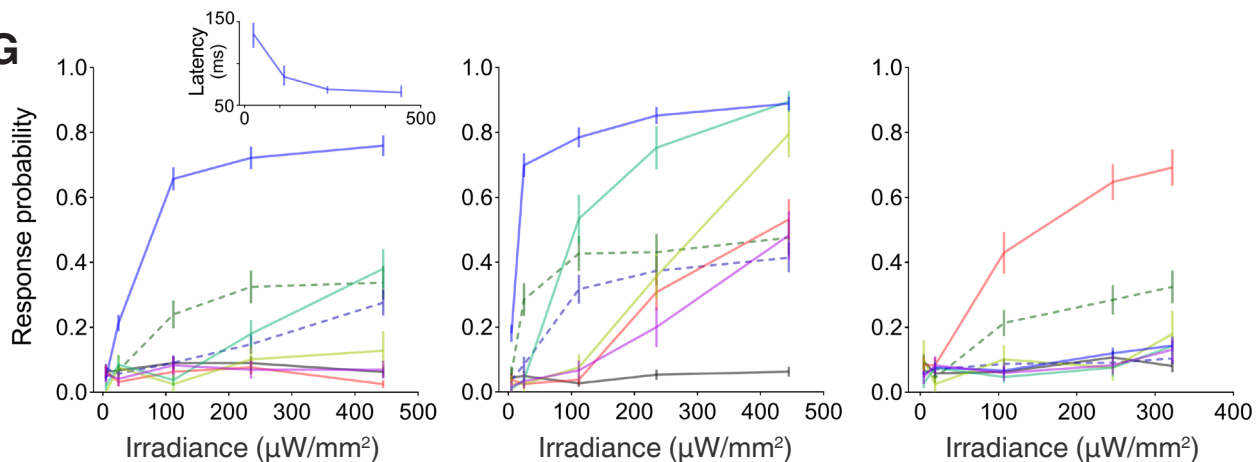


A**B****C** *Tg(isl2b:GAL4; UAS:CoChR-tdTomato)***D***Transient expression*

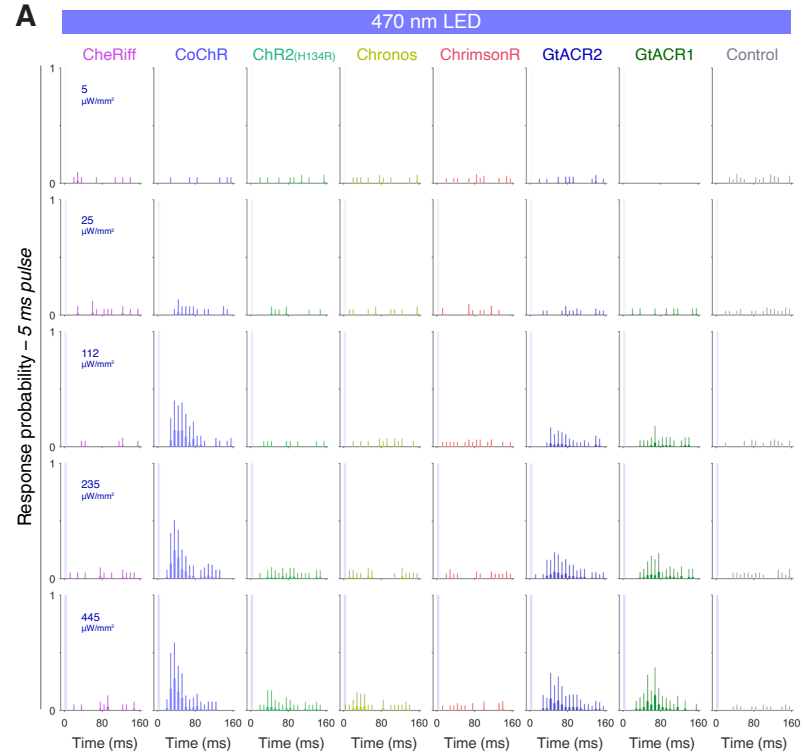
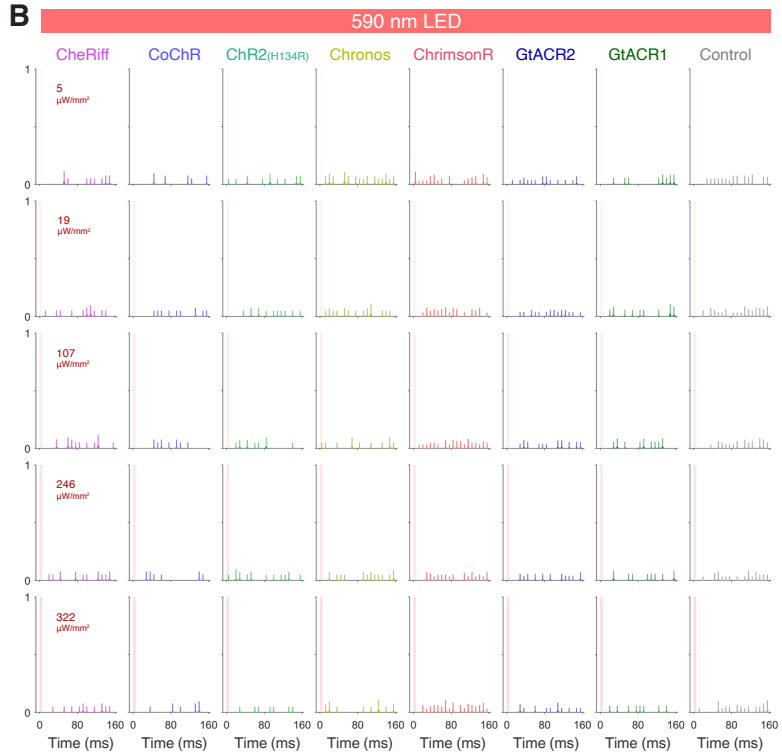
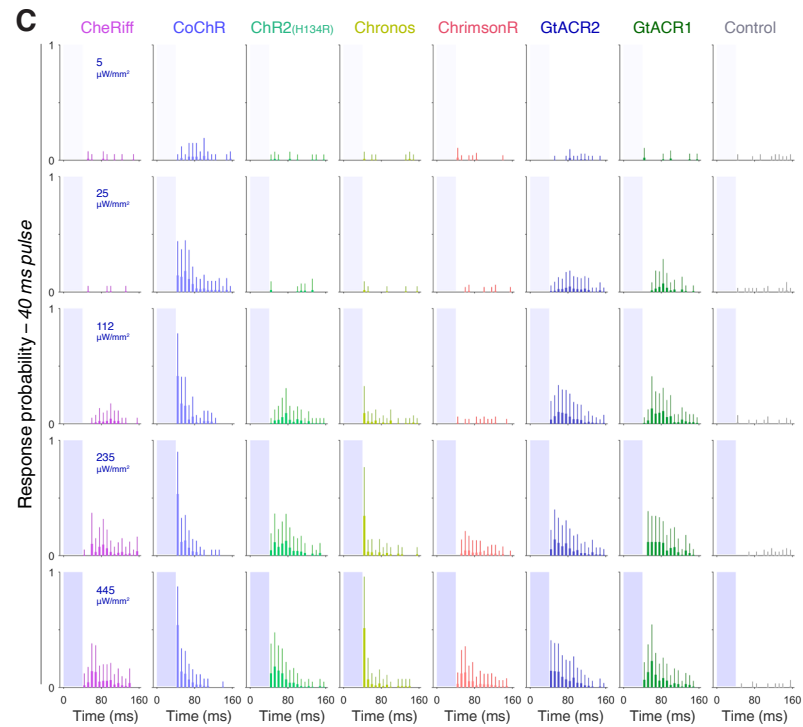
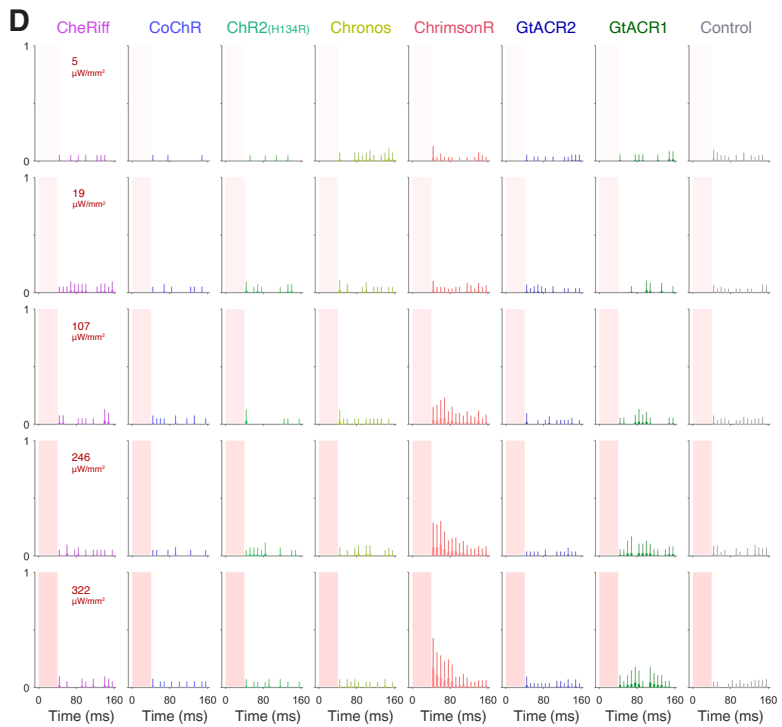
CheRiff (N = 52)
CoChR (N = 53)
ChR2(H134R) (N = 57)
Chronos (N = 57)
ChrimsonR (N = 111)
Uninjected (N = 107)
--- GtACR2 (N = 90)
--- GtACR1 (N = 52)

F*Stable lines*

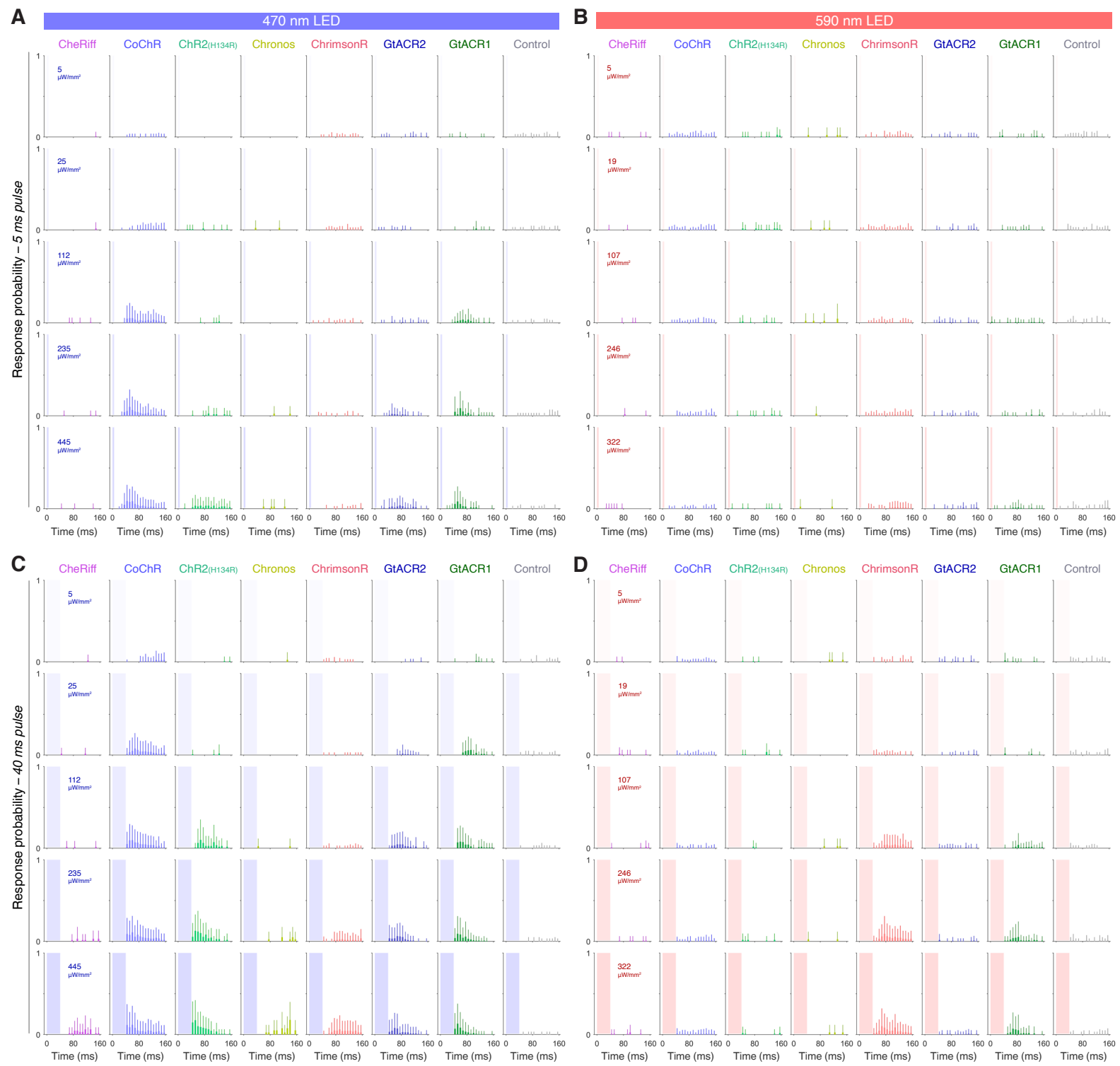
CheRiff (N = 28)
CoChR (N = 144)
ChR2(H134R) (N = 35)
Chronos (N = 13)
ChrimsonR (N = 52)
Control (N = 74)
--- GtACR2 (N = 99)
--- GtACR1 (N = 75)

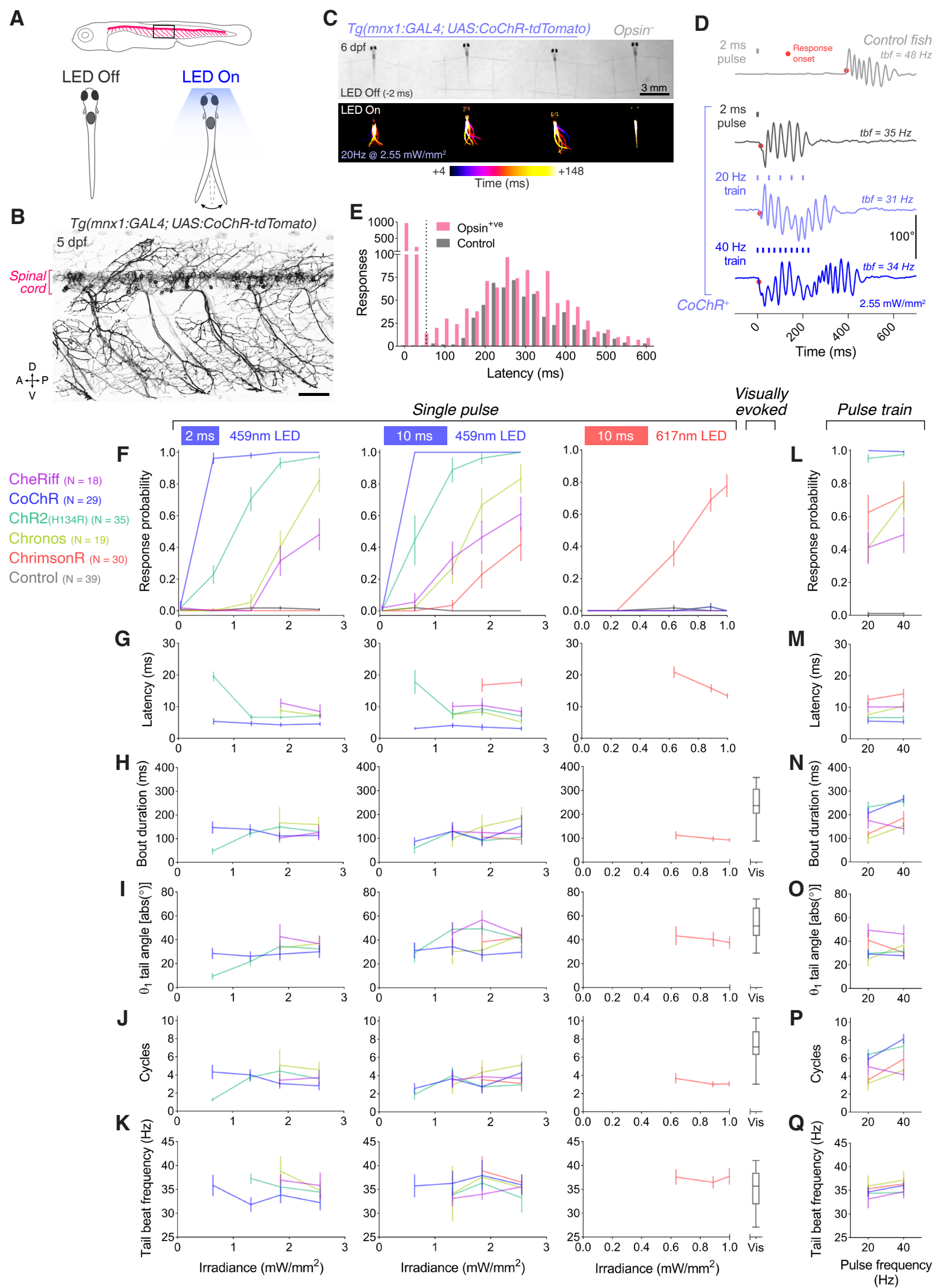
G

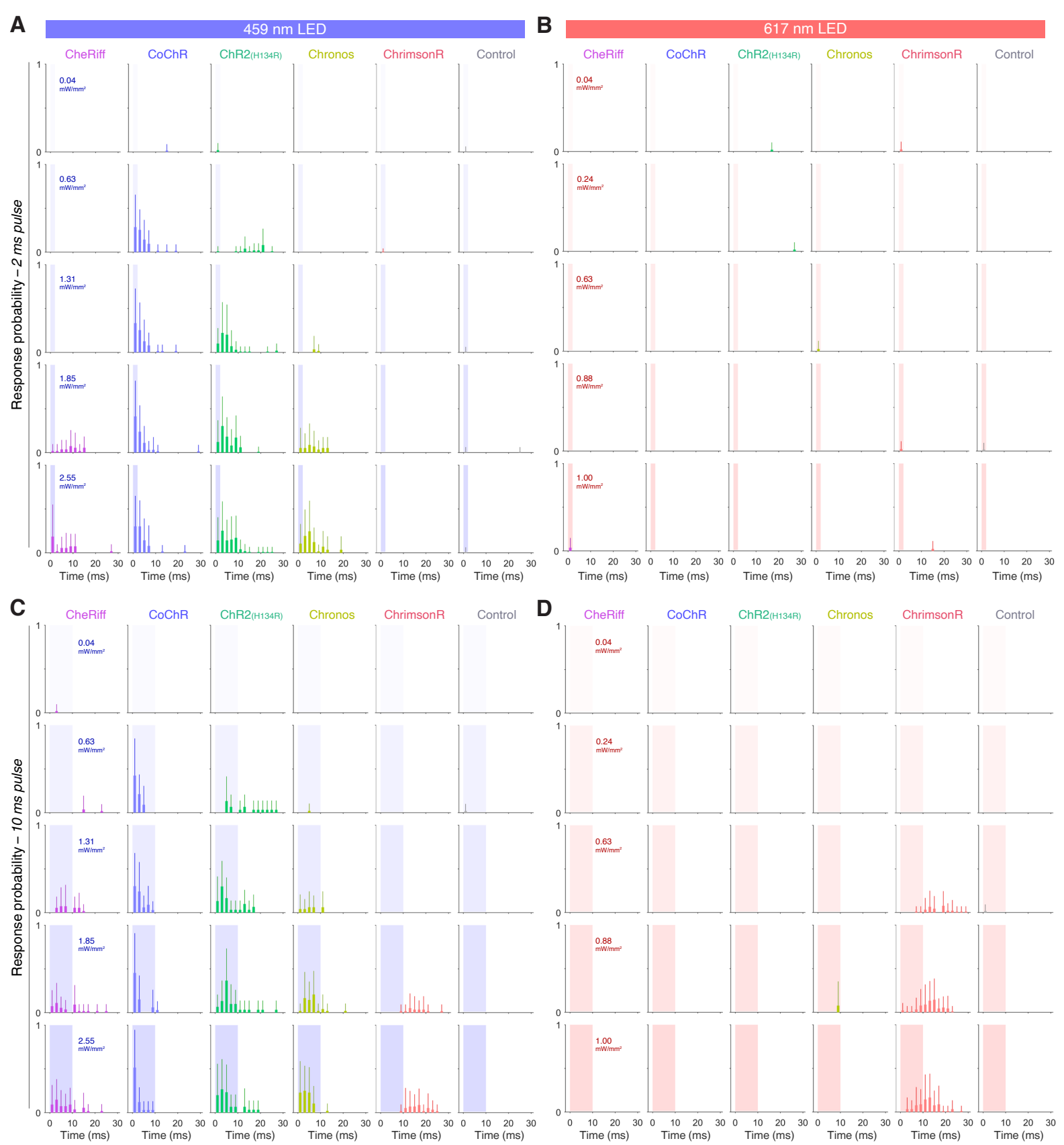
Transient expression

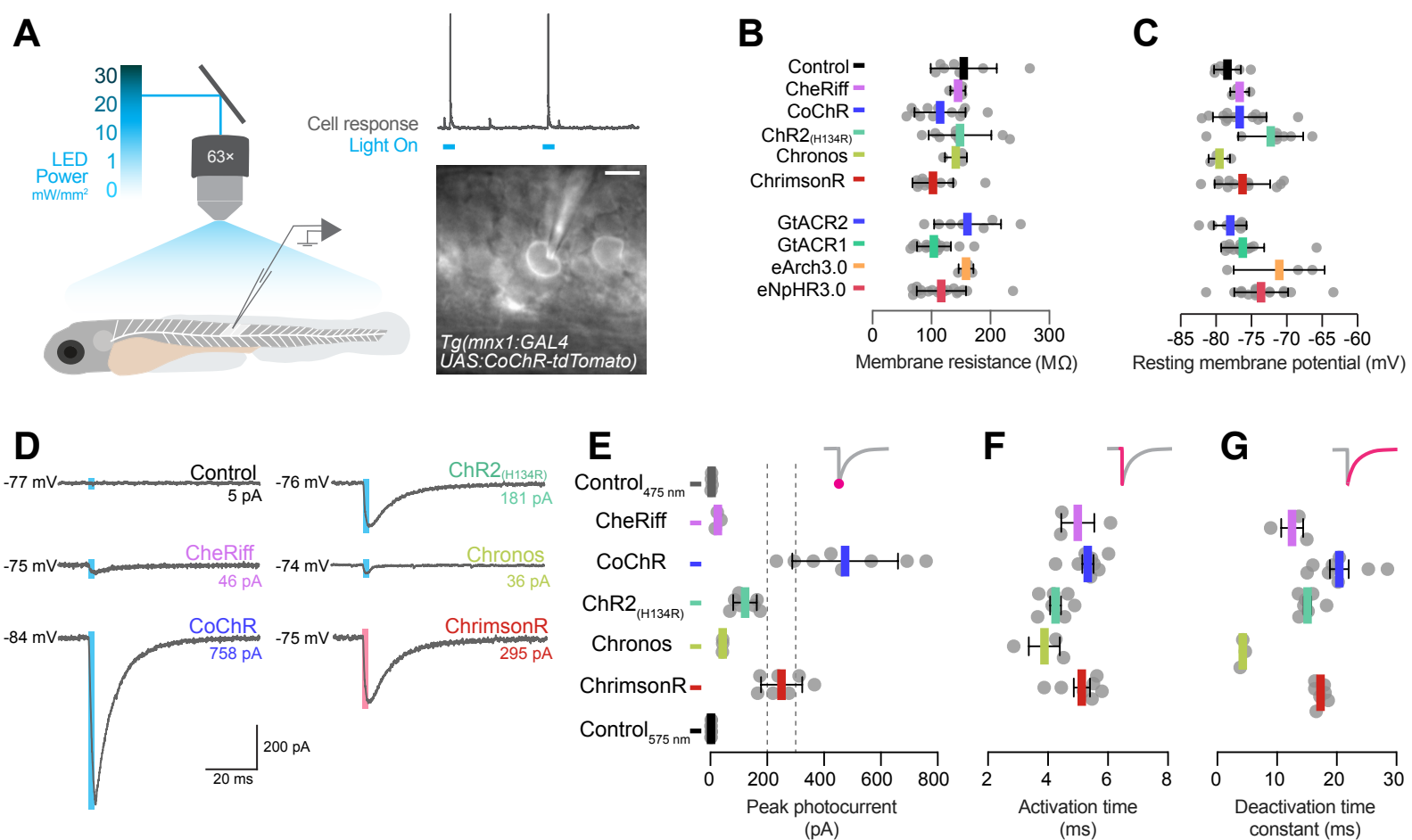
A

B

C

D


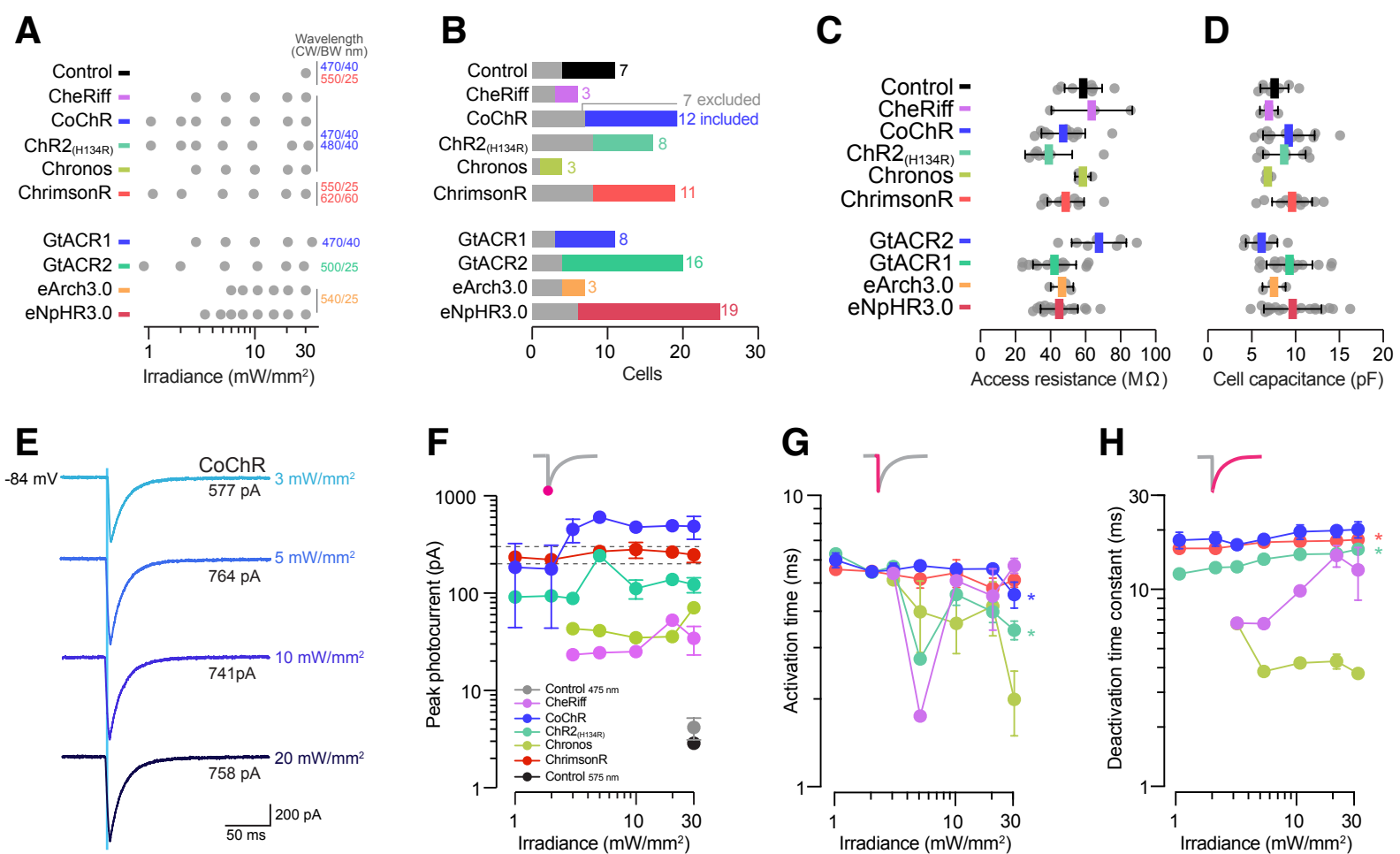
Stable lines

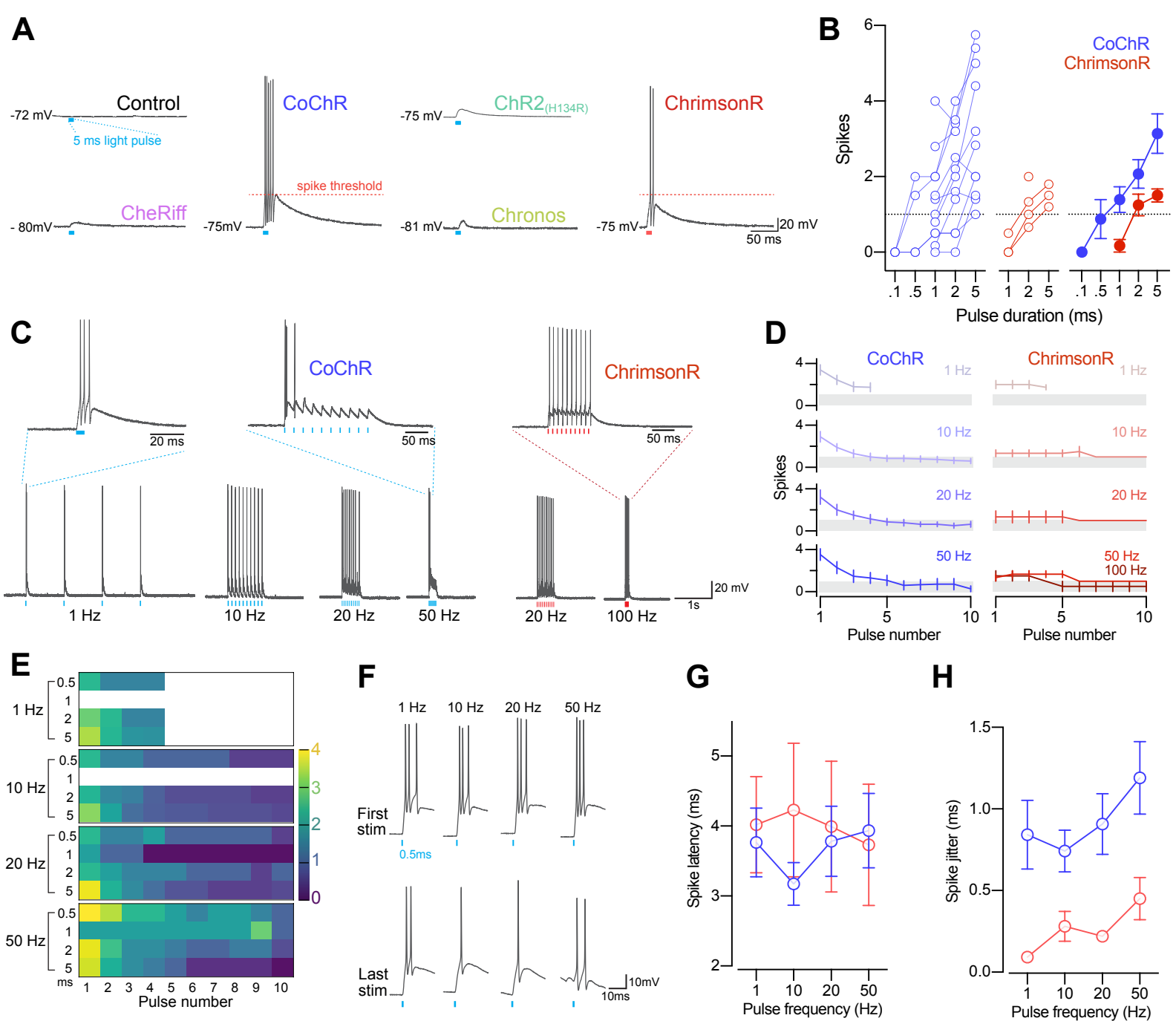


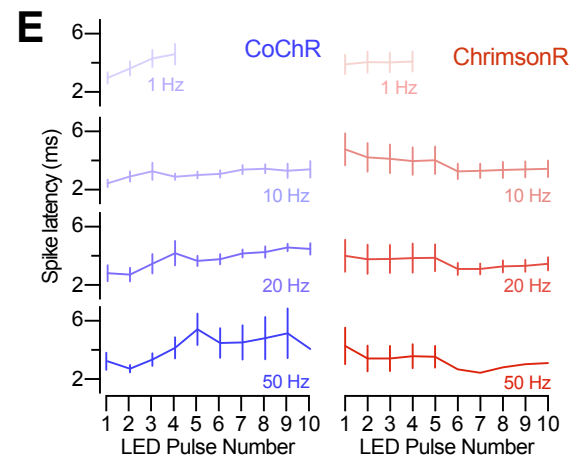
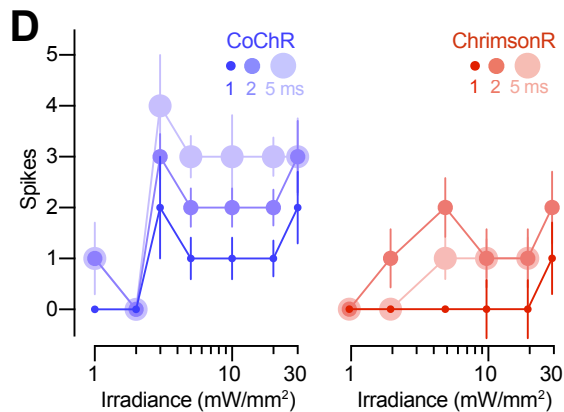
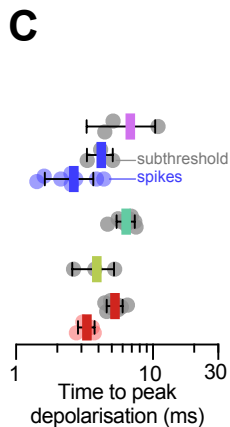
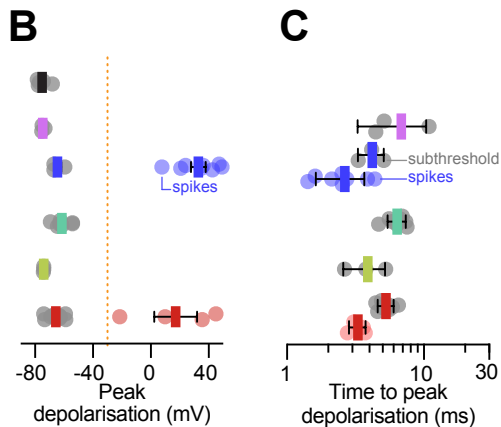
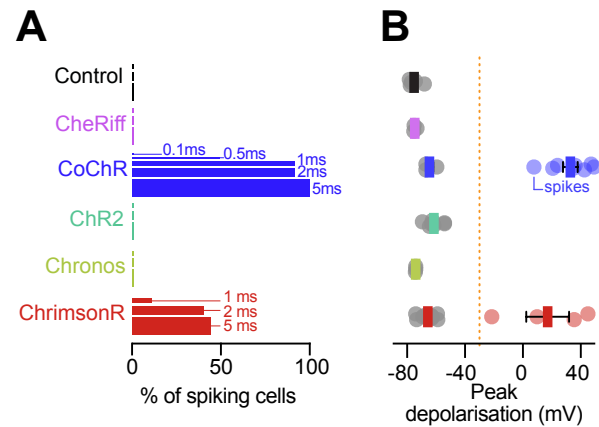


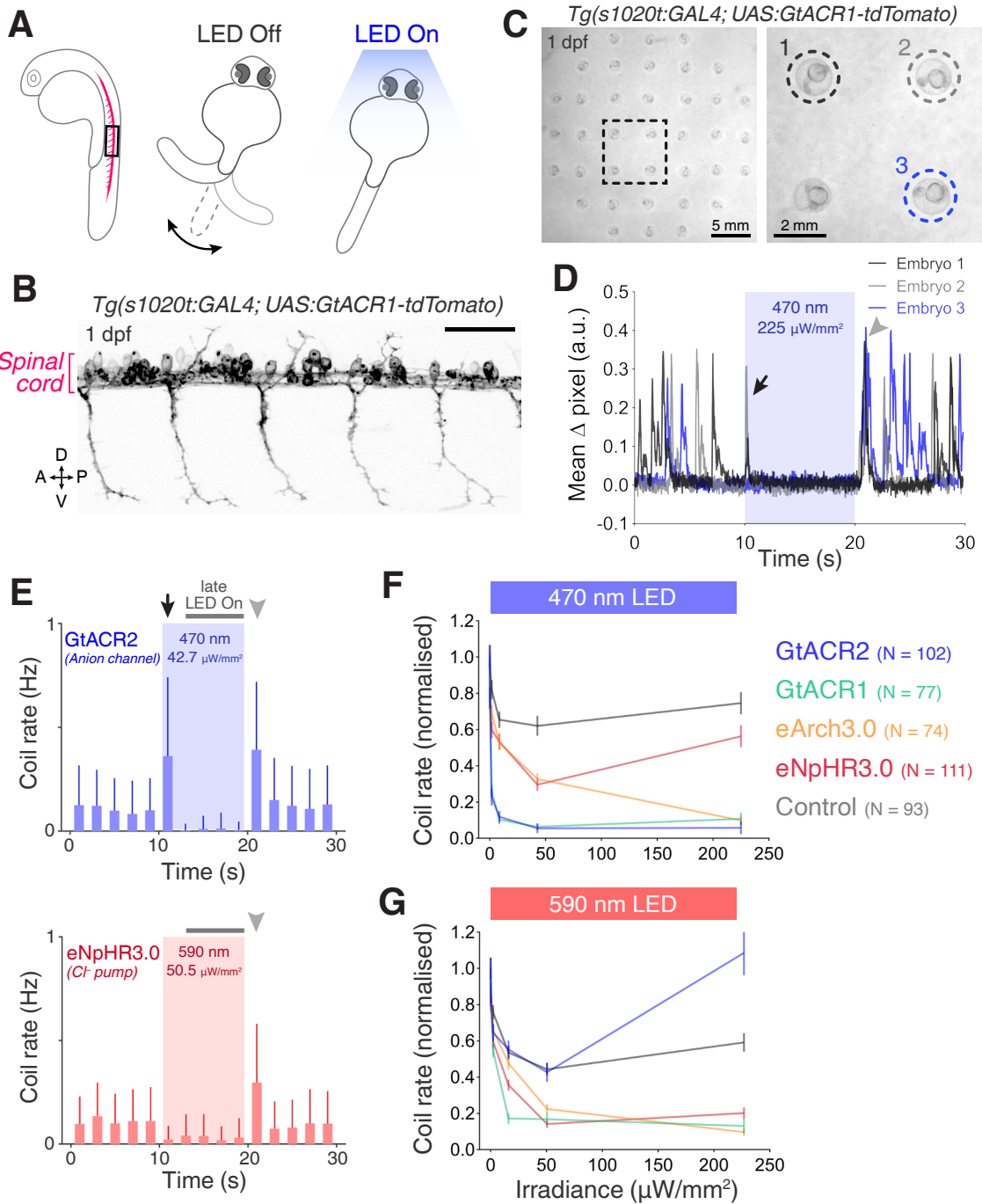






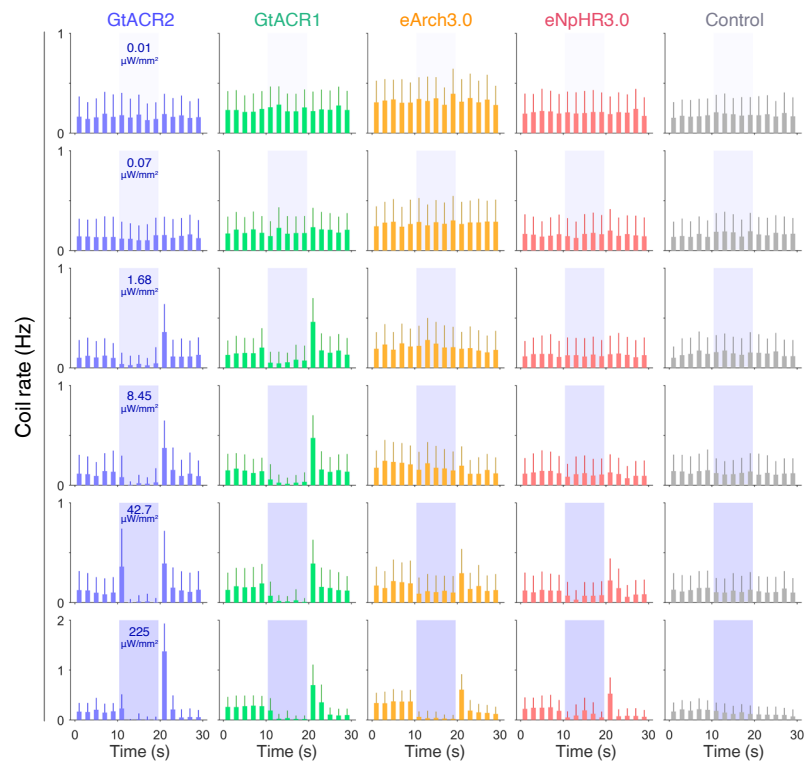




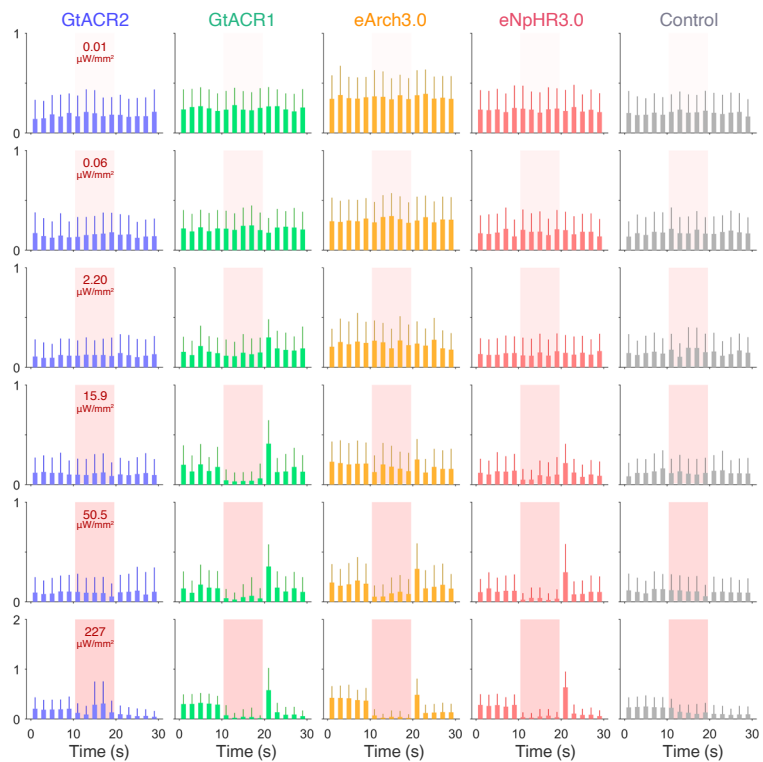


A

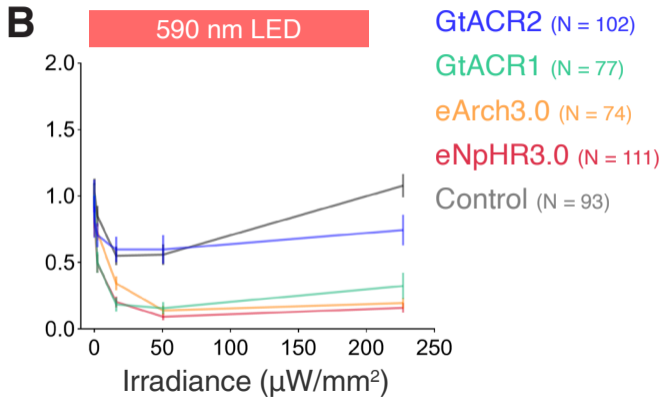
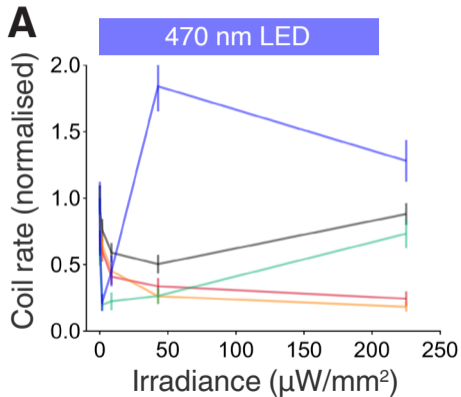
470 nm LED

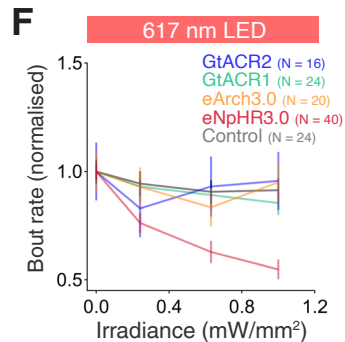
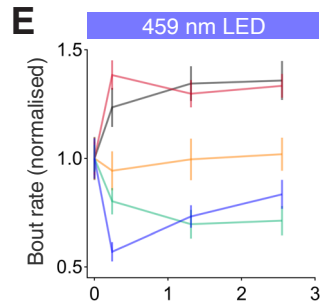
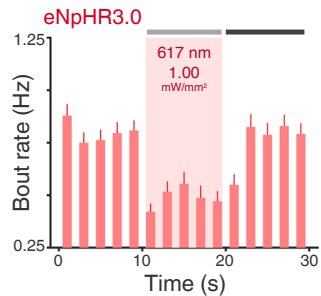
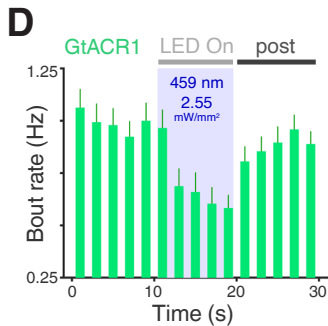
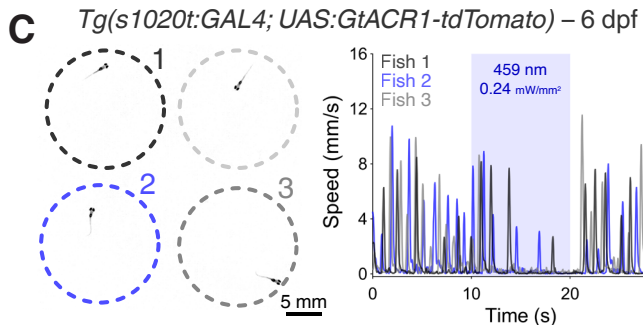
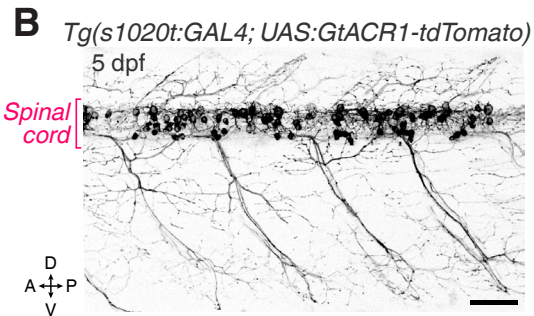
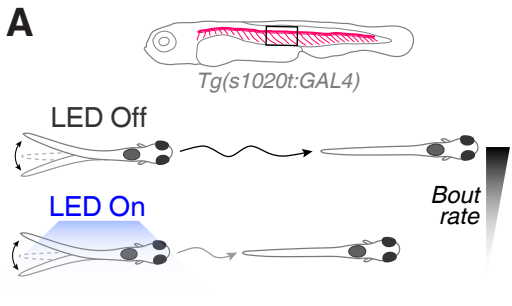
**B**

590 nm LED



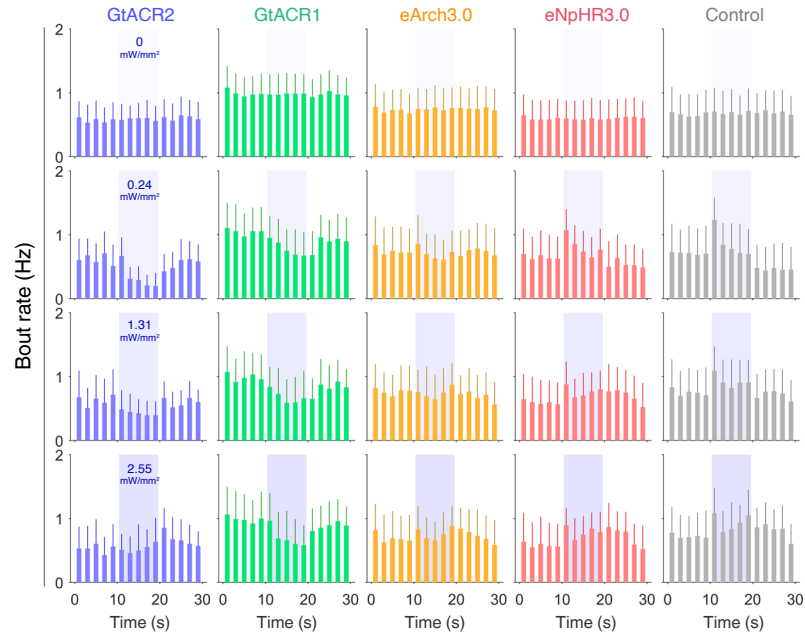
LED On – initial 2 seconds



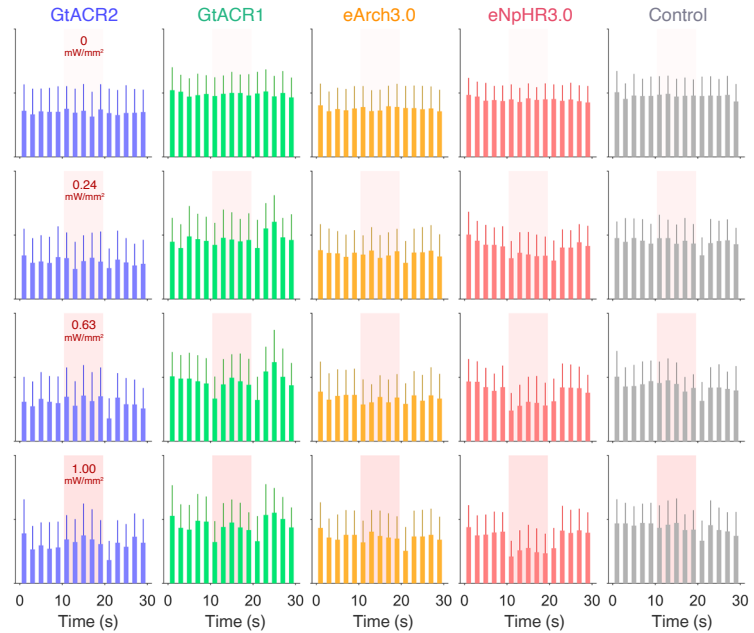


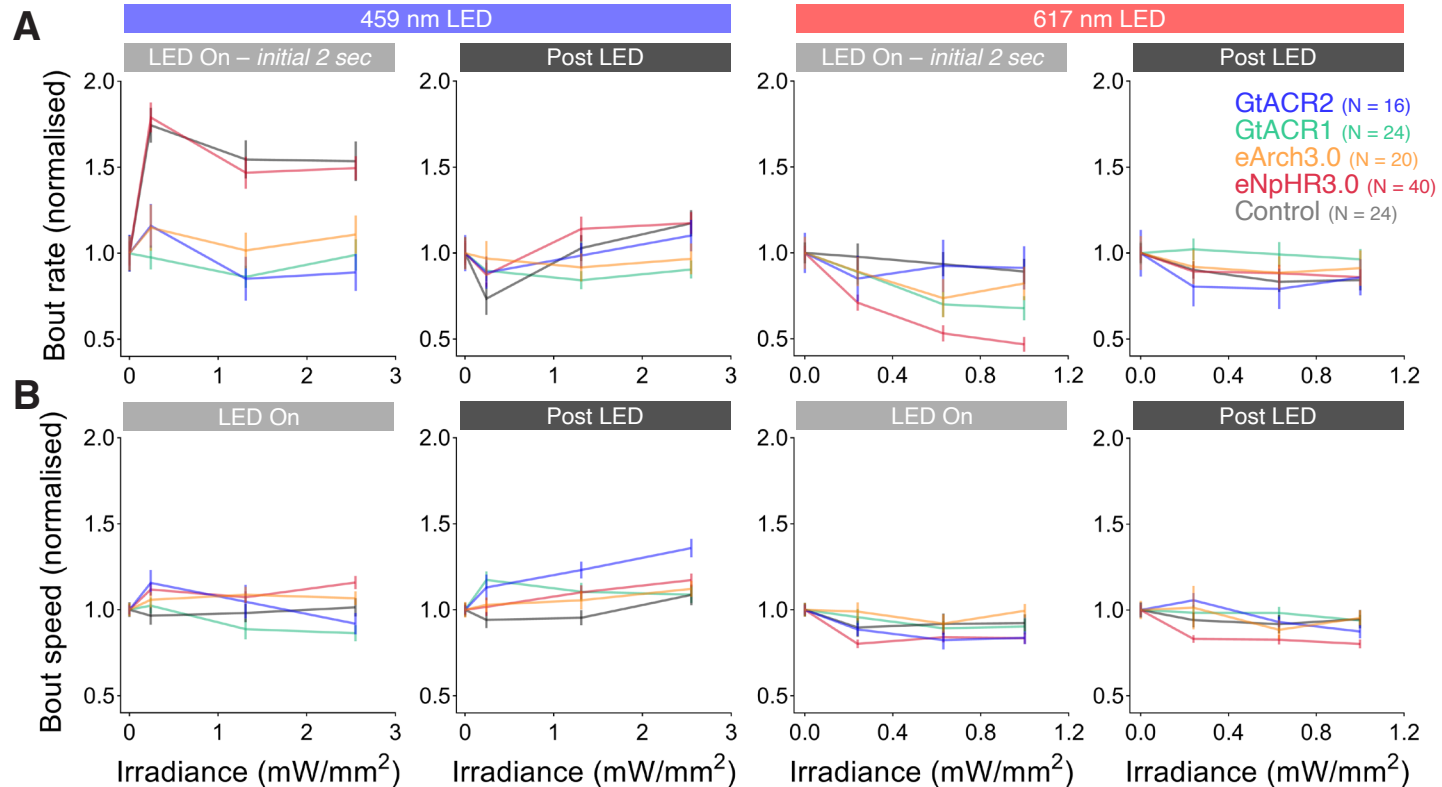
A

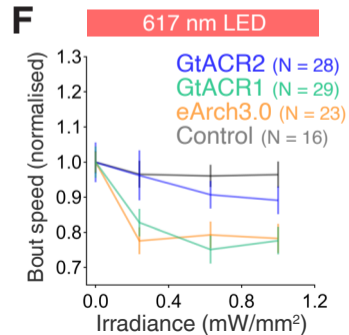
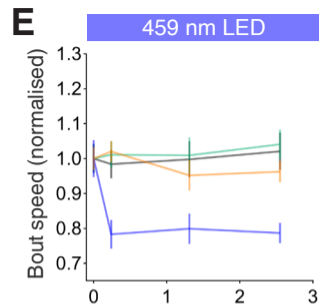
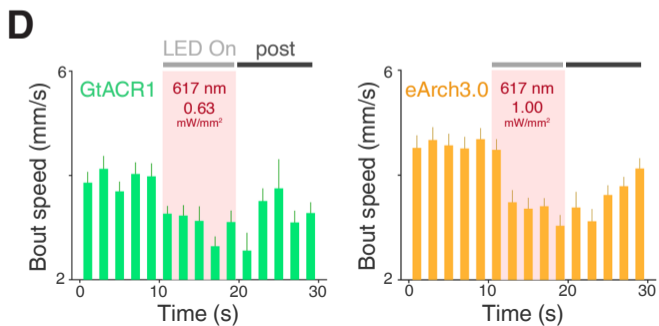
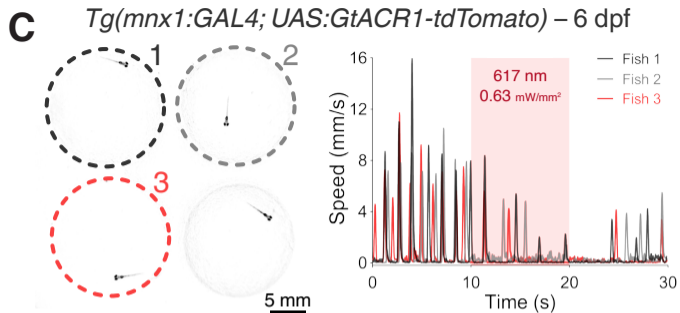
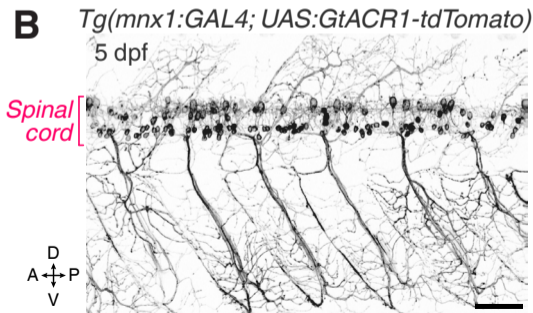
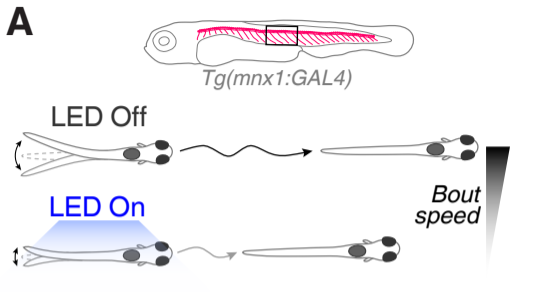
459 nm LED

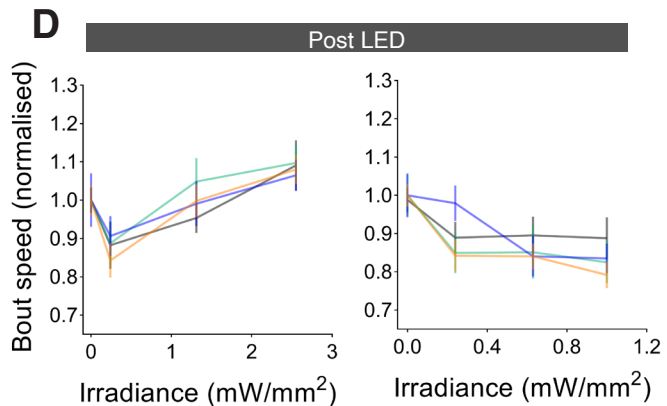
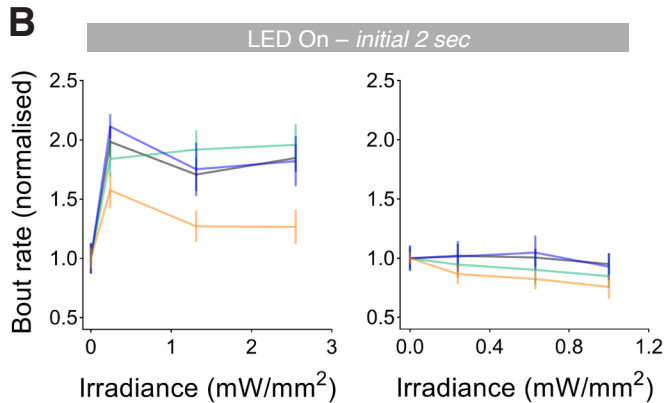
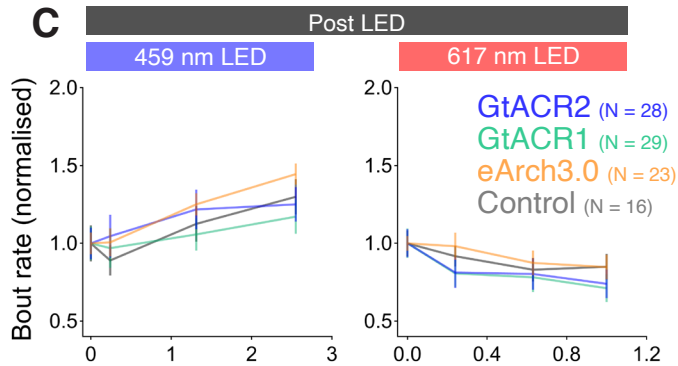
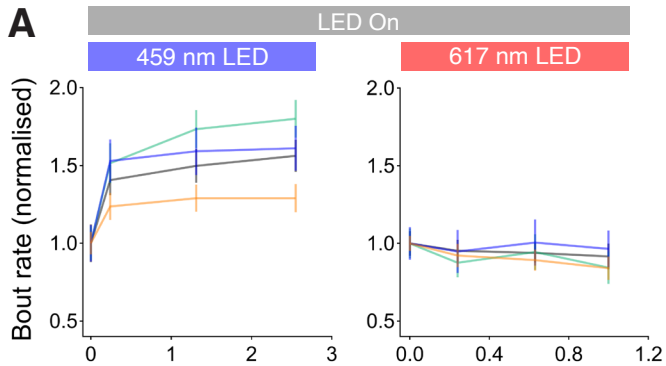
**B**

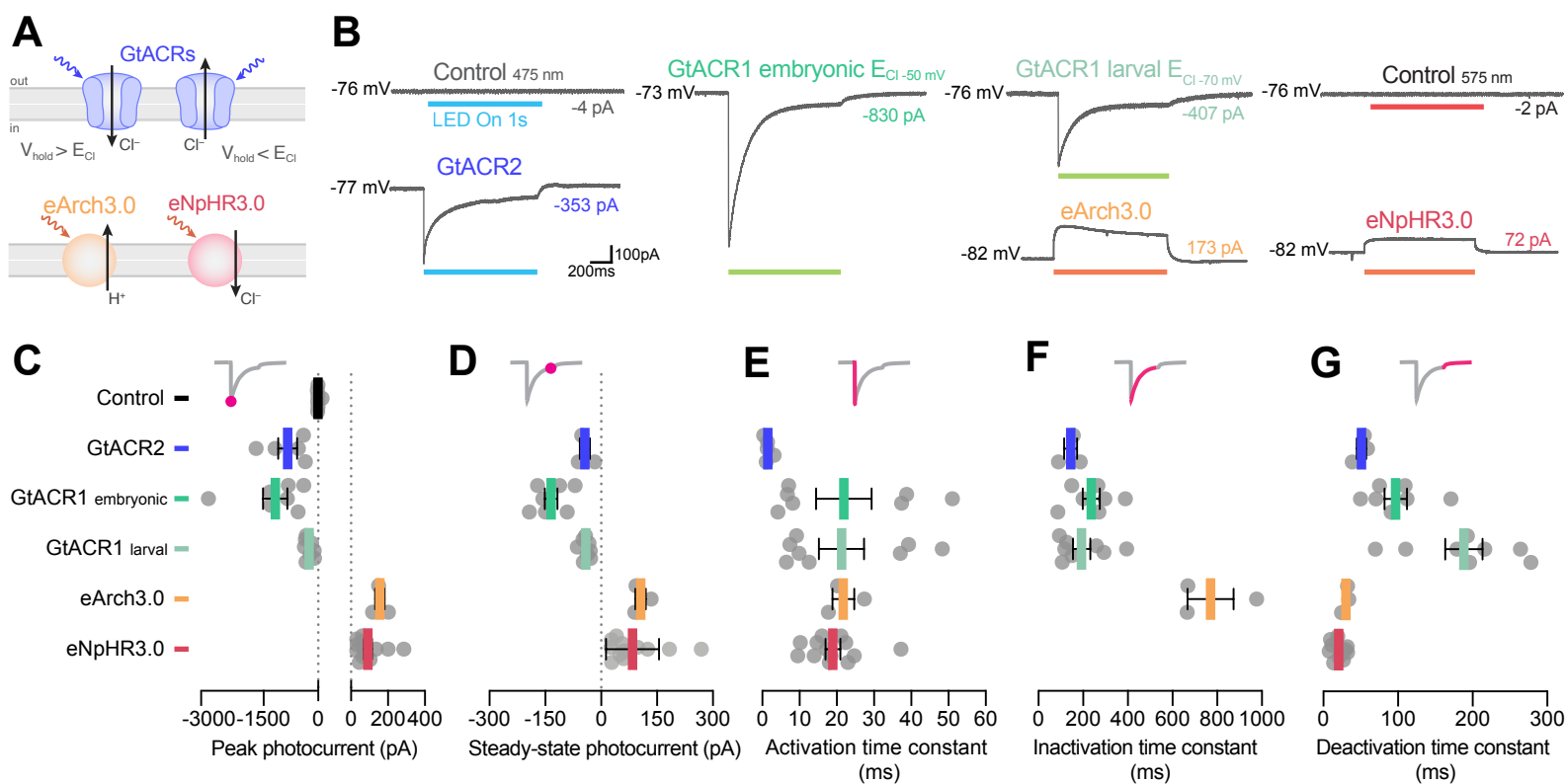
617 nm LED

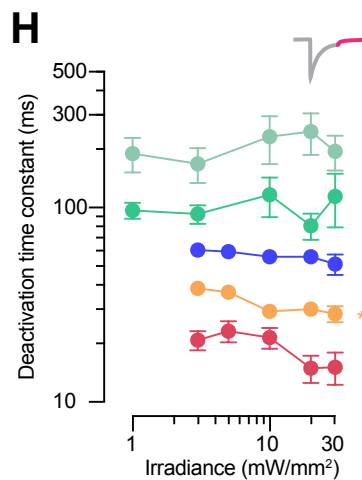
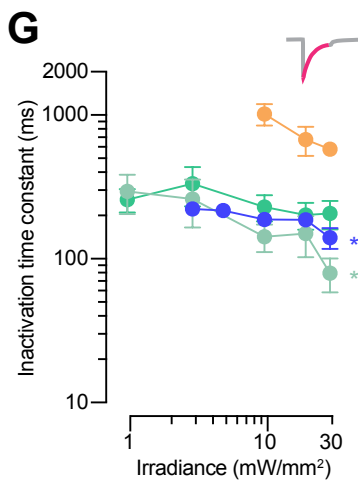
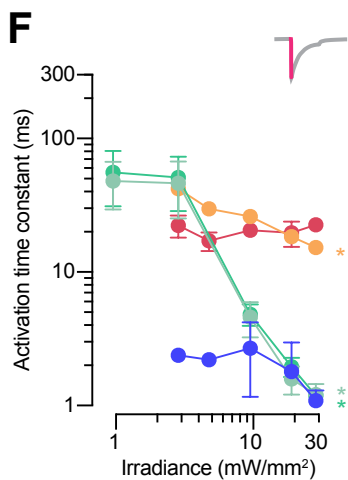
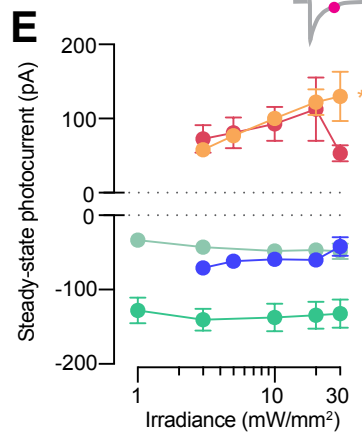
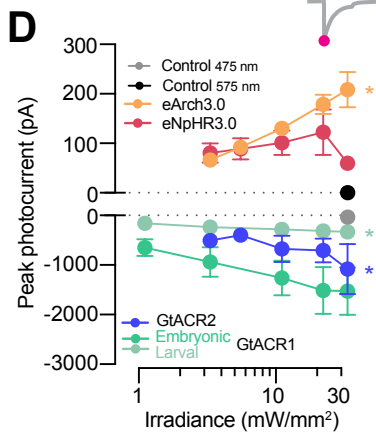
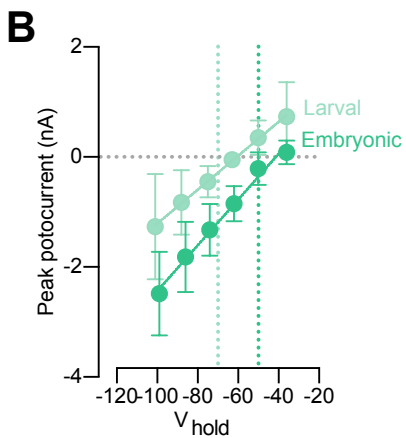
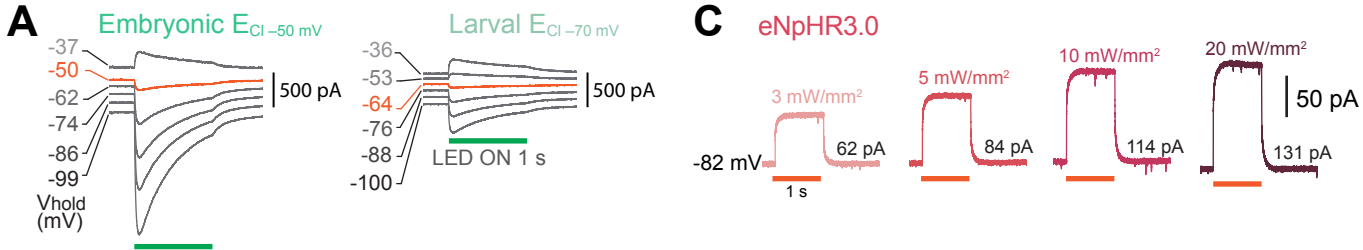


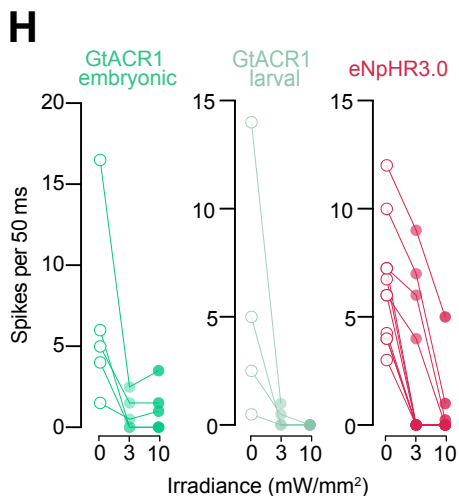
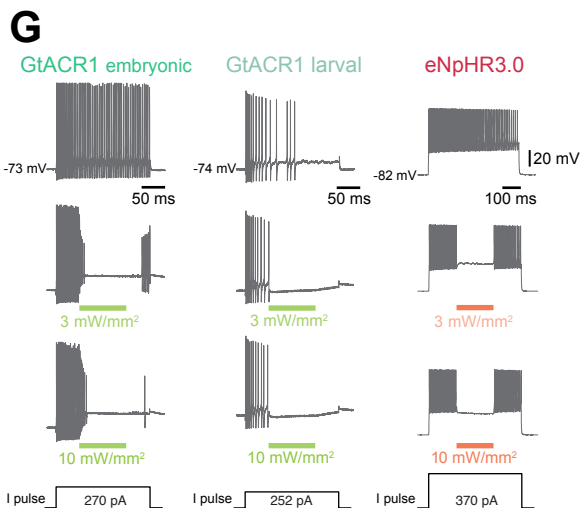
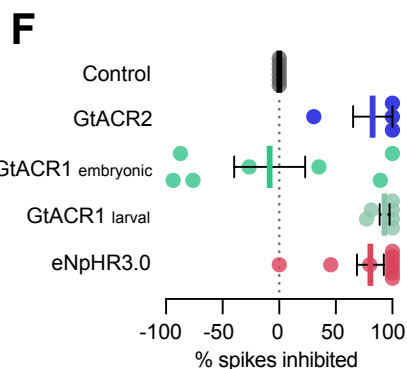
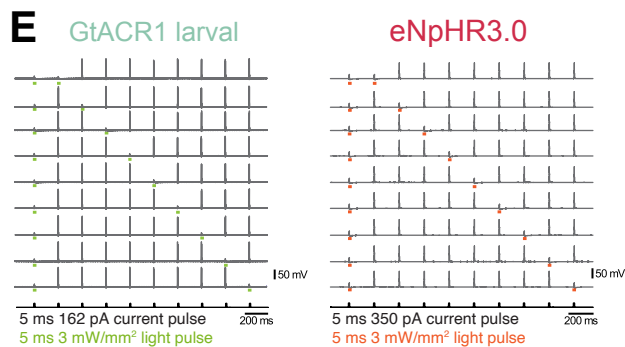
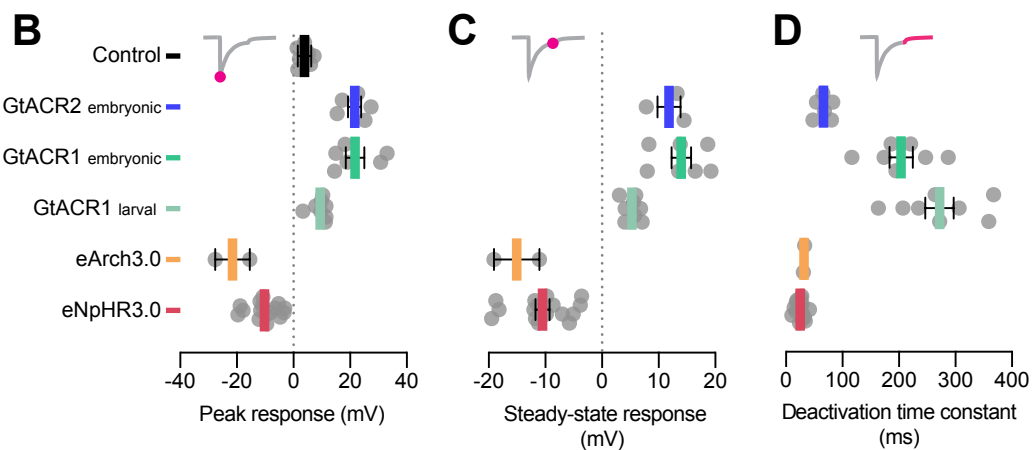
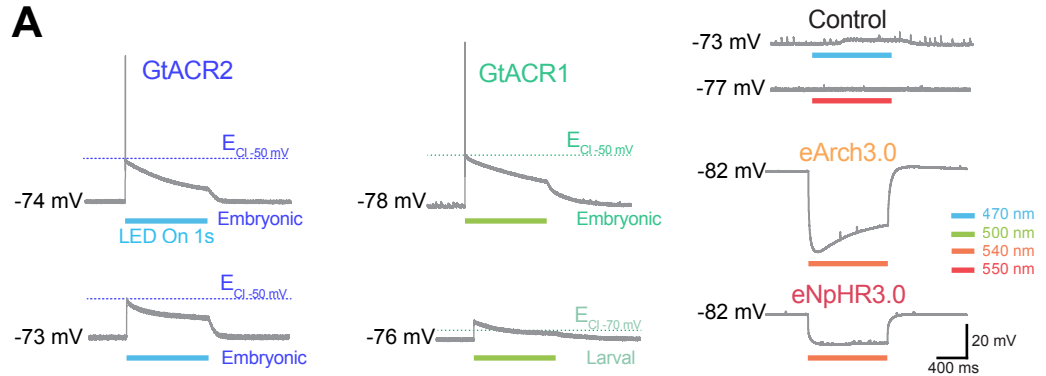


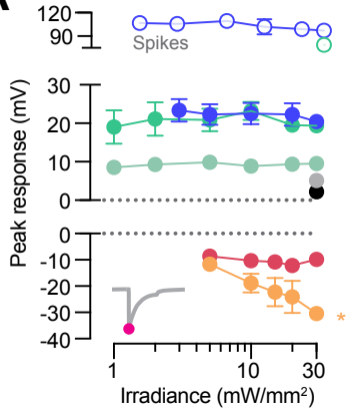
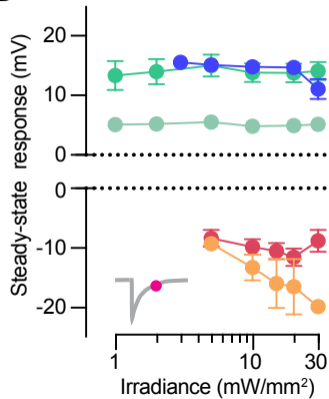
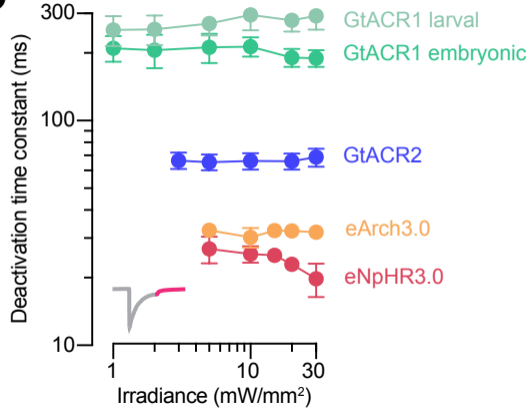


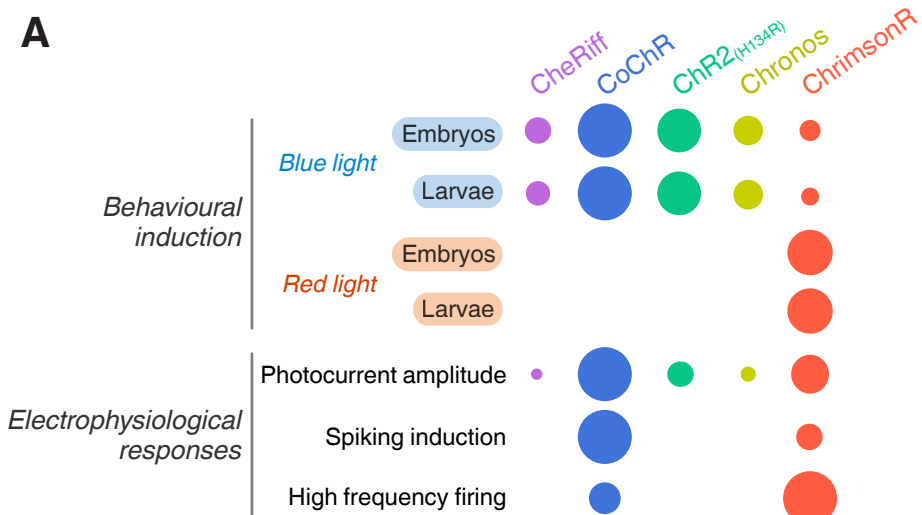








A**B****C**

A**B**